Monthly Notices of the ROYAL ASTRONOMICAL SOCIETY

MNRAS **519,** 6349–6380 (2023) https://doi.org/10.1093/mnras/stad060
Advance Access publication 2023 January 10

Optical/γ-ray blazar flare correlations: understanding the high-energy emission process using ASAS-SN and Fermi light curves

T. de Jaeger [1]★ B. J. Shappee,[1] C. S. Kochanek,[2,3] J. T. Hinkle [1] S. Garrappa,[4] I. Liodakis [5] A. Franckowiak [4] K. Z. Stanek,[2,3] J. F. Beacom[2,3,6] and J. L. Prieto[7,8]

[1]*Institute for Astronomy, University of Hawaii, 2680 Woodlawn Drive, Honolulu, HI 96822, USA*
[2]*Department of Astronomy, The Ohio State University, 140 W. 18th Avenue, Columbus, OH 43210, USA*
[3]*Center for Cosmology and AstroParticle Physics (CCAPP), The Ohio State University, 191 W. Woodruff Avenue, Columbus, OH 43210, USA*
[4]*Fakultät für Physik and Astronomie, Ruhr-Universität Bochum, D-44780 Bochum, Germany*
[5]*Finnish Centre for Astronomy with ESO, University of Turku, FI-20014 Turku, Finland*
[6]*Department of Physics, The Ohio State University, 191 W. Woodruff Ave., Columbus, OH 43210, USA*
[7]*Núcleo de Astronomía de la Facultad de Ingeniería y Ciencias, Universidad Diego Portales, Av. Ej ército 441, Santiago, Chile*
[8]*Millennium Institute of Astrophysics, Nuncio Monsenor Sótero Sanz 100, Providencia 8320000, Santiago, Chile*

Accepted 2023 January 6. Received 2022 December 15; in original form 2022 October 27

ABSTRACT

Using blazar light curves from the optical All-Sky Automated Survey for Supernovae (ASAS-SN) and the γ-ray *Fermi*-LAT telescope, we performed the most extensive statistical correlation study between both bands, using a sample of 1180 blazars. This is almost an order of magnitude larger than other recent studies. Blazars represent more than 98 per cent of the AGNs detected by *Fermi*-LAT and are the brightest γ-ray sources in the extragalactic sky. They are essential for studying the physical properties of astrophysical jets from central black holes. However, their γ-ray flare mechanism is not fully understood. Multiwavelength correlations help constrain the dominant mechanisms of blazar variability. We search for temporal relationships between optical and γ-ray bands. Using a Bayesian Block Decomposition, we detect 1414 optical and 510 γ-ray flares, we find a strong correlation between both bands. Among all the flares, we find 321 correlated flares from 133 blazars, and derive an average rest-frame time delay of only $1.1^{+7.1}_{-8.5}$ d, with no difference between the flat-spectrum radio quasars, BL Lacertae-like objects or low, intermediate, and high-synchrotron peaked blazar classes. Our time-delay limit rules out the hadronic proton-synchrotron model as the driver for non-orphan flares and suggests a leptonic single-zone model. Limiting our search to well-defined light curves and removing 976 potential but unclear 'orphan' flares, we find 191 (13 per cent) and 115 (22 per cent) clear 'orphan' optical and γ-ray flares. The presence of 'orphan' flares in both bands challenges the standard one-zone blazar flare leptonic model and suggests multizone synchrotron sites or a hadronic model for some blazars.

Key words: relativistic processes – galaxies: active – galaxies: jets.

1 INTRODUCTION

Blazars are a subclass of radio-loud active galactic nuclei (AGNs) characterized by a jet pointing within a few degrees of the observer's line of sight (Blandford & Ostriker 1978; Antonucci 1993; Urry & Padovani 1995). Due to the nearly aligned viewing angle, we observe strong relativistic effects such as beaming of the emitted power, causing blazars to be the brightest γ-ray sources in the extragalactic sky. They represent more than 98 per cent of the AGNs detected by the Large Area Telescope (LAT) onboard the *Fermi* γ-ray space observatory (Atwood et al. 2009; Acero et al. 2015; Abdollahi et al. 2020) and are ideal objects for studying the poorly understood physics of astrophysical jets.

Based on the strength of their optical emission lines, blazars are subdivided into flat-spectrum radio quasars (FSRQs) and BL Lacertae (BL Lac) objects (Urry & Padovani 1995). FSRQs have prominent broad emission lines, while BL Lacs have blue nearly featureless optical spectra with emission line equivalent width <5Å (Stickel et al. 1991). Padovani & Giommi (1995) proposed an independent classification based on the peak of their spectral energy distribution (SED; see also Abdo et al. 2010 and Ghisellini et al. 2011): low-synchrotron peaked blazars (LSP; $\nu_{\rm peak} \leq 10^{14}$ Hz), intermediate synchrotron peaked blazars (ISP; $10^{14} \leq \nu_{\rm peak} \leq 10^{15}$ Hz), and high-synchrotron peaked blazars (HSP; $\nu_{\rm peak} > 10^{15}$ Hz). The HSP and ISP blazar groups are mostly BL Lacs, while the LSP class is dominated by FSRQs.

All blazars emit across the electromagnetic spectrum. Their SED consists of two broad non-thermal peaks, one at radio to ultraviolet wavelengths and the second at X-ray to γ-ray energies (Impey & Neugebauer 1988; Fossati et al. 1998; Marscher et al. 2008). The low-frequency peak is generally agreed to be synchrotron emission from relativistic electrons spiralling in the jet magnetic field (Urry & Mushotzky 1982; Impey & Neugebauer 1988). However, the origin of the higher energy peak is not fully understood. It can be explained by leptonic, hadronic (Mücke et al. 2003; Böttcher et al. 2013;

★ E-mail: dejaeger@hawaii.edu

Madejski & Sikora 2016), or hybrid models (see Böttcher 2019 for a review).

In the leptonic model, electron pairs dominate the high-energy emissions, as the protons within the outflow are either not accelerated to sufficiently high energies or the injected energy in relativistic protons is much less than that in relativistic electrons to make a significant contribution. Therefore, GeV–TeV γ-rays are due to inverse-Compton scattering (ICS) of low-energy (IR-optical-UV) target photons by the same ultrarelativistic electrons producing the synchrotron emission at lower frequencies (Maraschi, Ghisellini & Celotti 1992; Sikora, Begelman & Rees 1994). Since the low and high-energy peaks are produced by the same population of electrons, the leptonic model predicts strong correlations between the optical and γ-ray emission. The origin of the seed photons is not clear. They could be produced within the jet (synchrotron self-Compton, SSC; e.g. Marscher & Gear 1985; Ghisellini & Maraschi 1989; Maraschi et al. 1992; Bloom & Marscher 1996; Mastichiadis & Kirk 1997; Chiang & Böttcher 2002; Arbeiter, Pohl & Schlickeiser 2005) or from external sources (external Compton, EC) such as the accretion disc, the 'dusty torus', or the broad-line region (Dermer & Schlickeiser 1993; Sikora et al. 1994; Ghisellini & Madau 1996; Boettcher, Mause & Schlickeiser 1997; Błażejowski et al. 2000; Dermer et al. 2009).

The absence of thermal emission in BL Lac blazar flares favours a one-zone leptonic SSC model, where a single emitting region with constant and homogeneous parameters dominates the emission (Costamante & Ghisellini 2002). One-zone leptonic SSC models are interesting because of their simplicity and their limited number of free parameters. However, unlike BL Lac, the FSRQ SED is not easily described by a simple one-zone SSC model. It is best modelled with a sum of the contribution from the SSC and the scattering of external photons with the EC contribution dominant during strong γ-ray flares (Sikora et al. 1994; Ghisellini et al. 2012; Williamson et al. 2014; Böttcher 2019).

In hadronic models, the high-energy emission is associated with ultrarelativistic protons emitted by proton–synchrotron radiation (Aharonian 2000; Mücke & Protheroe 2001; Mücke et al. 2003; Liodakis & Petropoulou 2020) or photo-pion production (Mannheim 1993). A strong long-term correlated variability between the low-energy bands and γ-rays is generally not expected for the hadronic model. However, we expect a correlation between the γ-ray and the neutrino fluxes, when the γ-rays from pion decay are emitted in a similar energy range as the neutrinos. Note that for GeV γ-rays and PeV neutrinos, a correlation is not always expected (Kelner, Aharonian & Bugayov 2006; Gao, Pohl & Winter 2017; IceCube Collaboration 2018). Note also, there could still be some correlation between optical and γ-ray emission, because the hadronic processes that produce high-energy γ-rays also produce high-energy electrons, which act just like those in leptonic models. However, the corresponding low-energy emission can be overwhelmed by other sources.

Understanding the dominant process for blazar's γ-ray emissions and the physics of the astrophysical jets can be done through two complementary approaches:

(i) The first is broad-band SED modelling of individual objects such as 3C 454.3, Mrk 421, Mrk 501, or PKS 2155-304. Unfortunately, for almost all blazars, leptonic, hadronic, and lepto-hadronic scenarios have all been able to reproduce the SEDs of blazars successfully (e.g. Punch et al. 1992; Dermer & Schlickeiser 1993; Mannheim 1993; Urry et al. 1997; Ghisellini et al. 1998; Mücke & Protheroe 2001; Błażejowski et al. 2005; Aharonian et al. 2007; Albert et al. 2007; Jorstad et al. 2010; Böttcher et al. 2013; Cerruti et al. 2019), so it has been difficult to constrain the dominant process. Note that in the case of TXS 0506+056, the SED modelling showed that lepto-hadronic models could not reproduce simultaneously the EM and neutrino observations (Keivani et al. 2018; Gao et al. 2019; Rodrigues et al. 2019). Obtaining the SED also requires intensive multiwavelength observational campaigns for each source.

(ii) An alternative method is to study flux variations and search for temporal correlations between the two major emission components (optical and γ-ray). This method can now be applied to a large number of blazars thanks to the well-sampled γ-ray light curves from *Fermi*-LAT and the optical light curves from new generations of optical surveys like the All-Sky Automated Survey for Supernovae (ASAS-SN; Shappee et al. 2014; Kochanek et al. 2017). This allows a significant expansion in the number of optically monitored blazars compared to previous campaigns studying individual objects such as Yale/SMARTS (Bonning et al. 2012; Chatterjee et al. 2012) or the Katzman Automatic Imaging Telescope (KAIT; Filippenko et al. 2001; Cohen et al. 2014; Liodakis et al. 2019).

Recent multiwavelength correlation investigations of large blazar samples have constrained the dominant mechanisms driving blazar variability. For example, Liodakis et al. (2019) studied 178 *Fermi*-LAT blazars regularly monitored by KAIT and SMARTS and found strong optical/γ-ray correlations with time delays of only a few days (1 to 30 d), supporting the leptonic models and confirming previous studies with smaller samples (Bonning et al. 2012; Chatterjee et al. 2012; Cohen et al. 2014; Hovatta et al. 2014; Liodakis et al. 2018a). However, the presence of γ-ray flares without a low-energy counterpart and optical flares without a high-energy counterpart (known as 'orphan' flares) in the same blazar sample challenges the standard one-zone leptonic blazar flare model (Chatterjee et al. 2012; Böttcher et al. 2013; Cohen et al. 2014; Liodakis et al. 2019). There are several models for the origin of orphan flares (see Böttcher 2019 for a review), including a hadronic synchrotron mirror model in which a flare is due to the interaction of relativistic protons within the jet with external photons from the reflected electron–synchrotron emission from a nearby external obstacle (Böttcher 2005), a two-zone model with a site of γ-ray production situated between the broad-line region and the jet recollimation shock (MacDonald et al. 2015), an encounter between relativistic blobs in the jet and a luminous star (Banasiński, Bednarek & Sitarek 2016), the effects of the magnetic fields (Joshi, Marscher & Böttcher 2016), or a stochastic dissipation model (Wang et al. 2022).

In this work, we investigate the question of the high-energy emission process by looking for optical/γ-ray flare correlations for 1180 blazar light curves from the *Fermi*-LAT Collaboration data base (Abdollahi et al. 2022). This sample represents the most extensive and homogeneous statistical study of blazar flares. Our paper is organized as follows. Section 2 describes our optical and γ-ray data. Section 3 presents our methodology to search for optical-γ-ray flares and measure rest-frame time lag. Section 4 presents our results. Finally, Section 5 contains a summary and conclusions. Appendix A and B present the sample and 'orphan' flare information.

2 DATA SAMPLES

We selected all the sources from the 12-yr *Fermi*-LAT point source (4FGL-DR3) catalogue (Abdollahi et al. 2022) with a variability index greater than 24.725. For these sources, the chance of being a steady source is < 1 per cent. This leads to a sample of 1695 sources ($\sim$ 25 per cent of the 4FGL-DR3 6659 source catalogue). Then, we remove all sources with any non-zero entry in the analysis

flags column indicating that they are affected by systematic errors (Abdollahi et al. 2022). Finally, we select only the blazars and blazar candidates – the sources classified as FSRQ, BL Lac, or blazar candidates of uncertain type (BCU) – with light curves in the Fermi LAT Light Curve Repository (LCR[1]). This leads to a final sample of 1180 sources consisting of 503 FSRQs, 437 BL Lacs, and 240 BCU (814 LSP, 123 ISP, and 127 HSP) sources. This source list is provided in Table A1.

2.1 γ-ray light curves

The γ-ray light curves were obtained from the LAT Light Curve Repository website and included data binned at three-day, one-week, and one-month intervals. For our analysis, we use the three-day binning to detect short flares, on a day scale. Using a daily binned light curves for the brightest sources would be useful for our analysis, however, is required a full likelihood analysis which is beyond the scope of this paper. A full description of the data reduction is found on the *Fermi*-LAT Light Curve Repository website and in Abdollahi et al. (2022). Therefore, we present only a brief description here.

The LAT sources are characterized using an unbinned maximum-likelihood analysis (Abdo et al. 2009) in which the complete spatial and spectral information of each photon is used in the maximum-likelihood optimization. Light curves from the LCR were created using the standard Fermi Tools 1.4.7 analysis suite with the $P8R3\_SOURCE\_V2$ instrument response functions on $P8R3\_SOURCE$ class photons selected over an energy range spanning 100 MeV–100 GeV. To select the photons, a region of interest with a radius of 12° is centred on the source localization with a zenith angle cut of 90° to prevent contamination from γ-rays from the Earth limb. Then, the region of interest is fitted as a point source plus a model including the diffuse γ-ray emission from our Galaxy (template: gll_iem_v07), the isotropic template to account for all remaining isotropic emission (template: $iso\_P8R3\_SOURCE\_V2\_v1.txt$), the Sun and Moon steady emission templates, and all point-like and extended sources from DR3. The significance of the source detections are quantified by a test statistic (TS). Here, we select a detection criterion such that the maximum-likelihood TS exceeds four ($\sim 2\sigma$). Note that no assumptions about the spectral shape of the γ-ray sources is made and the photon index fits are fixed.

2.2 Optical light curves

ASAS-SN is a ground-based survey able to observe the entire visible sky daily to a depth of $g = 18.5$ mag (Shappee et al. 2014; Kochanek et al. 2017). Starting in 2013, with its first unit (Brutus) located on Haleakalā in Hawaii (USA), ASAS-SN is now composed of five stations in both hemispheres. Two units at the Cerro Tololo International Observatory in Chile (Cassius and Paczynski), one at McDonald Observatory in Texas, USA (Leavitt), and finally, one at the South African Astrophysical Observatory in Sutherland, South Africa (Payne-Gaposchkin). Each unit consists of four 14-cm aperture Nikon telephoto lenses with back-illuminated, 2048^2 CCD cameras having a 4.47 by 4.47-degree field of view. Until late 2018, Brutus and Cassius units used a *V*-band filter and were switched to *g*-band filters after roughly 1 yr of *V*- and *g*-band overlap with the three new units.

[1]https://fermi.gsfc.nasa.gov/ssc/data/access/lat/LightCurveRepository/about.html.

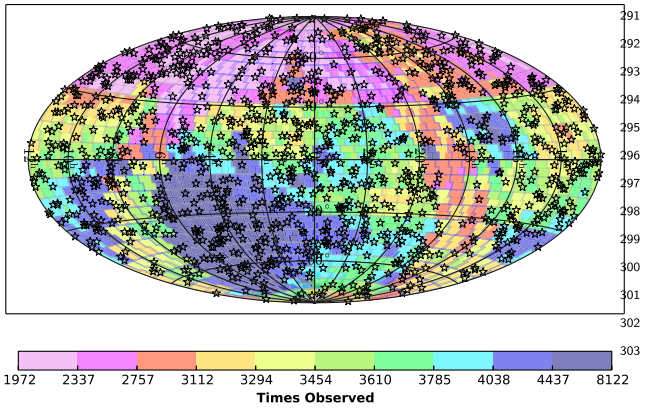

Figure 1. The all-sky, high-cadence, decade-long coverage of both ASAS-SN and *Fermi*-LAT makes the pairing of these two observational data sets compelling. ASAS-SN covers the entire visible sky with at least 1970 epochs and more than 8100 for some number of sky regions (as of 2022 October 11). The colour bar indicates the number of ASAS-SN epochs and the black stars indicate the 1180 *Fermi*-LAT sources.

For each ASAS-SN field, we take three dithered 90 s exposures. All the images are processed by the *ISIS* (Alard & Lupton 1998; Alard 2000) image subtraction ASAS-SN pipeline (Shappee et al. 2014; Kochanek et al. 2017; de Jaeger et al. 2022; Hart et al., in preparation). For photometry, we use the subtracted image with the reference flux of the source added back to the light curve (see https://www.astronomy.ohio-state.edu/asassn/public/examples.shtml). With a 2-pixel radius ($\sim$ 16 arcsec) and the *IRAF apphot* package, we conduct aperture photometry on the coadded image-subtracted data for each nightly epoch. Note that the blazar flux in the reference image leads to small offsets in the light curve for each ASAS-SN camera. To correct the light curves, we derive an average offset by comparing the average flux of each camera during the overlapping period. As the 'reference' flux, we choose the camera with a longer time coverage range. Then, we apply the different cameras' offsets to the rest of the light curve. Finally, we bin all the light curves to a three-day cadence to be consistent with the γ-ray light curves. No Milky Way or host–galaxy extinctions have been applied to the optical photometry as the extinction does not affect our methodology to detect flares. If we apply a dust correction, all the magnitudes will be offset but the ratio between the peak of the flares and the continuum will remain the same, therefore we will detect the same flares. For the blazars near the Galactic plane, affected by dust extinction, we will observe flares for only the brightest events.

ASAS-SN is ideal for searching for blazar flare correlations as it has two unique advantages over other optical surveys:

(i) Its observational baseline begins in 2013, covering the entire sky. For comparison, ZTF has observed only the Northern hemisphere since 2018 (Bellm et al. 2019). As seen in Fig. 1, there are at least 1970 and up to 8100 observations[2] of every point in the sky.
(ii) Unlike targeted optical blazar monitoring programmes, it has observations of all the *Fermi*-LAT sources.

Those two unique features allow us to do the most extensive statistical study of blazar flares to date with minimal selection biased, as we observe all the blazars independently of their properties or localization.

[2]One epoch consists of three observations of 90 s.

3 SEARCH FOR OPTICAL/γ-RAY CORRELATIONS

In this section, we detail our methodology to search for flares and how we derive the time lag between the optical and the γ-ray emissions.

3.1 Flares

In blazar studies, one of the most important goals is to search for and characterize flares. Flares are prominent outbursts lasting for days to months surrounded by period of relative quiescence. Unfortunately, there is no a consensus on a quantitative definition of a flare. Here, we give a non-exhaustive list of the approaches used in the literature:

(i) A flare is simply defined as the period when the flux level exceeds <F>+3σ_w where <F> is the average flux and σ_w is the weighted standard deviation (Williamson et al. 2014).
(ii) A flare is a contiguous period of time associated with a given flux peak, during which the flux exceeds half of the peak value, and this lower limit is attained exactly twice at the beginning and the end (Nalewajko 2013).
(iii) The blazar light curves are decomposed into individual flares (Valtaoja et al. 1999), each described by an exponential rise and decay (Chatterjee et al. 2008; Jorstad et al. 2010; Chatterjee et al. 2012; Liodakis et al. 2018b; Roy et al. 2019).
(iv) A flare is defined using the Bayesian block algorithm (Scargle 1998; Scargle et al. 2013). First, the Bayesian block algorithm is used to segment the blazar light curve into blocks with statistically constant fluxes. Then, we choose a flux threshold above which a block is designated as a flare (Liodakis et al. 2018a; Meyer, Scargle & Blandford 2019; Adams et al. 2022; Stathopoulos et al. 2022).
(v) A flare is the period of time where the fractional variability amplitude ($F_{\rm var}$), which characterizes the flux variability properties of a blazar, is above a threshold (Vaughan et al. 2003).

For this study, we use Bayesian Block Decomposition (BBD; Scargle 1998; Scargle et al. 2013), as it seems to be the most objective way to identify strong flares, for both the γ-ray and optical light curves. Additionally, it can identify significant data series changes independently of gaps or exposure variations and does not need a prior for the flare time-scale. BBD determines an optimal binning for the data, where the bin sizes do not have the same width but each bin has no statistically significant flux variations. This method requires a false-positive rate (p_0) associated with the prior estimate of the number of bins, ncrprior, defined as $4 - \log(73.53 p_0 N^{-0.478})$, where N is the number of photometric points. We choose a false-positive rate for the optical and the γ-ray data of $p_0 = 0.01$.

After running the BBD, the non-flaring and flaring levels are identified using a three-step procedure following Meyer et al. (2019, see also Wagner et al. 2022 for PYTHON codes).

(i) We select all the local maxima[3] with a peak higher than $\widetilde{F}+\sigma_F$, where $\widetilde{F}$ is the median flux and σ_F is the standard deviation of the whole light curve. Note that a block peak is defined as the average flux in the block ($\overline{F_{\rm blocks}}$).
(ii) We regroup blocks using the HOP algorithm (Eisenstein & Hut 1998) based on a bottom-up hill-climbing concept. We proceed downward from the peak, and every block subsequently lower in both directions (left and right) belongs to that peak. The flux exceeding our quiescent level ($\widetilde{F} + \sigma_F$) determines the start/end of the flare. Note that using the median flux for our quiescent level yields an upward bias for the true quiescent level estimate. However, this has little effect for our results, as we focus only on the most prominent flares (see Section 4.2).
(iii) Finally, for our work, we study only the prominent flares. First, from all the flares defined above, we select only the flares with at least two flux points ($N > 2$). Then, we apply a threshold which depends on the number of points in the flare (see equation 1).

$$\overline{F_{\rm blocks}} > 3 \times \frac{\overline{F_{\rm blocks}} - \widetilde{F}}{\sigma_F} \times \sqrt{N}. \quad (1)$$

Finally, we visually inspect all the flare candidates and remove the bad candidates: flares with large photometric errors, optical flares due to seasonal gap edges (e.g. higher airmass), or optical flares seen only in one optical band (V or g) during the V/g band overlap period. Then, we classify each source as:

(i) Having at least one flare in both bands (both).
(ii) Only in optical (opt).
(iii) Only in γ-ray (gam).
(iv) Without flares (none).

Table A1 shows a summary of the results of our visual inspections. Fig. 2 shows an example of a blazar with flares detected in both bands after applying our methodology. We highlight correlated flares, 'orphan' flares, candidate 'orphan' flares, and the flares removed after our visual inspection in different colours. We select only the clearest examples for our 'orphan' flare analysis, as explained in Section 4.3. For example, we do not consider the first 'orphan' flare candidate at $\sim$ MJD 58050 as a true 'orphan' flare. At the same epoch, the γ-ray light curve presents a small flux rise, not enough to be considered a flare according to our definition but enough to consider the optical flare as not an 'orphan'. Note also that the two 'orphan' γ-ray flares detected by our methodology (magenta) are removed from the sample because they occurred during an optical observational gap.

3.2 Time lags

To resolve the structure of relativistic jets and the localization of the emission along the length of the jet, we can study the time lags between flares in different energy bands. For example, in the leptonic single-zone model (SSC and EC), one expects time delays of only a few days because the same electrons produce flares in both bands. For example, we find short delays (on hour-day scale) when the EC is the dominant mechanism due to the stratification with the distance from the black hole of the jet regarding the amount of emitted energy and the profile of the magnetic field (Janiak et al. 2012). For some hadronic models, the low- and high-energy SED peaks vary independently and we do not expect a correlation between the optical and γ-ray flares. This is the case for the proton–synchrotron model (Sikora et al. 1994; Sokolov, Marscher & McHardy 2004; Cohen et al. 2014; Böttcher 2019; Liodakis et al. 2019) but not for photohadronic cascade models (Mastichiadis, Petropoulou & Dimitrakoudis 2013) or purely hadronic models (Mastichiadis & Petropoulou 2021). Different works using different techniques and samples have found a strong temporal correlation between optical and γ-ray flares ruled out the proton–synchrotron model for the blazar flares. In particular, Bonning et al. (2012), Cohen et al. (2014), Liodakis et al. (2019), and Bhatta (2021) only found short time delays of the order of days to tens of days.

In the literature, two methods are commonly used to study the cross-correlation between time-series and estimate lags:

[3] All the blocks that are higher than both the previous and subsequent blocks.

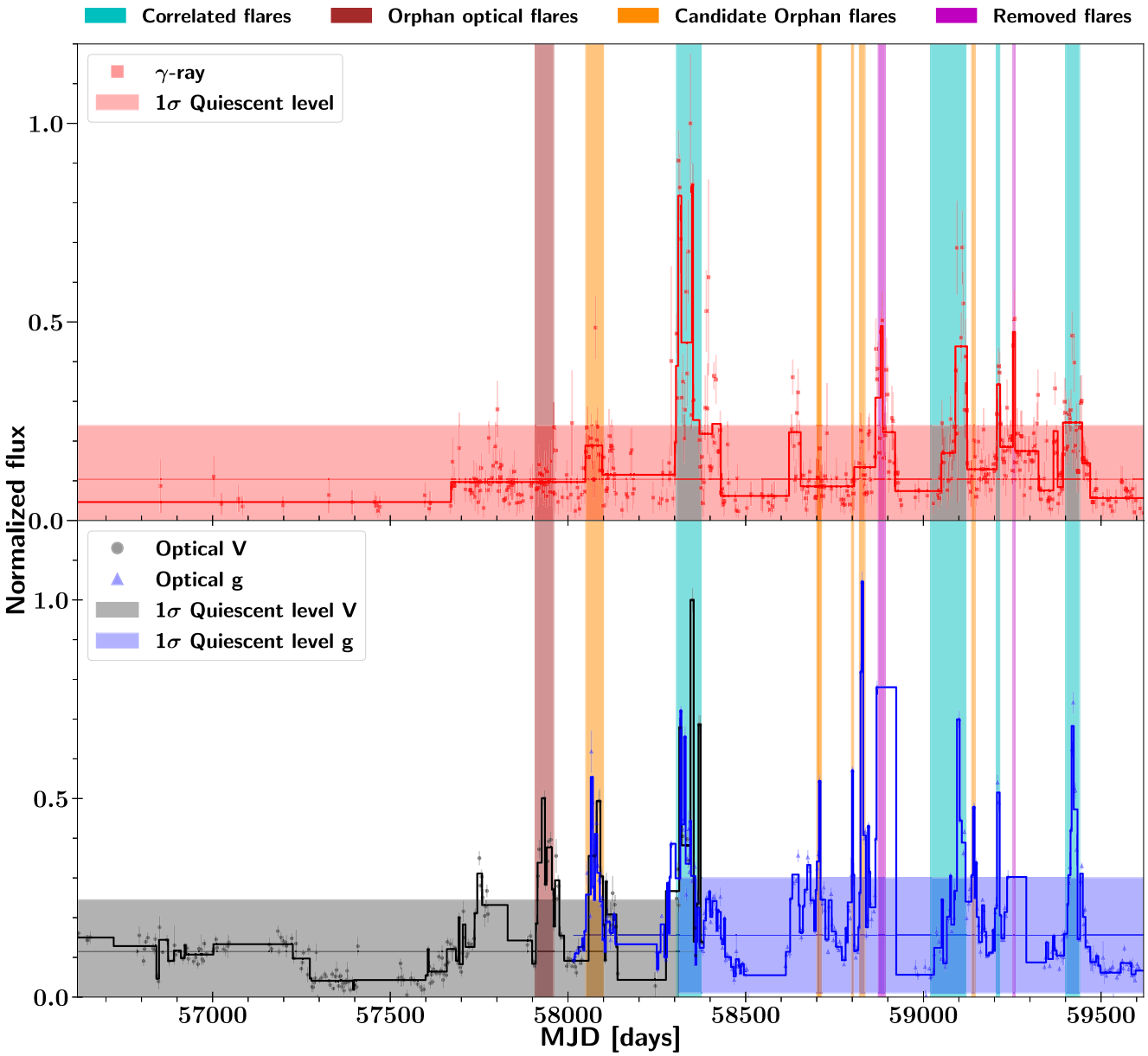

Figure 2. Upper panel: *Fermi*-LAT γ-ray light curves for J0038.2-2459 and its Bayesian Block Decomposition (solid line), together with the identified HOP groups shown by the shaded regions. Bottom panel: Optical *V* and *g* light curves from ASAS-SN and their BBD are shown, respectively, in red and black. In both panels, the vertical cyan, brown, orange, and magenta-shaded regions represent the correlated flares, the flares seen in the optical but not in γ-rays ('orphan' optical flares), the 'orphan' candidate flares, and the flares removed after visual inspection, respectively.

(i) Discrete correlation function (DCF): this method is based on the discrete correlation function (Edelson & Krolik 1988), which, unlike the autocorrelation function, allows an estimates from unevenly sampled data.

(ii) Z-transformed discrete correlation function (ZDCF): this is a modified version of the DCF (Alexander 1997, 2013) where the cross-correlation coefficients, r, are z-transformed using Fisher transformations. Unlike the DCF, the data are rebinned with an equal numbers of data points in each lag bin. The ZDCF reduces biases and gives better estimates of the uncertainties.

In general, one computes the DCF and the ZDCF for a range of time lags. Then, the correlation peak is fit with a Gaussian to determine the time lag and its uncertainty.

Here, we focus on the lags for individual correlated flares instead of cross-correlations the entire light curve. By looking only at flares, we are less sensitive to seasonal systematics, especially for sources near the detection limits of ASAS-SN and Fermi. This technique is better for objects where the DCF or the ZDCF curves do not show a peak in the correlation function, but the optical and γ-ray light curves clearly have correlated flares. An example is shown in Fig. 3. For this source, both DCF and ZDCF correlation functions lack a well-defined peak. However, both light curves clearly have correlated flares. For example, around MJD 56550, a flare is visible in both bands, with the γ-ray emission leading the optical. Another possible less significant correlated flare is visible around MJD 57250 but it was not detected by the Bayesian Block Decomposition of the γ-ray light curve.

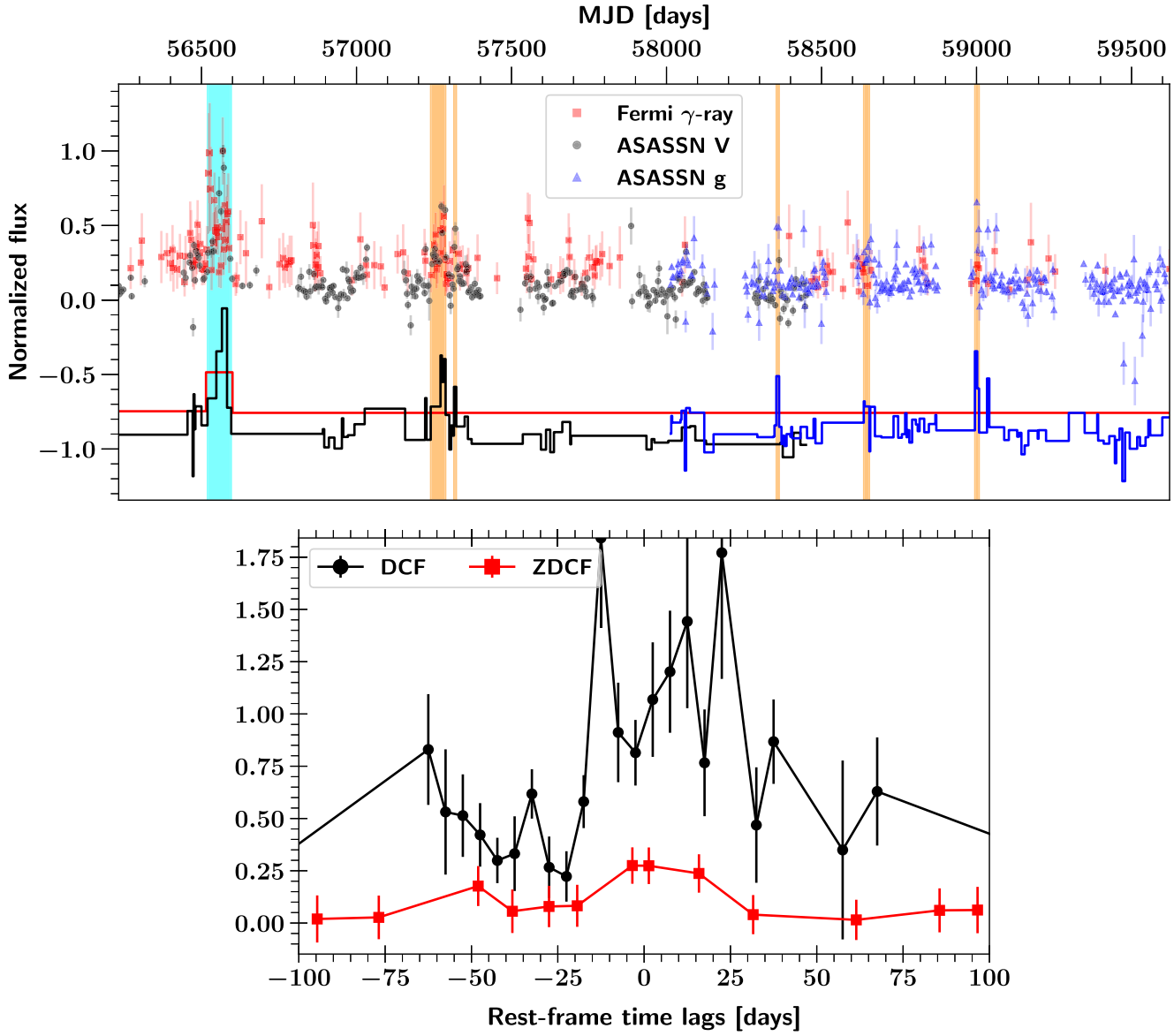

Figure 3. Upper panel: Correlated flares in the normalized light curves of J0050.4-0452 between the *Fermi*-LAT γ-ray (red squares) and the optical *V*-band (black dots), and *g*-band (blue triangles). The cyan shaded region indicates the flares in both bands and used to derive the time lag. The orange shaded regions represent the flare detected in the optical light curves but not in the γ-ray light curve. The black, red, and blue lines are the Bayesian Block Decompositions for each band shifted downwards for clarity. Bottom panel: Discrete correlation function (DCF; in black) and Z-transformed discrete correlation function (ZDCF; in red) between the optical and γ-ray light curves. A positive observed time lag corresponds to the γ-ray emission leading to the optical emission.

For all the blazars, we define the rest-frame time lag ($\tau_{\rm lag}$) as the difference in the epochs of the Bayesian block peaks (the middle of the block) and the associated uncertainty as half the block widths. For the object presented in Fig. 3, the γ-ray and optical observed flare epochs are, respectively, MJD 56557.25 $\pm$ 42.8 and MJD 56574.12 $\pm$ 38.2. So the rest-frame is $\tau_{\rm lag} = 8.8 \pm 21.1$ d. A positive $\tau_{\rm lag}$ corresponds to the γ-ray emission leading to the optical emission.

4 RESULTS

In this section, we investigate if flaring activities are stronger in one of the bands. One metric for this is the number of flares (correlated and 'orphan') observed in each band and for each blazar class. Then, we measure the time lag between optical and γ-ray emissions.

4.1 Flares

After applying our search methodology from Section 3.1, we end up with a total of 2584 flares in 421 blazars[4]: 1624 optical and 960 γ-ray flares. If we remove all the flares in observational gaps (at least 50 d without data) to keep only flares with overlapping optical and γ-ray observation periods – the total decreases to 1924 flares: 1414 optical and 510 γ-ray flares. Roughly $\sim$ 50 per cent of γ-ray flares occur during optical observing gaps. This is consistent with the 43 per cent found by Liodakis et al. (2019).

Finally, we investigate how the statistics are affected by our instrument limiting magnitude. Fig. 4 shows the histogram of a rough estimate of the *g*-band magnitude for blazars with (red) or

[4]Blazars labelled as 'opt', 'both' or 'gam' in Table A1.

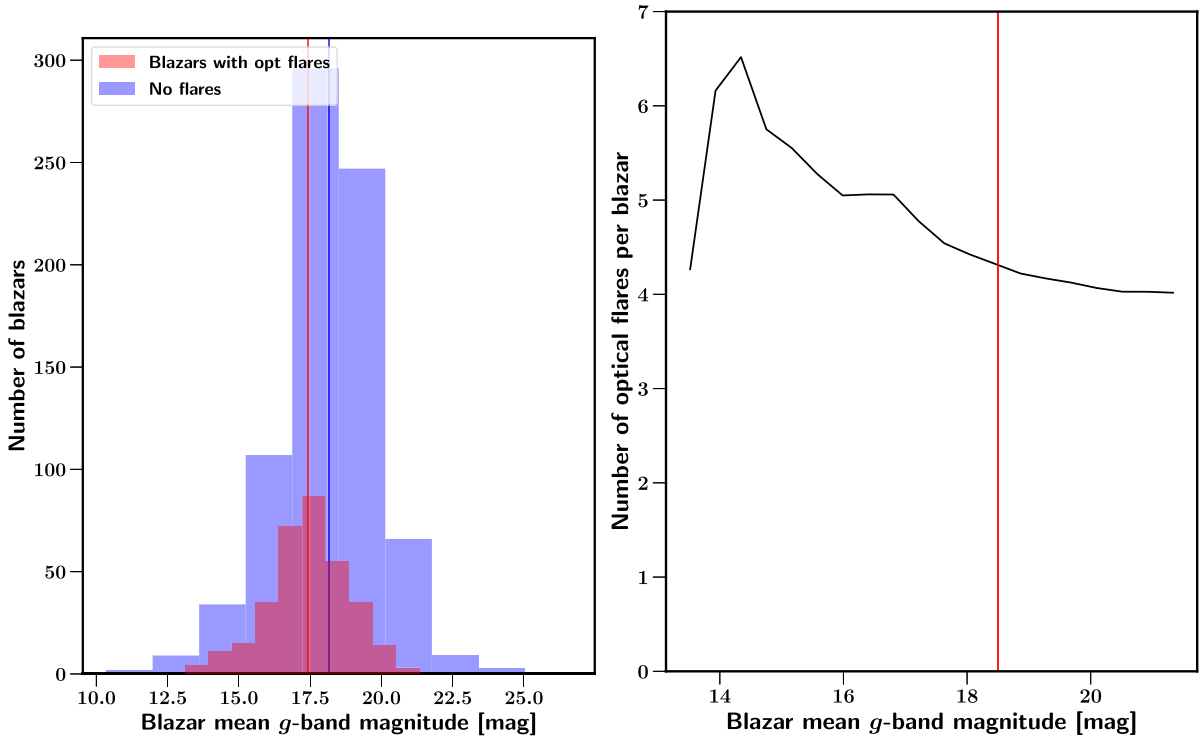

Figure 4. Optical flaring versus optical magnitude. Left-hand panel: Histogram of the mean g-band blazar magnitude for the objects with at least one optical flare (red) and the sources without flares (blue). The vertical lines correspond to the average values. Right-hand panel: Number of optical flares versus the mean g-band blazar magnitude. The red vertical line represents our magnitude cut at $g = 18.5$ mag.

without optical flares (blue). The g-band magnitudes are derived using an average weighted g-band flux over all the years (negative and positive values) and a zero point of 16.4. As expected, blazars without optical flares are on average fainter than those with flares, almost one magnitude. Also, as seen in Fig. 4 (right-hand panel), brighter blazars have more detected flares than fainter objects ($\sim$ 6 versus 3 flares). Therefore, as a conservative approach, we select only the optical flares in blazars with a mean $m_g < 18.5$ mag. This corresponds to our limiting magnitude and the magnitude where the number of flares per object flattens (see Fig. 4). This is a conservative approach and some of the optical flares detected in fainter blazars are well-defined and also correlated with the γ-ray emission (see Section 4.2). In Fig. 5, we present examples of two clear optical flares and two correlated flares in fainter blazars.

After all the cuts, we end up with 1230 optical and 510 γ-ray flares, so, we detect $\sim$ 42 per cent more flares in optical than in γ-ray. Liodakis et al. (2018a) found the same trend and obtained $\sim$ 3.5 times more optical flares than γ-ray events. However, in a more recent study, Liodakis et al. (2019) increased their previous sample (178 versus 145 blazars) and derived a similar number of flares for each band: 4277 for optical and 4384 for γ-ray. It is important to note that with the BBD method, the number of flares varies with binning, with more flares for smaller temporal bins (Liodakis et al. 2019). The flare number is also sensitive to the photometric uncertainties, so the flare numbers change for different bin size and methodologies. This could explain our differences with Liodakis et al. (2019) and the different flare numbers between the optical and γ-ray bands. For example, the BBD method can explain the larger optical flare rate, as it creates several small false flares due to the smaller photometric errors and higher dispersion of the optical light curves. If we concentrate our study on only the strongest flares and increase our threshold in equation (1) from 3 to 10 (i.e. the flare flux must exceed ten times our quiescent level), we only detect 273 optical flares and 161 γ-ray flares.

We also investigate the number of flares for each blazar class. In our sample of 421 blazars (with at least one flare), there are 220 FSRQs, 160 BL Lacs, and 41 BCU. We detect 874, 774, and 92 flares for the FSRQ, BL Lac, and BCU classes. Like Liodakis et al. (2018a), we find that FSRQs tend to exhibit more γ-ray flares per source than the BL Lacs with 520/650 optical and 354/124 γ-ray flares for the FSRQ/BL Lac classes. The trend is not statistically significant to conclude if the difference between the two sub-classes is intrinsic or because FSRQs are on average brighter in γ-rays than BL Lacs. However, the BL Lacs seem to have more optical flares than the FSRQs. Finally, we consider all the FSRQs and BL Lacs of our sample and not only those with at least one flare. We obtain a rate of 1.73/1.77 flares per source (503/437) for FSRQ/BL Lac classes. For optical and γ-ray, the rates are 1.03/1.48 and 0.70/0.28 flares per source for FSRQ/BL Lac classes, respectively.

4.2 Time lags

Time lags between optical and γ-ray flares are of the order of only a few days (Bonning et al. 2012; Cohen et al. 2014; Liodakis et al. 2019; Bhatta 2021), so we look for correlated flares within a 30-d rest-frame window. For each of these 175 objects with flares in both bands, the final rest-frame $\tau_{\rm lag}$ is the average of correlated flare lags, and the error is the quadratic sum of the block widths. In the cases where two flares in one band could be correlated with a simple flare in the other band (i.e. within 30 d), we include both time lags. Our final rest-frame $\tau_{\rm lag}$ and their associated errors are in Table A1.

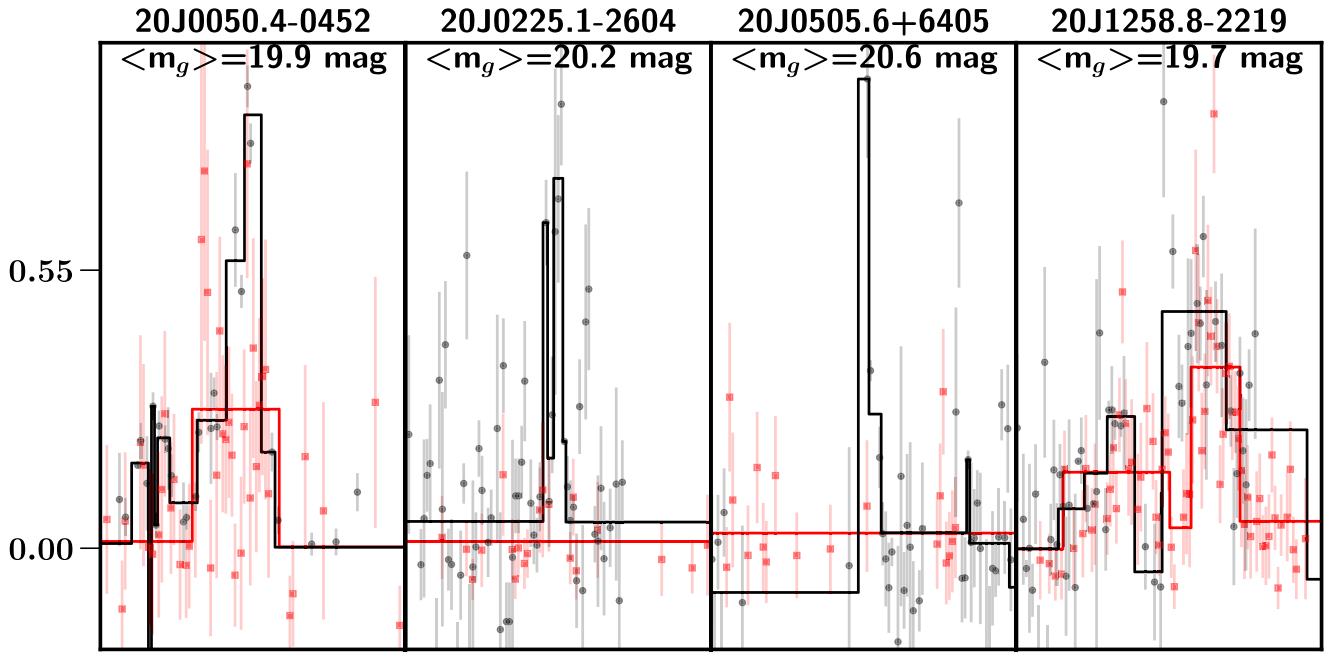

Figure 5. Example of optical flares observed in faint optical blazars ($m_g > 18.5$ mag). In each panel the optical blazar magnitude is shown. The black dots and red squares represent the *V*-band and γ-ray light curves and the red and black lines are the Bayesian Block Decompositions for each band. For 20J0050.4-0452 and 20J1258.8-2219 we clearly see a γ-ray counterpart.

Unlike Section 4.1, here we do not remove the optical flares seen in faint blazars because we only consider correlated flares. Even in faint blazars, if a γ-ray emission is seen at roughly the same epoch as the optical flares, it is likely that the optical flare is real. An example of two correlated flares in faint blazars are displayed in Fig. 5.

From the 175 objects with flares in both bands, we found 133 blazars with correlated flares and a redshift. Fig. 6 shows the rest-frame time lag distribution between both bands. We obtain an average rest-frame time lag of $1.1^{+7.1}_{-8.5}$ d, and the quoted uncertainties (hereafter) represent the 68 per cent confidence interval obtained from a bootstrapping simulation of 10 000 events. To estimate the uncertainties from the bootstrapping, we select 133 random rest-frame time lags for each event from our distribution and measure the standard deviation. Finally, from those 10 000 measurements, we derive our 68 per cent confidence interval. Note that, if we simply use the scatter in the 10 000 median lags, the dispersion is only $\sim$ 1 d which it is not representative of our distribution (standard deviation $\sim$ 7–8 d). Among the 133 objects, only three have a rest-frame time lag greater than 20 d and are not consistent with 0 (20J0133.1−5201, 20J1006.7−2159, 20J1604.6+5714). Our distribution is almost centred on 0 d and it is consistent with previous works (Bonning et al. 2012; Cohen et al. 2014; Liodakis et al. 2019; Bhatta 2021). For example, Liodakis et al. (2019) derived a median time lag of -0.24 ± 20.5 d using 117 objects, so, it is consistent with no time lag. Their time lag distribution is similar to ours but has a tail towards longer time lags (see Fig. 6). However, the difference may be due to our 30 d search window. If we increase our window to 60 d, the number of objects increases to 143, extending the distribution from -55 to 56 d. However, the median value changes only to $2.9^{+15.9}_{-13.1}$ d. We also find no correlations between our time lags and the redshift or the synchrotron peak frequency. If we remove the 17 blazars with $m_g > 18.5$ mag, we do not see significant difference in our average rest-frame time lag ($0.2^{+5.0}_{-10.1}$).

Investigating time lags between flares in different energy bands probes the origin of the seed photon for the leptonic model. For example, using 13 FSRQs and 17 BL Lacs, Cohen et al. (2014) found that FSRQs tend to have γ-rays leading the optical by a few days, while for the BL Lacs, they did not find a clear offset. This suggests that the seed photons for FSRQs are from external sources,

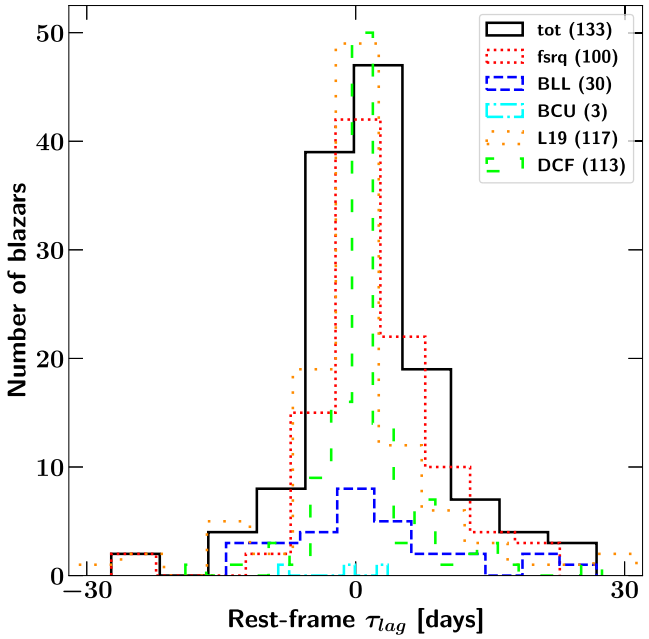

Figure 6. Distribution of all rest-frame time lags between the optical and γ-ray flares (solid black). The distributions for the classes are also shown: FSRQ (dotted red), BL Lac (dashed blue), and BCU (dash-dotted cyan). For comparison, the result obtained by Liodakis et al. (2019) is shown in loosely dotted orange, and the DCF lag distribution derived from the DCF is the loosely dashed lime. A positive $\tau_{\rm lag}$ corresponds to the γ-ray emission leading the optical emission.

while it is within the jet for BL Lacs (Böttcher et al. 2013). However, Liodakis et al. (2019) did not find such differences using a larger sample (53 FSRQs and 67 BL Lacs).

Fig. 6 shows the time lag distribution of our 100 FSRQs and 30 BL Lacs with median values of $0.9^{+6.3}_{-8.0}$ and $1.5^{+8.2}_{-10.9}$ d for FSRQs and BL Lacs, respectively. A Kolmogorov–Smirnov test also confirms the distribution are consistent with each other. These results support Liodakis et al. (2019) in finding no evidence for a difference in the seed photon source of the two blazar classes. However, this is only a statistical statement; individual objects could have different high-energy emission mechanisms, as has already been seen for individual blazars (e.g. Punch et al. 1992; Dermer & Schlickeiser 1993; Mannheim 1993; Urry et al. 1997; Ghisellini et al. 1998; Mücke & Protheroe 2001; Błażejowski et al. 2005; Aharonian et al. 2007; Albert et al. 2007; Jorstad et al. 2010; Böttcher et al. 2013; Cerruti et al. 2019).

We also separate our sample based on their SED class (LSP, ISP, and HSP). Of 133 objects with $\tau_{\rm lag}$ measurements, we have 118 LSP (96 FSRQs, 19 BL Lacs, 3 BCU), five ISP (1 FSRQ, 4 BL Lacs), and seven HSP (all BL Lacs), and three without an SED class. We derive a median lags of $\tau_{\rm lag}$ of $0.90^{+6.2}_{-8.1}$, $3.6^{+1.8}_{-4.6}$, and $5.6^{+15.1}_{-10.3}$ d for the LSP, ISP, and HSP classes, respectively. We do not see any significant lags between the optical and γ-ray flares for the three SED classes. All are consistent with no lag given their uncertainties.

Finally, as different studies have used the DCF to derive time lags, Fig. 6 shows our DCF lag distribution for the 113 objects with well-measured DCF peaks. The DCF sample is smaller because 20 sources have correlated flares, but the DCF does not show a well-defined peak (e.g. Fig. 3). Note that the lack of well-defined peak in the DCF could be due to the methodology. With the DCF, we analyse the entire light curve while with our methodology, we look only at correlated flares. Therefore, if there is only 1 flare in each band but the rest of the light curve is noisy, it will be difficult for the DCF to find a strong correlation between both signals. The DCF lag distribution is also statistically consistent with the lag distribution from the correlated peak analysis (Pearson correlation factor of 0.33, p-value of 0.009) and it has a median rest-frame $\tau_{\rm lag}$ of $0.6^{+4.8}_{-6.2}$ d.

To summarize our time lag analysis, we find that the majority of blazars have a strong optical/γ-ray correlation with time-scales on the order of days to tens of days, and are on average consistent with no delay for all blazar classes. Our results are in good agreement with previous studies (Bonning et al. 2012; Cohen et al. 2014; Liodakis et al. 2019; Bhatta 2021) and our work rules out the hadronic proton–synchrotron model as the driver for non-orphan flares and supports leptonic single-zone model.

4.3 Orphan flares

Our study of time lags presented in Section 4.2 supports a leptonic single-zone model for the non-orphan flares. However, some blazars show behaviours not expected in such a model. One of the most peculiar is the presence of 'orphan' flares – γ-ray flares with no visible counterpart or optical flares without γ-ray counterparts (Krawczynski et al. 2004; Błażejowski et al. 2005). As in Section 4.1, we remove all the 'orphan' flare candidates which occur during optical or γ-ray observational gaps[5] (see Fig. 2). This cut removes 979 'orphan' flare candidates: 500 optical (29 per cent) and 479 γ-ray (48 per cent).

[5]We have only upper limits.

To be sure that the existence of 'orphan' flares is not due to sensitivity limitations, we compare the optical and γ-ray flare amplitudes using all the correlated flares from Section 4.2. The flare amplitude is defined as the difference between the height of the block and the median flux of the light curve. Then, we measure the amplitude ratio $A_{\rm opt}/A_{\gamma}$. This ratio could give information regarding the structure of the jet as it expected to be different for different mechanisms. For example, for PKS 1510–089 Marscher et al. (2010) have shown that the dichotomy in the ratio suggests that as the emission feature moves down the jet, different sources of seed photons dominate the inverse Compton scattering. For another object, Bonnoli et al. (2011), demonstrated that larger variation in the flux of the γ-ray light curve with respect to the optical can be explained by a decreasing magnetic field when the observed γ-ray luminosity increases. We do not find a strong correlation between the amplitudes (Pearson factor of 0.18, p-value of 0.002). Thus to estimate the expected γ-ray flux amplitude for any 'orphan' optical flare candidate, we assume the median of $1.3^{+1.6}_{-1.2}$ of the $A_{\rm opt}/A_{\gamma}$ distribution. This value is consistent with Liodakis et al. (2019), who also found that optical flares have a larger average amplitude than γ-ray flares ($A_{\rm opt}/A_{\gamma} \sim 2.7$).

Next, we visually inspect all the 'orphan' flare candidates and select only the clearest ones, those with at least 2 points, not close to observational gaps, not likely due to photometric noise (see Fig. 2), and seen only in one optical band during *V*/*g* bands overlap period. We found a total of $\sim$ 306 'orphan' flares: 191 'orphan' optical flares and 115 'orphan' γ-ray flares. From those 306 'orphan' flares, we also construct a 'gold' sample of flares for future individual analysis. Fig. 7 shows those 28 'orphan' optical flares and 28 'orphan' γ-ray flares. Our fraction of 'orphan' γ-ray flares (115) relative to the total number of γ-ray flares (507) is consistent with Liodakis et al. (2019). We estimate that $\sim$22 per cent of γ-ray flares are 'orphan' events compared to $\sim$20 per cent in Liodakis et al. (2019). This is not surprising as we use the same photometric data for the γ-ray light curves (from *Fermi*-LAT). However, we find a different fraction percentage of 'orphan' optical flares. We find that $\sim$13.5 per cent (191/1414) of optical flares are orphan events as compared to $\sim$54 per cent in Liodakis et al. (2019). A difference in methodology and photometric data could explain the difference. First, we only use the strongest flares, while Liodakis et al. (2019) considered all local maxima (centre of three Bayesian blocks) as flares, independent of their amplitudes. With a blazar sample roughly three times larger, we find only $\sim$ 2000 flares while they detected more than 8600 flares. Secondly, unlike the γ-ray data, we are using optical photometry from different telescopes with different limiting magnitudes. We use data from ASAS-SN, which has a limiting magnitude of 18.5 mag (Kochanek et al. 2017). Most of the optical light curves used in Liodakis et al. (2019) are from the KAIT telescope (Filippenko et al. 2001) with a limiting magnitude of 19.5 mag, which allows Liodakis et al. (2019) to detect fainter optical flares which presumably leads to more 'orphan' optical flares. Liodakis et al. (2018a) also found that 'orphan' optical flares in their sample have lower amplitudes and are likely random fluctuations, not real flares. Note also, if we remove all the 'orphan' optical flares in the blazars with $m_g > 18.5$ mag, our 'orphan' optical flare fraction decreases to 12 per cent (from 191 to 153).

We also estimate the 'orphan' flare fraction for each blazar class. We obtained a similar optical 'orphan' flare number for the two classes (91/91) but we see a different rates of 'orphan' γ-ray flares (85/18) for the FSRQ/B LLac classes. Given the number of FSRQs (220) and BL Lacs (160) in our sample (+41 BCU), we find more 'orphan' γ-ray flares among the FSRQs than among the BL Lacs: 0.38/0.11 'orphan' γ-ray flare per object for FSRQ/BL Lac classes. However, we obtain more 'orphan' optical flares in BL

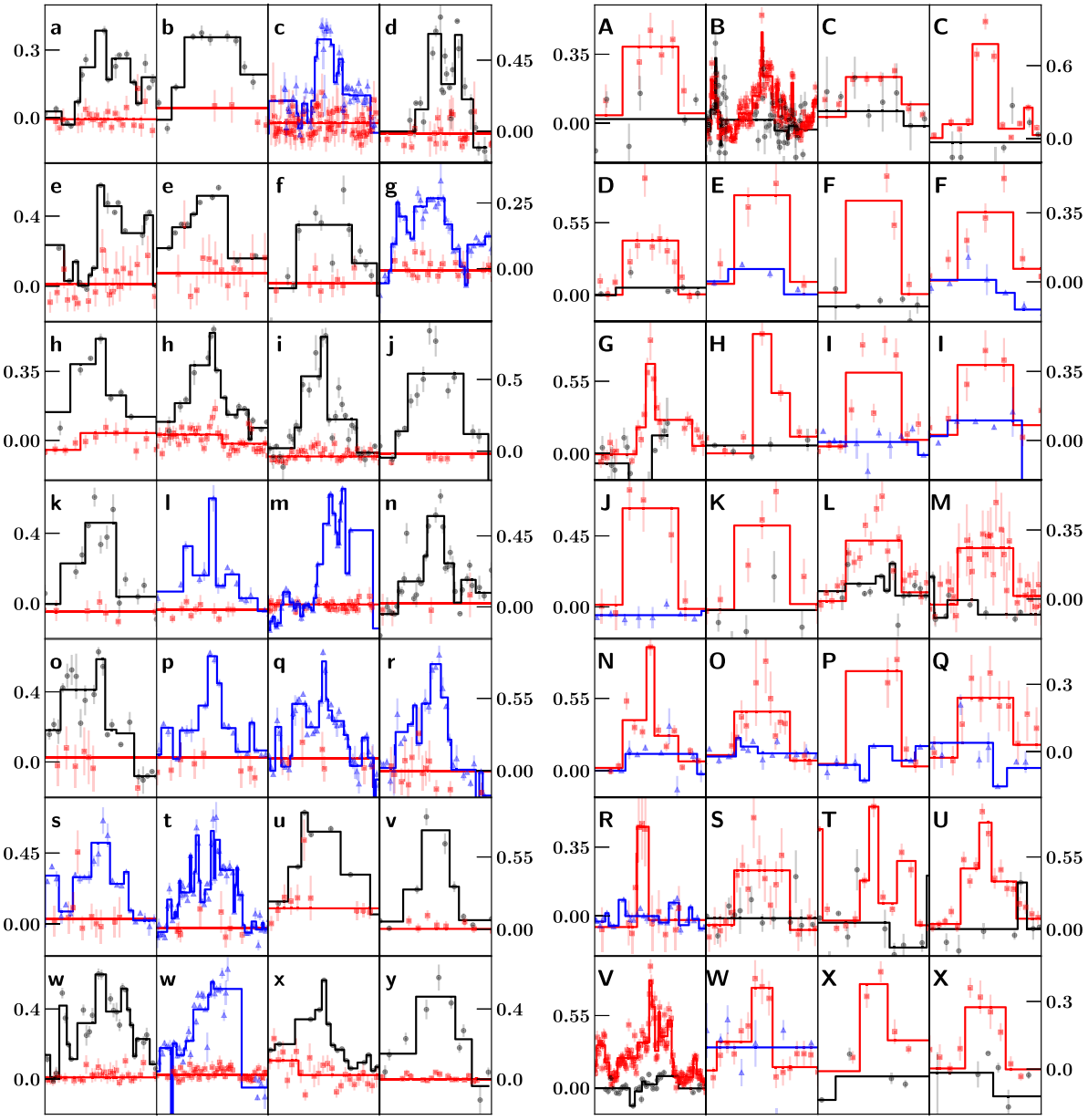

(a) optical "orphan" flares (b) γ-ray "orphan" flares

Figure 7. Gold sample of optical (left-hand panel) and γ-ray (right-hand panel) 'orphan' flares. The black dots, blue triangles, and red squares are optical V, optical g, and γ-ray fluxes, respectively. The letter in each panel corresponds to the blazar name in Table B1.

Lacs than FSRQs: 0.41/0.57 'orphan' optical flare per object for FSRQ/BL Lac classes. The presence of 'orphan' flares argues for multizone synchrotron sites or a hadronic origin for some blazar flares. However, as suggested by Liodakis et al. (2019), the small orphan γ-ray flare fraction favours a single-zone leptonic mechanism for the high-energy emission in most blazars.

4.4 Fractional variability

We use the fractional variability to characterize the average variability of the blazars (Vaughan et al. 2003). It is defined as

$$F_{\rm var} = \sqrt{\frac{S^2 - \langle \sigma_{\rm err}^2 \rangle}{\langle F \rangle^2}}, \qquad (2)$$

where $S^2 = (N-1)^{-1} \sum_{i=1}^{N} (F_i - < F >)^2$ is the variance, $<F>$ is the mean flux, and $< \sigma_{\rm err}^2 >$ is the mean square uncertainty. First, we compare the variability properties using the whole light curves. We measure the variability for 166 objects among the 175 with flares in both bands (for 9 blazars S^2 is smaller than $< \sigma_{\rm err}^2 >$). We obtain a mean value and a standard deviation of $F_{\rm var} = 0.60 \pm 0.42$ and $F_{\rm var} = 0.66 \pm 0.34$ for the optical and γ-ray bands, respectively. Even if both bands have a consistent fractional variability, a Kolmogorov–Smirnov test indicates that the fractional variability distributions are not the same ($p = 0.0078$). For the different blazar classes, we find $F_{\rm var} = 0.66 \pm 0.44$ and $F_{\rm var} = 0.73 \pm 0.33$ for FSRQs and the optical and γ-ray bands, respectively and $F_{\rm var} = 0.45 \pm 0.27$ and $F_{\rm var} = 0.49 \pm 0.25$ for BL Lacs. For the γ-ray band and FSRQs, our fractional variability

values are higher but consistent with the value of 0.55 ± 0.33 found by Rajput, Stalin & Rakshit (2020). We also find that the FSRQ class has a higher fractional variability than the BL Lac class in both the γ-ray and optical. A Kolmogorov–Smirnov test shows that FSRQ and BL Lac distributions are not from the same distribution at 95 per cent confidence with statistics of 0.39/0.34 and a p-value of 0.00006/0.0008 (for γ-ray/optical).

Finally, because $F_{\rm var}$ is sensitive to the photometric uncertainties, we checked our analysis by doubling the uncertainties of both bands. We find different values for $F_{\rm var}$ but the FSRQs still have larger variability in both bands (Opt: FSRQs: 0.63 ± 0.45, BL Lacs: 0.55 ± 0.24; γ-ray FSRQs: 0.79 ± 0.35, BL Lacs: 0.65 ± 0.27).

5 CONCLUSIONS

Using blazar light curves from the optical All-Sky Automated Survey for Supernovae and the γ-ray *Fermi*-LAT telescope, we performed the most extensive statistical correlation study between both bands to date for a sample of 1180 blazars. This is almost an order of magnitude larger than other recent studies (Cohen et al. 2014; Liodakis et al. 2019). We decompose both light curves into histograms using the Bayesian Block Decomposition method. Then, we select only the prominent flares to study the time delays and the relative rates of 'orphan' flares. Of the 1180 blazars, 421 objects have at least one flare and 133 sources have at least one correlated flare within a 30-d window. Our six main conclusions are:

(i) Based on the 143 sources with correlated flares, the time lag distribution between both bands is consistent with no lags (16th, 50th, and 84th percentiles of −8.5, 1.1, and 7.1 d).

(ii) We do not find differences in the time lags for different blazar classes. Both distributions are consistent, with median value of $0.9^{+6.3}_{-8.0}$ and $1.5^{+8.2}_{-10.9}$ d for our 100 FSRQs and 30 BL Lacs, respectively.

(iii) In the 421 blazars with flares, we detect $\sim$ 1400 optical and 500 γ-ray flares. The exact numbers are sensitive to parameter choices but FSRQs tend to exhibit more γ-ray flares per source than the BL Lacs while BL Lacs have more optical flares than FSRQs.

(iv) We measure a median amplitude ratio between optical and γ-ray flares of $A_{\rm opt}/A_{\gamma} = 1.3^{+1.6}_{-1.2}$.

(v) We search for good example of 'orphan' flares and found a total of 306 'orphan' flares: 191 'orphan' optical flares and 115 'orphan' γ-ray flares. These represent $\sim$13 per cent of optical and $\sim$22 per cent of γ-ray flares. We find more 'orphan' γ-ray flares in FSRQs than BL Lacs but, more 'orphan' optical flares in BL Lacs than FSRQs.

(vi) We compare the variability properties in the optical and γ-ray bands. Both bands have a consistent fractional variability amplitude, but FSRQs have higher a fractional variability in both the γ-ray and optical than BL Lacs.

Our work rules out the hadronic proton–synchrotron model and supports the leptonic single-zone models where the low and high-energy emissions come from the same population of electrons as the dominant driver of blazar flares. However, the presence of 'orphan' flares in some blazars argues for the occasional presence of a more complex emission mechanism, such as multizone synchrotron models or another hadronic models for some flares.

Even if we performed the largest statistical study and independently confirmed previous work with a smaller sample, our work does not help distinguishing between SSC or EC models. The main reason is the signal-to-noise ratio of our optical light curves due to the limiting magnitude of ASAS-SN. However, it has been shown in the literature that the distinction between different models is doable for individual well-studied blazar. For this reason, to put better constraints on the models and derive more precise time delays, instead of increasing the sample size, we need to obtain optical light curves with a better signal-to-noise ratio.

ACKNOWLEDGEMENTS

We thank the referee for the comments on the manuscript. We thank Las Cumbres Observatory and its staff for their continued support of ASAS-SN. ASAS-SN is funded in part by the Gordon and Betty Moore Foundation through grants GBMF5490 and GBMF10501 to the Ohio State University, and also funded in part by the Alfred P. Sloan Foundation grant G-2021-14192.

TdJ thanks Colby Haggerty for discussions and Jedidah Isler for useful discussions in the early stages of this work. Support for TdJ has been provided by NSF grants AST-1908952 and AST-1911074. BJS is supported by NSF grants AST-1907570, AST-1908952, AST-1920392, and AST-1911074. CSK and KZS are supported by NSF grants AST-1814440 and AST-1908570. AF acknowledges funding from the German Science Foundation DFG, via the Collaborative Research Center SFB1491 'Cosmic Interacting Matters – From Source to Signal'. Support for TW-SH was provided by NASA through the NASA Hubble Fellowship grant HST-HF2-51458.001-A awarded by the Space Telescope Science Institute, which is operated by the Association of Universities for Research in Astronomy, Inc., for NASA, under contract NAS5-265. JFB is supported by National Science Foundation grant No. PHY-2012955.

This work is based on observations made by ASAS-SN. We wish to extend our special thanks to those of Hawaiian ancestry on whose sacred mountains of Maunakea and Haleakalā, we are privileged to be guests. Without their generous hospitality, the observations presented herein would not have been possible.

Facilities: Fermi-LAT telescope, Haleakala Observatories (USA), Cerro Tololo International Observatory (Chile), McDonald Observatory (USA), South African Astrophysical Observatory (South Africa).

Software: ASTROPY (Astropy Collaboration 2013), MATPLOTLIB (Hunter 2007), NUMPY (Harris et al. 2020), SCIPY (Virtanen et al. 2020), Z-transformed discrete correlation function (Alexander 1997, 2013)

DATA AVAILABILITY STATEMENTS

The optical and γ-ray light curves have already been made available to the community. γ-ray light curves can be downloaded from https://fermi.gsfc.nasa.gov/ssc/data/access/lat/LightCurveRepository/source.html? while optical light-curves from ASAS-SN can be obtained via their ASAS-SN sky patrol webpage (https://asas-sn.osu.edu/). All the data sets used in this work will be also available on the author's Github (https://github.com/tdejaeger).

REFERENCES

Abdo A. A. et al., 2009, ApJS, 183, 46
Abdo A. A. et al., 2010, ApJ, 716, 30
Abdollahi S. et al., 2020, ApJS, 247, 33
Abdollahi S. et al., 2022, ApJS, 260, 53
Acero F. et al., 2015, ApJS, 218, 23
Adams C. B. et al., 2022, ApJ, 924, 95
Aharonian F. A., 2000, New Astron., 5, 377
Aharonian F. et al., 2007, ApJ, 664, L71

Alard C., 2000, A&AS, 144, 363
Alard C., Lupton R. H., 1998, ApJ, 503, 325
Albert J. et al., 2007, ApJ, 669, 862
Alexander T., 1997, in Maoz D., Sternberg A., Leibowitz E. M., eds, Astrophysics and Space Science Library Vol. 218, Astronomical Time Series. Springer, Berlin, p. 163
Alexander T., 2013, preprint (arXiv:1302.1508)
Antonucci R., 1993, ARA&A, 31, 473
Arbeiter C., Pohl M., Schlickeiser R., 2005, ApJ, 627, 62
Astropy Collaboration 2013, A&A, 558, A33
Atwood W. B. et al., 2009, ApJ, 697, 1071
Ballet J., Burnett T. H., Digel S. W., Lott B., 2020, preprint (arXiv:2005.11208)
Banasiński P., Bednarek W., Sitarek J., 2016, MNRAS, 463, L26
Bellm E. C. et al., 2019, PASP, 131, 018002
Bhatta G., 2021, ApJ, 923, 7
Blandford R. D., Ostriker J. P., 1978, ApJ, 221, L29
Błażejowski M., Sikora M., Moderski R., Madejski G. M., 2000, ApJ, 545, 107
BłażejowskiM. et al., 2005, ApJ, 630, 130
Bloom S. D., Marscher A. P., 1996, ApJ, 461, 657
Boettcher M., Mause H., Schlickeiser R., 1997, A&A, 324, 395
Bonning E. et al., 2012, ApJ, 756, 13
Bonnoli G., Ghisellini G., Foschini L., Tavecchio F., Ghirlanda G., 2011, MNRAS, 410, 368
Böttcher M., 2005, ApJ, 621, 176
Böttcher M., 2019, Galaxies, 7, 20
Böttcher M., Reimer A., Sweeney K., Prakash A., 2013, ApJ, 768, 54
Cerruti M., Zech A., Boisson C., Emery G., Inoue S., Lenain J. P., 2019, MNRAS, 483, L12
Chatterjee R. et al., 2008, ApJ, 689, 79
Chatterjee R. et al., 2012, ApJ, 749, 191
Chiang J., Böttcher M., 2002, ApJ, 564, 92
Cohen D. P., Romani R. W., Filippenko A. V., Cenko S. B., Lott B., Zheng W., Li W., 2014, ApJ, 797, 137
Costamante L., Ghisellini G., 2002, A&A, 384, 56
de Jaeger T. et al., 2022, MNRAS, 509, 3427
Dermer C. D., Schlickeiser R., 1993, ApJ, 416, 458
Dermer C. D., Finke J. D., Krug H., Böttcher M., 2009, ApJ, 692, 32
Edelson R. A., Krolik J. H., 1988, ApJ, 333, 646
Eisenstein D. J., Hut P., 1998, ApJ, 498, 137
Filippenko A. V., Li W. D., Treffers R. R., Modjaz M., 2001, in Paczynski B., Chen W.-P., Lemme C., eds, ASP Conf. Ser. Vol. 246, IAU Colloq. 183: Small Telescope Astronomy on Global Scales. Astron. Soc. Pac., San Francisco, p. 121
Fossati G., Maraschi L., Celotti A., Comastri A., Ghisellini G., 1998, MNRAS, 299, 433
Gao S., Pohl M., Winter W., 2017, ApJ, 843, 109
Gao S., Fedynitch A., Winter W., Pohl M., 2019, Nat. Astron., 3, 88
Ghisellini G., Madau P., 1996, MNRAS, 280, 67
Ghisellini G., Maraschi L., 1989, ApJ, 340, 181
Ghisellini G., Celotti A., Fossati G., Maraschi L., Comastri A., 1998, MNRAS, 301, 451
Ghisellini G., Tavecchio F., Foschini L., Ghirlanda G., 2011, MNRAS, 414, 2674
Ghisellini G., Tavecchio F., Foschini L., Sbarrato T., Ghirlanda G., Maraschi L., 2012, MNRAS, 425, 1371
Harris C. R. et al., 2020, Nature, 585, 357
Hovatta T. et al., 2014, MNRAS, 439, 690
Hunter J. D., 2007, Comput. Sci. Eng., 9, 90
IceCube Collaboration 2018, Science, 361, 147
Impey C. D., Neugebauer G., 1988, AJ, 95, 307
Janiak M., Sikora M., Nalewajko K., Moderski R., Madejski G. M., 2012, ApJ, 760, 129
Jorstad S. G. et al., 2010, ApJ, 715, 362
Joshi M., Marscher A., Böttcher M., 2016, Galaxies, 4, 45
Keivani A. et al., 2018, ApJ, 864, 84
Kelner S. R., Aharonian F. A., Bugayov V. V., 2006, Phys. Rev. D, 74, 034018
Kochanek C. S. et al., 2017, PASP, 129, 104502
Krawczynski H. et al., 2004, ApJ, 601, 151
Liodakis I., Petropoulou M., 2020, ApJ, 893, L20
Liodakis I., Romani R. W., Filippenko A. V., Kiehlmann S., Max-Moerbeck W., Readhead A. C. S., Zheng W., 2018a, MNRAS, 480, 5517
Liodakis I., Hovatta T., Huppenkothen D., Kiehlmann S., Max-Moerbeck W., Readhead A. C. S., 2018b, ApJ, 866, 137
Liodakis I., Romani R. W., Filippenko A. V., Kocevski D., Zheng W., 2019, ApJ, 880, 32
MacDonald N. R., Marscher A. P., Jorstad S. G., Joshi M., 2015, ApJ, 804, 111
Madejski G. G., Sikora M., 2016, ARA&A, 54, 725
Mannheim K., 1993, A&A, 269, 67
Maraschi L., Ghisellini G., Celotti A., 1992, ApJ, 397, L5
Marscher A. P., Gear W. K., 1985, ApJ, 298, 114
Marscher A. P. et al., 2008, Nature, 452, 966
Marscher A. P. et al., 2010, preprint (arXiv:1002.0806)
Mastichiadis A., Kirk J. G., 1997, A&A, 320, 19
Mastichiadis A., Petropoulou M., 2021, ApJ, 906, 131
Mastichiadis A., Petropoulou M., Dimitrakoudis S., 2013, MNRAS, 434, 2684
Meyer M., Scargle J. D., Blandford R. D., 2019, ApJ, 877, 39
Mücke A., Protheroe R. J., 2001, Astropart. Phys., 15, 121
Mücke A., Protheroe R. J., Engel R., Rachen J. P., Stanev T., 2003, Astropart. Phys., 18, 593
Nalewajko K., 2013, MNRAS, 430, 1324
Padovani P., Giommi P., 1995, ApJ, 444, 567
Punch M. et al., 1992, Nature, 358, 477
Rajput B., Stalin C. S., Rakshit S., 2020, A&A, 634, A80
Rodrigues X., Gao S., Fedynitch A., Palladino A., Winter W., 2019, ApJ, 874, L29
Roy N., Chatterjee R., Joshi M., Ghosh A., 2019, MNRAS, 482, 743
Scargle J. D., 1998, ApJ, 504, 405
Scargle J. D., Norris J. P., Jackson B., Chiang J., 2013, ApJ, 764, 167
Shappee B. J. et al., 2014, ApJ, 788, 48
Sikora M., Begelman M. C., Rees M. J., 1994, ApJ, 421, 153
Sokolov A., Marscher A. P., McHardy I. M., 2004, ApJ, 613, 725
Stathopoulos S. I., Petropoulou M., Giommi P., Vasilopoulos G., Padovani P., Mastichiadis A., 2022, MNRAS, 510, 4063
Stickel M., Padovani P., Urry C. M., Fried J. W., Kuehr H., 1991, ApJ, 374, 431
Urry C. M., Mushotzky R. F., 1982, ApJ, 253, 38
Urry C. M., Padovani P., 1995, PASP, 107, 803
Urry C. M. et al., 1997, ApJ, 486, 799
Valtaoja E., Lähteenmäki A., Teräsranta H., Lainela M., 1999, ApJS, 120, 95
Vaughan S., Edelson R., Warwick R. S., Uttley P., 2003, MNRAS, 345, 1271
Virtanen P. et al., 2020, Nat. Methods, 17, 261
Wagner S. M. et al., 2022, in Proceeding of Science 37th International Cosmic Ray Conference. 12-23 July 2021. ICRC, Berlin, p. 868
Wang Z.-R., Liu R.-Y., Petropoulou M., Oikonomou F., Xue R., Wang X.-Y., 2022, Phys. Rev. D, 105, 023005
Williamson K. E. et al., 2014, ApJ, 789, 135

APPENDIX A: PROPERTIES OF BLAZARS USED IN OUR SAMPLE

In this appendix, we list relevant information from Abdollahi et al. (2022) and Ballet et al. (2020) of our blazar sample together with the results obtained in Section 4.

Table A1. Blazar properties.

4FGL Name	RA deg	Dec deg	Association	Class	SED class	redshift	Flares	Lags days
J0001.2-0747	0.315100	−7.797100	PMN J0001-0746	BL Lac	LSP	···	opt	···
J0001.5+2113	0.381500	21.218300	TXS 2358+209	FSRQ	ISP	1.106	both	0.25 (4.64)
J0003.3-1928	0.846500	−19.467600	PKS 0000-197	BCU	LSP	···	none	···
J0004.3+4614	1.075700	46.242699	MG4 J000421+4615	FSRQ	LSP	1.810	none	···
J0004.4-4737	1.109100	−47.623299	PKS 0002-478	FSRQ	LSP	0.880	none	···
J0005.9+3824	1.498600	38.401001	S4 0003+38	FSRQ	LSP	0.229	none	···
J0007.7+4008	1.927500	40.133999	NVSS J000741+400830	BCU	···	···	none	···
J0009.3+5030	2.346600	50.511501	NVSS J000922+503028	BL Lac	HSP	···	none	···
J0010.6+2043	2.650200	20.733200	TXS 0007+205	FSRQ	LSP	0.600	none	···
J0010.6-3025	2.667500	−30.425800	PKS 0008-307	FSRQ	LSP	1.190	none	···
J0011.4+0057	2.855100	0.964600	RX J0011.5+0058	FSRQ	LSP	1.492	gam	···
J0014.1+1910	3.536800	19.171301	MG3 J001356+1910	BL Lac	LSP	0.477	none	···
J0014.9+3212	3.726800	32.216202	3C 6	BCU	LSP	···	none	···
J0016.2-0016	4.061000	−0.280600	S3 0013-00	FSRQ	LSP	1.576	none	···
J0017.0-0649	4.263500	−6.831700	PMN J0017-0650	BCU	LSP	···	none	···
J0017.5-0514	4.394900	−5.234700	PMN J0017-0512	FSRQ	LSP	0.227	both	16.38 (26.92)
J0019.2-5640	4.810600	−56.682598	PMN J0019-5641	BCU	LSP	···	none	···
J0019.6+7327	4.903100	73.456001	S5 0016+73	FSRQ	LSP	1.781	both	999.90 (999.90)
J0021.5-2552	5.391200	−25.868099	CRATES J002132.55-255049.3	BL Lac	ISP	···	opt	···
J0021.9-5140	5.498500	−51.672798	1RXS J002159.2-514028	BL Lac	ISP	0.250	opt	···
J0022.5+0608	5.637600	6.134300	PKS 0019+058	BL Lac	LSP	···	both	999.90 (999.90)
J0023.7-6820	5.934700	−68.338097	PKS 0021-686	FSRQ	LSP	0.354	none	···
J0024.4+4647	6.121200	46.797001	B3 0021+464	BCU	···	···	none	···
J0024.7+0349	6.197500	3.832100	GB6 J0024+0349	FSRQ	···	0.545	none	···
J0025.7-4801	6.435100	−48.019100	SUMSS J002545-480356	BCU	LSP	···	none	···
J0028.4+2001	7.126200	20.017000	TXS 0025+197	FSRQ	LSP	1.552	both	−5.19 (12.89)
J0029.0-7044	7.250900	−70.741402	PKS 0026-710	BL Lac	LSP	···	none	···
J0030.2-1647	7.564300	−16.797501	2MASS J00302045-1647130	BL Lac	HSP	0.237	none	···
J0030.3-4224	7.595800	−42.412701	PKS 0027-426	FSRQ	LSP	0.495	both	0.78 (29.93)
J0030.6-0212	7.655800	−2.201400	PKS B0027-024	FSRQ	LSP	1.804	both	999.90 (999.90)
J0032.3-5522	8.077800	−55.366798	SUMSS J003210-552228	BCU	···	···	none	···
J0033.5-1921	8.395400	−19.359301	KUV 00311-1938	BL Lac	HSP	0.610	none	···
J0033.9+3858	8.483000	38.971600	MG3 J003408+3901	BCU	LSP	···	opt	···
J0034.0-4116	8.514200	−41.270802	PKS 0031-415	BCU	LSP	···	none	···
J0035.2+1514	8.812300	15.240500	RX J0035.2+1515	BL Lac	ISP	1.090	none	···
J0035.9+5950	8.982300	59.833401	1ES 0033+595	BL Lac	HSP	···	none	···
J0036.9+1832	9.234000	18.542400	CRATES J003659.39+183203.7	BCU	···	1.595	gam	···
J0037.8+1239	9.469500	12.652700	NVSS J003750+123818	BL Lac	HSP	0.089	none	···
J0038.2-2459	9.558900	−24.994101	PKS 0035-252	FSRQ	LSP	1.196	both	0.22 (9.16)
J0039.1+4330	9.799400	43.512199	NVSS J003907+433015	BCU	ISP	···	opt	···
J0043.8+3425	10.971700	34.431599	GB6 J0043+3426	FSRQ	LSP	0.966	none	···
J0044.2-8424	11.071100	−84.401604	PKS 0044-84	FSRQ	LSP	1.032	none	···
J0045.1-3706	11.293600	−37.106499	PKS 0042-373	FSRQ	LSP	···	none	···
J0045.3+2128	11.339600	21.466801	GB6 J0045+2127	BL Lac	HSP	···	none	···
J0045.7+1217	11.430900	12.292000	GB6 J0045+1217	BL Lac	···	···	none	···
J0047.0+5657	11.753500	56.960098	GB6 J0047+5657	BL Lac	LSP	0.747	none	···
J0047.9+2233	11.998100	22.563200	GB6 J0048+2234	FSRQ	LSP	1.161	opt	···
J0047.9+3947	11.976300	39.797501	B3 0045+395	BL Lac	···	0.252	none	···
J0049.7+0237	12.437700	2.627300	PKS 0047+023	BL Lac	LSP	1.474	none	···
J0050.4-0452	12.612100	−4.880600	PKS 0047-051	FSRQ	LSP	0.920	both	8.79 (21.13)
J0050.7-0929	12.675300	−9.493600	PKS 0048-09	BL Lac	ISP	0.635	opt	···
J0051.1-0648	12.782400	−6.809600	PKS 0048-071	FSRQ	LSP	1.975	none	···
J0051.2-6242	12.824300	−62.703701	1RXS J005117.7-624154	BL Lac	HSP	0.300	none	···
J0055.1-1219	13.780500	−12.320400	TXS 0052-125	BCU	LSP	···	none	···
J0056.3-0935	14.087400	−9.599700	TXS 0053-098	BL Lac	ISP	0.103	none	···
J0056.4-2118	14.120400	−21.302900	PMN J0056-2117	BL Lac	ISP	···	opt	···
J0056.6-5317	14.159100	−53.295601	CRATES J005630.93-531931.5	BCU	ISP	···	none	···
J0058.0-0539	14.510800	−5.655000	PKS 0055-059	FSRQ	LSP	1.246	none	···
J0058.0-3233	14.513200	−32.565800	PKS 0055-328	BL Lac	LSP	···	none	···
J0058.4+3315	14.610100	33.250500	MG3 J005830+3311	FSRQ	LSP	1.369	none	···
J0100.3+0745	15.093200	7.764700	GB6 J0100+0745	BL Lac	ISP	···	none	···
J0102.4+4214	15.606900	42.237099	GB6 J0102+4214	FSRQ	LSP	0.874	none	···

Table A1 – *continued*

4FGL Name	RA deg	Dec deg	Association	Class	SED class	redshift	Flares	Lags days
J0102.8+5824	15.701000	58.409199	TXS 0059+581	FSRQ	LSP	0.644	opt	···
J0103.5+5337	15.878700	53.626202	RX J0103.3+5337	BL Lac	···	···	none	···
J0103.8+1321	15.969000	13.353600	NVSS J010345+132346	BL Lac	···	0.490	none	···
J0104.8-2416	16.214600	−24.280800	PKS 0102-245	FSRQ	LSP	1.747	none	···
J0105.1+3929	16.291300	39.496300	GB6 J0105+3928	BL Lac	LSP	0.440	opt	···
J0107.4+0334	16.850800	3.569100	PMN J0107+0333	BL Lac	LSP	···	none	···
J0108.6+0134	17.169500	1.581900	4C +01.02	FSRQ	LSP	2.099	both	3.99 (23.06)
J0109.7+6133	17.445000	61.561501	TXS 0106+612	FSRQ	LSP	0.783	gam	···
J0112.0-6634	18.023600	−66.575203	PKS 0110-668	FSRQ	LSP	1.189	none	···
J0112.1+2245	18.029400	22.751499	S2 0109+22	BL Lac	LSP	0.265	both	7.53 (19.94)
J0112.8+3208	18.222700	32.139900	4C +31.03	FSRQ	LSP	0.603	both	−2.40 (6.93)
J0113.1-3553	18.289301	−35.894001	PMN J0113-3551	FSRQ	LSP	1.220	none	···
J0113.4+4948	18.368200	49.805401	S4 0110+49	FSRQ	LSP	0.389	both	−8.96 (40.15)
J0114.0+6418	18.515100	64.304001	GB6 J0113+6416	BCU	ISP	···	none	···
J0114.8+1326	18.711901	13.434200	GB6 J0114+1325	BL Lac	ISP	0.583	opt	···
J0115.1+2622	18.778400	26.373301	1RXS J011451.8+262337	BCU	ISP	···	none	···
J0115.1-0129	18.785900	−1.496200	PKS 0112-017	FSRQ	LSP	1.365	none	···
J0115.8+2519	18.953899	25.332399	RX J0115.7+2519	BL Lac	HSP	0.358	opt	···
J0116.0-1136	19.000601	−11.606000	PKS 0113-118	FSRQ	LSP	0.670	opt	···
J0117.8-2109	19.454300	−21.157801	PKS 0115-214	FSRQ	LSP	1.490	none	···
J0118.7-0848	19.688400	−8.808000	AT20G J011844-085058	BCU	LSP	···	none	···
J0118.9-2141	19.725401	−21.694799	PKS 0116-219	FSRQ	LSP	1.165	both	0.92 (21.47)
J0120.4-2701	20.122700	−27.022900	PKS 0118-272	BL Lac	ISP	···	none	···
J0124.8-0625	21.217800	−6.432800	PMN J0124-0624	BL Lac	LSP	2.117	none	···
J0125.3-2548	21.347401	−25.807400	PKS 0122-260	BL Lac	LSP	···	none	···
J0126.0-2221	21.520399	−22.361000	PKS 0123-226	FSRQ	LSP	0.720	none	···
J0127.2+0324	21.823700	3.413000	NVSS J012713+032259	BL Lac	HSP	···	none	···
J0128.5+4440	22.143801	44.677700	GB6 J0128+4439	FSRQ	LSP	0.228	none	···
J0131.1+6120	22.792400	61.337200	RX J0131.0+6120	BL Lac	HSP	···	none	···
J0132.7-1654	23.176001	−16.910299	PKS 0130-17	FSRQ	LSP	1.020	both	5.32 (51.68)
J0133.1-5201	23.293800	−52.020199	PKS 0131-522	FSRQ	LSP	0.925	both	20.39 (3.84)
J0134.3-3842	23.588699	−38.708500	PMN J0134-3843	FSRQ	LSP	2.140	none	···
J0137.0+4751	24.260300	47.863701	OC 457	FSRQ	LSP	0.859	both	2.22 (9.45)
J0137.6-2430	24.406900	−24.516300	PKS 0135-247	FSRQ	LSP	0.835	opt	···
J0137.9+5814	24.495701	58.249401	TXS 0134+579	BL Lac	HSP	···	none	···
J0138.0+2247	24.506300	22.796200	GB6 J0138+2248	BL Lac	HSP	···	none	···
J0140.6+8736	25.168800	87.606201	WN B0126.6+8722	BCU	LSP	···	none	···
J0141.4-0928	25.362600	−9.482500	PKS 0139-09	BL Lac	LSP	0.730	both	9.97 (33.89)
J0143.1-3622	25.785601	−36.367401	PMN J0143-3623	BCU	LSP	···	gam	···
J0143.7-5846	25.948000	−58.771801	SUMSS J014347-584550	BL Lac	HSP	···	opt	···
J0144.6+2705	26.150200	27.089899	TXS 0141+268	BL Lac	LSP	···	none	···
J0145.0-2732	26.258499	−27.536301	PKS 0142-278	FSRQ	LSP	1.148	none	···
J0146.0-6746	26.518200	−67.774803	SUMSS J014554-674646	BL Lac	ISP	···	none	···
J0152.2+2206	28.072701	22.113300	PKS 0149+21	FSRQ	LSP	1.320	opt	···
J0152.2+3714	28.063101	37.234100	B2 0149+37	BCU	LSP	0.761	none	···
J0152.6+0147	28.161400	1.789400	PMN J0152+0146	BL Lac	HSP	0.080	opt	···
J0153.9+0823	28.497200	8.393100	GB6 J0154+0823	BL Lac	ISP	0.681	none	···
J0156.5+3914	29.132500	39.249298	MG4 J015630+3913	FSRQ	LSP	···	none	···
J0156.9-5301	29.232800	−53.030800	1RXS J015658.6-530208	BL Lac	HSP	···	none	···
J0157.7-4614	29.435301	−46.243099	PMN J0157-4614	FSRQ	LSP	2.287	none	···
J0158.5-3932	29.646000	−39.535801	PMN J0158-3932	BL Lac	ISP	···	none	···
J0159.5+1046	29.885799	10.773700	RX J0159.5+1047	BL Lac	HSP	0.195	none	···
J0200.6-6637	30.159901	−66.625999	PMN J0201-6638	FSRQ	LSP	···	none	···
J0202.7+4204	30.686199	42.071400	B3 0159+418	BL Lac	LSP	···	opt	···
J0203.6+7233	30.911400	72.553001	S5 0159+723	BL Lac	LSP	···	none	···
J0203.7+3042	30.932699	30.713900	NVSS J020344+304238	BL Lac	LSP	0.761	opt	···
J0204.8+1513	31.218201	15.232600	4C +15.05	BCU	LSP	0.833	none	···
J0205.0-1700	31.263700	−17.002199	PKS 0202-17	FSRQ	LSP	1.740	both	4.83 (17.01)
J0205.2+3212	31.308901	32.202999	B2 0202+31	FSRQ	LSP	1.466	gam	···
J0206.4-1151	31.601801	−11.857600	PMN J0206-1150	FSRQ	LSP	1.663	both	10.29 (23.41)
J0207.5-2402	31.898899	−24.048401	NVSS J020733-240202	BCU	···	···	none	···
J0209.9+7229	32.497898	72.487701	S5 0205+722	BL Lac	LSP	0.895	none	···
J0210.7-5101	32.694599	−51.021801	PKS 0208-512	FSRQ	LSP	1.003	both	5.93 (29.36)

Table A1 – *continued*

4FGL Name	RA deg	Dec deg	Association	Class	SED class	redshift	Flares	Lags days
J0211.2+1051	32.809101	10.856900	MG1 J021114+1051	BL Lac	ISP	0.200	both	5.05 (12.75)
J0212.9+2244	33.242699	22.746599	MG3 J021252+2246	BL Lac	ISP	0.459	none	···
J0214.4-5822	33.602402	−58.369801	PMN J0214-5822	BCU	···	···	none	···
J0216.6-1015	34.165298	−10.266200	PMN J0216-1017	BCU	LSP	···	both	999.90 (999.90)
J0216.8-6635	34.216801	−66.589699	RBS 0300	BL Lac	HSP	0.330	none	···
J0217.2+0837	34.316299	8.623400	ZS 0214+083	BL Lac	LSP	0.085	opt	···
J0217.4+7352	34.353298	73.880402	S5 0212+73	FSRQ	LSP	2.367	none	···
J0217.8+0144	34.462101	1.734600	PKS 0215+015	FSRQ	LSP	1.715	opt	···
J0218.9+3643	34.747299	36.717602	MG3 J021846+3641	BCU	···	···	gam	···
J0221.1+3556	35.280998	35.935902	B2 0218+357	FSRQ	LSP	0.944	gam	···
J0221.5+2513	35.380901	25.230499	2MASS J02212698+2514338	BL Lac	ISP	0.482	none	···
J0222.0-1616	35.519699	−16.278700	PKS 0219-164	FSRQ	LSP	0.698	both	4.57 (9.12)
J0222.6+4302	35.669601	43.035702	3C 66A	BL Lac	ISP	0.444	both	999.90 (999.90)
J0224.2+0700	36.057701	7.012600	PKS 0221+067	FSRQ	LSP	0.511	opt	···
J0225.1-2604	36.282902	−26.077400	PMN J0225-2603	BCU	LSP	···	opt	···
J0226.5+0938	36.631302	9.635100	NVSS J022634+093843	FSRQ	LSP	2.605	none	···
J0226.5-4441	36.648102	−44.685902	RBS 0318	BL Lac	HSP	···	none	···
J0227.8+2246	36.954399	22.777500	NVSS J022744+224834	BCU	LSP	0.428	none	···
J0229.5-3644	37.387699	−36.738800	PKS 0227-369	FSRQ	LSP	2.115	both	15.99 (9.05)
J0230.8+4032	37.708599	40.541599	B3 0227+403	FSRQ	LSP	1.019	gam	···
J0231.2-4745	37.820900	−47.765400	PMN J0231-4746	FSRQ	LSP	0.765	both	−2.05 (8.87)
J0231.8+1322	37.961601	13.369200	4C +13.14	FSRQ	LSP	2.065	none	···
J0236.8-6136	39.202099	−61.610600	PKS 0235-618	FSRQ	LSP	0.467	opt	···
J0237.6-3602	39.424400	−36.042198	RBS 0334	BL Lac	HSP	0.411	none	···
J0237.8+2848	39.473701	28.804399	4C +28.07	FSRQ	LSP	1.206	both	8.18 (23.08)
J0238.1-3905	39.529900	−39.087399	1RXS J023800.5-390505	BL Lac	HSP	0.200	none	···
J0238.2+1531	39.561699	15.517500	CRATES J023819+153323	BCU	LSP	···	gam	···
J0238.4-3116	39.620899	−31.282801	1RXS J023832.6-311658	BL Lac	HSP	0.232	opt	···
J0238.6+1637	39.667999	16.617901	PKS 0235+164	BL Lac	LSP	0.940	both	1.74 (25.23)
J0239.5+1326	39.884701	13.436600	GB6 J0239+1327	BCU	···	···	none	···
J0239.7+0415	39.940300	4.264300	PKS 0237+040	FSRQ	LSP	0.978	none	···
J0243.4+7119	40.867901	71.324898	S5 0238+711	BL Lac	LSP	···	none	···
J0244.6-5819	41.157600	−58.325600	RBS 0351	BL Lac	HSP	0.265	opt	···
J0244.7+1316	41.192001	13.279900	GB6 J0244+1320	BCU	LSP	···	none	···
J0245.1-0257	41.291401	−2.955000	PMN J0245-0255	BL Lac	LSP	···	none	···
J0245.4+2408	41.354500	24.149799	B2 0242+23	FSRQ	LSP	2.243	none	···
J0245.9-4650	41.496601	−46.846298	PKS 0244-470	FSRQ	LSP	1.385	none	···
J0250.2-8224	42.573200	−82.403702	PMN J0251-8226	BCU	LSP	···	none	···
J0251.5-5958	42.897598	−59.973900	PKS 0250-602	FSRQ	LSP	1.373	opt	···
J0252.8-2219	43.200699	−22.320299	PKS 0250-225	FSRQ	LSP	1.419	gam	···
J0253.5+3216	43.382900	32.282600	MG3 J025334+3217	FSRQ	LSP	0.859	none	···
J0253.9+5103	43.493301	51.063301	TXS 0250+508	FSRQ	LSP	1.732	none	···
J0257.9-1215	44.492001	−12.263700	PMN J0257-1211	FSRQ	LSP	1.391	opt	···
J0258.1+2030	44.542198	20.513700	MG3 J025805+2029	BL Lac	LSP	···	none	···
J0259.4+0746	44.857800	7.783300	PKS 0256+075	FSRQ	LSP	0.893	both	999.90 (999.90)
J0301.6-7155	45.403599	−71.927902	PKS 0301-721	FSRQ	LSP	0.823	both	−5.99 (11.50)
J0303.4-2407	45.862499	−24.122499	PKS 0301-243	BL Lac	HSP	0.266	opt	···
J0303.4-5232	45.870602	−52.534901	AT20G J030328-523433	BCU	LSP	···	none	···
J0303.6+4716	45.909801	47.275902	4C +47.08	BL Lac	LSP	···	opt	···
J0303.6-6211	45.924500	−62.189899	PKS 0302-623	FSRQ	LSP	1.351	both	−1.79 (4.95)
J0304.5+3349	46.137901	33.826099	4C +33.06	BCU	LSP	···	none	···
J0309.0+1029	47.261700	10.492700	PKS 0306+102	FSRQ	LSP	0.863	none	···
J0309.9-6058	47.492100	−60.973301	PKS 0308-611	FSRQ	LSP	1.479	both	9.87 (8.58)
J0310.6-5017	47.654400	−50.290100	1RXS J031036.0-501615	BL Lac	HSP	···	none	···
J0312.8+0134	48.222198	1.572400	PKS 0310+013	FSRQ	LSP	0.664	none	···
J0314.3-5103	48.592899	−51.055000	PMN J0314-5104	BL Lac	LSP	···	none	···
J0315.9-1033	48.992199	−10.552200	PKS 0313-107	FSRQ	LSP	1.565	gam	···
J0316.2+0905	49.058300	9.094600	GB6 J0316+0904	BL Lac	LSP	0.372	none	···
J0318.7+2135	49.694599	21.596800	MG3 J031849+2135	BL Lac	···	···	none	···
J0319.8+1845	49.972198	18.753201	1E 0317.0+1835	BL Lac	HSP	0.190	none	···
J0319.9-3821	49.997501	−38.357700	NVSS J031957-381527	BCU	···	···	none	···
J0325.5-5635	51.379398	−56.591000	1RXS J032521.8-563543	BL Lac	HSP	0.060	opt	···

Table A1 – *continued*

4FGL Name	RA deg	Dec deg	Association	Class	SED class	redshift	Flares	Lags days
J0325.6-1646	51.417900	−16.781000	RBS 0421	BL Lac	HSP	0.291	opt	···
J0325.7+2225	51.442101	22.432600	TXS 0322+222	FSRQ	LSP	2.066	gam	···
J0327.5-1805	51.890701	−18.088499	CRATES J032743.34-180342.0	BCU	···	···	none	···
J0330.6+0438	52.672699	4.634900	GB6 J0330+0439	BCU	LSP	···	none	···
J0331.3-6156	52.843800	−61.936501	PMN J0331-6155	BL Lac	HSP	···	none	···
J0331.9+6307	52.990898	63.130901	GB6 J0331+6307	BL Lac	ISP	···	none	···
J0332.1-1123	53.033501	−11.394900	1RXS J033223.2-111938	FSRQ	LSP	0.207	none	···
J0333.9+6537	53.476700	65.618797	TXS 0329+654	BL Lac	LSP	···	none	···
J0334.2-3725	53.555599	−37.432701	PMN J0334-3725	BL Lac	LSP	···	opt	···
J0334.2-4008	53.556599	−40.145000	PKS 0332-403	BL Lac	LSP	1.445	opt	···
J0335.1-4459	53.784599	−44.991600	SUMSS J033513-445939	BL Lac	HSP	···	none	···
J0336.4+3224	54.101501	32.411098	NRAO 140	FSRQ	LSP	1.259	none	···
J0338.5+1302	54.635502	13.041900	RX J0338.4+1302	BL Lac	HSP	···	none	···
J0338.9-2848	54.744701	−28.800900	NVSS J033859-284619	BCU	···	···	none	···
J0339.5-0146	54.877102	−1.776900	PKS 0336-01	FSRQ	LSP	0.850	both	0.09 (13.39)
J0340.5-2118	55.147701	−21.315800	PKS 0338-214	BL Lac	LSP	0.233	opt	···
J0342.2+3858	55.573002	38.978001	GB6 J0342+3858	FSRQ	LSP	0.945	none	···
J0343.2-2529	55.813599	−25.494301	PKS 0341-256	FSRQ	LSP	1.419	none	···
J0343.2-6444	55.816299	−64.734901	PMN J0343-6442	BL Lac	ISP	···	none	···
J0345.2-2353	56.318699	−23.885000	NVSS J034518-235218	BL Lac	ISP	0.104	none	···
J0347.7-3616	56.946999	−36.280800	PKS 0346-364	BCU	LSP	···	none	···
J0348.5-2749	57.153801	−27.821501	PKS 0346-27	FSRQ	LSP	0.991	both	6.92 (9.73)
J0348.6-1609	57.153198	−16.165400	PKS 0346-163	BL Lac	LSP	···	none	···
J0349.6+2410	57.423000	24.177500	TXS 0346+241	BCU	···	···	opt	···
J0349.8-2103	57.469898	−21.057600	PKS 0347-211	FSRQ	LSP	2.944	none	···
J0350.6-3226	57.659401	−32.447300	PKS 0348-326	BCU	LSP	···	none	···
J0353.0+5654	58.271999	56.902599	GB6 J0353+5654	BL Lac	HSP	···	none	···
J0354.4+4643	58.609001	46.723099	B3 0350+465	BCU	···	···	none	···
J0354.7+8009	58.691898	80.164703	S5 0346+80	BL Lac	LSP	···	none	···
J0354.7-1617	58.677898	−16.287001	PKS 0352-164	FSRQ	LSP	1.187	none	···
J0358.6+0634	59.665600	6.575900	PMN J0358+0629	BCU	LSP	···	none	···
J0358.9+6004	59.732800	60.076698	TXS 0354+599	FSRQ	LSP	0.455	none	···
J0359.6+5057	59.915798	50.959000	NRAO 150	FSRQ	LSP	1.520	gam	···
J0401.7+2112	60.449600	21.200701	TXS 0358+210	FSRQ	LSP	0.834	gam	···
J0401.9-2034	60.486698	−20.580400	PMN J0401-2034	BCU	LSP	···	both	999.90 (999.90)
J0402.0-2616	60.510300	−26.273001	PKS 0359-264	BL Lac	LSP	1.920	none	···
J0403.9-3605	60.974998	−36.087002	PKS 0402-362	FSRQ	LSP	1.417	both	1.20 (16.07)
J0405.6-1308	61.418900	−13.143800	PKS 0403-13	FSRQ	LSP	0.571	gam	···
J0407.0-3826	61.762699	−38.439400	PKS 0405-385	FSRQ	LSP	1.285	both	5.01 (11.59)
J0407.5+0741	61.892101	7.699800	TXS 0404+075	BL Lac	LSP	1.133	opt	···
J0409.8-0359	62.462898	−3.986500	NVSS J040946-040003	BL Lac	ISP	···	opt	···
J0410.9+4216	62.736000	42.277699	B3 0407+421	BCU	LSP	···	none	···
J0416.2-4353	64.072197	−43.887901	SUMSS J041613-435057	FSRQ	LSP	0.398	none	···
J0416.5-1852	64.137299	−18.872400	PKS 0414-189	FSRQ	LSP	1.536	none	···
J0416.9+0105	64.226898	1.088000	1ES 0414+009	BL Lac	HSP	0.287	opt	···
J0420.3-3745	65.093597	−37.752201	NVSS J042025-374443	BCU	LSP	···	none	···
J0422.1-0644	65.534302	−6.741000	PMN J0422-0643	FSRQ	LSP	0.242	both	999.90 (999.90)
J0423.3-0120	65.825996	−1.334200	PKS 0420-01	FSRQ	LSP	0.916	both	999.90 (999.90)
J0424.7+0036	66.194504	0.602800	PKS 0422+00	BL Lac	LSP	0.268	opt	···
J0424.9-5331	66.249802	−53.525700	PMN J0425-5331	BL Lac	LSP	0.390	opt	···
J0427.3-3900	66.825996	−39.009701	PMN J0427-3900	BCU	LSP	···	none	···
J0428.6-3756	67.172997	−37.940300	PKS 0426-380	BL Lac	LSP	1.110	both	−9.39 (50.58)
J0430.3+1654	67.590103	16.909300	MG1 J043022+1655	BCU	···	···	none	···
J0431.8+7403	67.951698	74.055199	GB6 J0431+7403	BL Lac	HSP	···	none	···
J0433.6+2905	68.410698	29.097500	MG2 J043337+2905	BL Lac	LSP	0.970	gam	···
J0433.6-6030	68.401199	−60.511101	PKS 0432-606	FSRQ	LSP	0.930	opt	···
J0434.1-2014	68.529297	−20.244400	TXS 0431-203	BL Lac	ISP	0.928	none	···
J0434.7+0922	68.688599	9.378300	TXS 0431+092	BL Lac	···	···	none	···
J0436.8-5223	69.219803	−52.393398	AT20G J043652-521639	BCU	LSP	···	none	···
J0438.4-1254	69.609901	−12.905300	PKS 0436-129	FSRQ	LSP	1.276	none	···
J0438.9-4521	69.744698	−45.358398	PKS 0437-454	BL Lac	LSP	2.017	none	···
J0440.3-4333	70.082901	−43.544800	PKS 0438-43	FSRQ	···	2.852	both	3.21 (7.79)

Table A1 – *continued*

4FGL Name	RA deg	Dec deg	Association	Class	SED class	redshift	Flares	Lags days
J0442.6-0017	70.661201	−0.296100	PKS 0440-00	FSRQ	LSP	0.449	none	···
J0443.3-6652	70.848297	−66.867302	PMN J0443-6651	FSRQ	LSP	···	none	···
J0445.1-6012	71.285797	−60.212200	PMN J0444-6014	FSRQ	···	0.097	none	···
J0449.1+1121	72.282303	11.356900	PKS 0446+11	FSRQ	LSP	2.153	none	···
J0449.4-4350	72.358200	−43.834999	PKS 0447-439	BL Lac	HSP	0.205	both	3.40 (39.74)
J0451.8-4651	72.955597	−46.857498	PKS 0450-469	FSRQ	LSP	0.602	both	15.89 (56.38)
J0453.1-2806	73.288696	−28.114401	PKS 0451-28	FSRQ	LSP	2.564	none	···
J0455.7-4617	73.946297	−46.287102	PKS 0454-46	FSRQ	LSP	0.858	opt	···
J0456.2+2702	74.067299	27.040300	MG2 J045613+2702	BCU	LSP	···	none	···
J0457.0+0646	74.254501	6.780400	4C +06.21	FSRQ	LSP	0.405	none	···
J0457.0-2324	74.260803	−23.414900	PKS 0454-234	FSRQ	LSP	1.003	both	3.02 (11.79)
J0501.2-0158	75.302299	−1.974900	S3 0458-02	FSRQ	LSP	2.291	gam	···
J0502.4+0609	75.618103	6.162700	PKS 0459+060	FSRQ	LSP	1.106	none	···
J0502.5+1340	75.634102	13.668500	PKS 0459+135	BL Lac	LSP	···	none	···
J0502.5+3438	75.636597	34.633801	MG2 J050234+3436	BCU	···	···	none	···
J0505.3+0459	76.343102	4.999400	PKS 0502+049	FSRQ	LSP	0.954	both	3.02 (5.67)
J0505.6+6405	76.424400	64.087700	TXS 0500+640	BCU	LSP	···	opt	···
J0505.8-0419	76.459801	−4.318200	S3 0503-04	FSRQ	LSP	1.481	none	···
J0507.7-6104	76.932701	−61.081402	PMN J0507-6104	FSRQ	LSP	1.089	none	···
J0507.9+6737	76.995598	67.622299	1ES 0502+675	BL Lac	HSP	0.416	none	···
J0509.4+0542	77.359299	5.701400	TXS 0506+056	BL Lac	ISP	0.336	both	3.61 (18.39)
J0509.4+1012	77.350998	10.200800	PKS 0506+101	FSRQ	LSP	0.621	none	···
J0509.9-6417	77.487602	−64.289101	RBS 0625	BL Lac	HSP	···	none	···
J0510.0+1800	77.518097	18.013500	PKS 0507+17	FSRQ	LSP	0.416	both	999.90 (999.90)
J0510.4-1809	77.611603	−18.164301	CRATES J051015.50-181227.8	BCU	LSP	···	none	···
J0512.8+4041	78.218597	40.694500	B3 0509+406	BCU	LSP	···	none	···
J0515.6-4556	78.905899	−45.948299	PKS 0514-459	FSRQ	LSP	0.194	both	−2.02 (24.70)
J0515.8+1527	78.953003	15.461400	GB6 J0515+1527	BL Lac	ISP	···	none	···
J0516.7-6207	79.179802	−62.124802	PKS 0516-621	BL Lac	LSP	1.300	both	999.90 (999.90)
J0521.7+2112	80.444504	21.213100	TXS 0518+211	BL Lac	HSP	0.108	both	21.11 (94.34)
J0521.8-3848	80.471802	−38.806599	PKS 0520-388	BCU	···	···	none	···
J0524.6-2819	81.173203	−28.328800	PMN J0524-2818	BCU	LSP	···	none	···
J0525.8-0052	81.466599	−0.870900	PMN J0525-0051	BL Lac	LSP	1.200	none	···
J0526.2-4830	81.571404	−48.515099	PKS 0524-485	FSRQ	LSP	1.300	both	6.35 (14.00)
J0529.3-7243	82.329300	−72.733002	PKS 0530-727	BCU	LSP	···	none	···
J0530.9+1332	82.736397	13.540200	PKS 0528+134	FSRQ	LSP	2.070	none	···
J0532.0-4827	83.002197	−48.460701	PMN J0531-4827	BL Lac	ISP	···	none	···
J0532.6+0732	83.171997	7.549300	OG 050	FSRQ	LSP	1.254	none	···
J0532.8-3941	83.199997	−39.685299	PKS 0531-397	BCU	LSP	···	none	···
J0533.0-8446	83.267700	−84.778297	PMN J0532-8447	BCU	LSP	···	none	···
J0533.3+4823	83.333801	48.383400	TXS 0529+483	FSRQ	LSP	1.160	none	···
J0533.8-3749	83.474899	−37.830898	PKS 0532-378	FSRQ	LSP	1.668	none	···
J0538.2-3910	84.574600	−39.169601	NVSS J053810-390844	BL Lac	HSP	0.440	none	···
J0538.8-4405	84.708900	−44.086201	PKS 0537-441	BL Lac	LSP	0.892	both	−14.46 (7.67)
J0539.6+1432	84.905197	14.544300	TXS 0536+145	FSRQ	LSP	2.690	gam	···
J0539.9-2839	84.995201	−28.658501	PKS 0537-286	FSRQ	LSP	3.104	gam	···
J0540.8-5415	85.206902	−54.257500	PKS 0539-543	FSRQ	LSP	1.185	none	···
J0542.9-0913	85.740898	−9.220800	PMN J0542-0913	BCU	LSP	···	none	···
J0543.9-5531	85.981400	−55.532700	1RXS J054357.3-553206	BL Lac	HSP	0.273	opt	···
J0555.6+3947	88.901497	39.787800	B2 0552+39A	FSRQ	LSP	2.365	both	999.90 (999.90)
J0556.2-4352	89.074898	−43.869598	SUMSS J055618-435146	BL Lac	LSP	···	none	···
J0601.1-7035	90.295799	−70.589500	PKS 0601-70	FSRQ	LSP	2.409	both	−0.28 (2.09)
J0607.4+4739	91.857101	47.663502	TXS 0603+476	BL Lac	LSP	···	both	999.90 (999.90)
J0608.0+6721	92.005699	67.351196	S4 0602+67	FSRQ	LSP	1.970	none	···
J0608.0-0835	92.010101	−8.585700	PKS 0605-08	FSRQ	LSP	0.870	none	···
J0608.1-1521	92.030197	−15.363900	PMN J0608-1520	FSRQ	LSP	1.094	none	···
J0608.9-5456	92.238701	−54.942501	PKS 0607-549	BCU	LSP	···	none	···
J0609.0-2219	92.262001	−22.331600	PKS 0606-223	FSRQ	LSP	1.926	opt	···
J0610.1-1848	92.545502	−18.807600	PMN J0610-1847	BL Lac	LSP	···	opt	···
J0610.9-6054	92.730499	−60.916401	PKS 0609-609	FSRQ	LSP	1.773	none	···
J0611.6-2712	92.911499	−27.215200	PMN J0611-2709	BCU	···	···	none	···
J0612.5-3138	93.127998	−31.638100	PKS 0610-316	FSRQ	LSP	0.873	none	···
J0612.8+4122	93.221802	41.371700	B3 0609+413	BL Lac	ISP	···	opt	···

Table A1 – *continued*

4FGL Name	RA deg	Dec deg	Association	Class	SED class	redshift	Flares	Lags days
J0614.8+6136	93.721298	61.607899	GB6 J0614+6139	BCU	···	···	none	···
J0615.3-3117	93.839401	−31.285299	PKS 0613-312	BL Lac	ISP	···	none	···
J0617.2+5701	94.316200	57.024899	87GB 061258.1+570222	BL Lac	LSP	···	none	···
J0620.5-2512	95.144501	−25.212900	PKS 0618-252	BCU	LSP	1.900	none	···
J0622.3-2605	95.595596	−26.096300	PMN J0622-2605	BL Lac	HSP	0.414	both	999.90 (999.90)
J0622.9+3326	95.729599	33.433498	B2 0619+33	BCU	LSP	1.062	none	···
J0623.0-3010	95.764603	−30.182800	PMN J0623-3010	BCU	···	···	none	···
J0625.3+4439	96.328796	44.664799	GB6 J0625+4440	BL Lac	LSP	···	opt	···
J0625.8-5441	96.452301	−54.691898	PMN J0625-5438	FSRQ	LSP	2.051	none	···
J0628.8-6250	97.217400	−62.840500	PKS 0628-627	BL Lac	LSP	···	none	···
J0629.3-1959	97.347801	−19.999901	PKS 0627-199	BL Lac	LSP	1.724	none	···
J0631.1+2020	97.776604	20.340599	TXS 0628+203	BCU	···	···	none	···
J0633.4-2222	98.369598	−22.372400	PMN J0633-2223	FSRQ	LSP	1.508	none	···
J0635.6-7518	98.902199	−75.304604	PKS 0637-75	FSRQ	LSP	0.653	none	···
J0636.5+7138	99.182800	71.661499	GB6 J0636+7138	BCU	LSP	···	none	···
J0638.6+7320	99.671097	73.343803	S5 0633+73	FSRQ	LSP	1.850	none	···
J0641.7-0320	100.437103	−3.346600	PMN J0641-0320	FSRQ	LSP	1.196	gam	···
J0643.2-5356	100.815399	−53.936401	PMN J0643-5358	BCU	LSP	···	none	···
J0643.3+0857	100.834503	8.952500	PMN J0643+0857	FSRQ	LSP	0.882	gam	···
J0644.4-6712	101.105301	−67.212402	PKS 0644-671	FSRQ	LSP	···	none	···
J0644.6+6039	101.162300	60.656200	NVSS J064435+603849	BL Lac	ISP	0.358	none	···
J0646.7-3913	101.678398	−39.217701	PKS 0644-390	FSRQ	LSP	0.681	none	···
J0647.7-6058	101.931396	−60.978100	PMN J0647-6058	BL Lac	LSP	···	none	···
J0648.7+1516	102.190498	15.280800	RX J0648.7+1516	BL Lac	HSP	0.179	none	···
J0649.5-3139	102.394501	−31.657301	NVSS J064933-313917	BL Lac	···	0.563	none	···
J0650.5-2851	102.628998	−28.861000	PMN J0650-2849	BCU	LSP	···	none	···
J0650.7+2503	102.698601	25.054800	1ES 0647+250	BL Lac	HSP	0.203	opt	···
J0654.3+5042	103.596199	50.702702	GB6 J0654+5042	FSRQ	LSP	1.253	none	···
J0654.4+4514	103.606003	45.244598	B3 0650+453	FSRQ	LSP	0.928	none	···
J0659.6-2742	104.906601	−27.701300	TXS 0657-276	FSRQ	LSP	1.727	none	···
J0659.9+1709	104.984703	17.152201	TXS 0657+172	FSRQ	···	1.080	none	···
J0700.5-6610	105.129303	−66.180298	PKS 0700-661	BL Lac	ISP	···	opt	···
J0701.5-4634	105.390602	−46.572899	PKS 0700-465	FSRQ	LSP	0.822	both	4.65 (21.58)
J0702.7-1951	105.678001	−19.851700	TXS 0700-197	BL Lac	LSP	···	none	···
J0703.3-0050	105.836700	−0.843600	TXS 0700-007	BL Lac	ISP	···	opt	···
J0704.8+4907	106.206703	49.131802	87GB 070112.8+491056	BCU	LSP	···	none	···
J0706.8+7742	106.724899	77.700203	NVSS J070651+774137	BL Lac	ISP	···	none	···
J0709.1+2241	107.276901	22.684700	GB6 J0708+2241	BL Lac	ISP	···	opt	···
J0709.7-0255	107.445099	−2.930100	PMN J0709-0255	FSRQ	LSP	1.472	gam	···
J0710.4+5908	107.623398	59.135201	1H 0658+595	BL Lac	HSP	0.125	none	···
J0710.8-3851	107.724503	−38.851299	AT20G J071043-385037	FSRQ	LSP	0.129	none	···
J0710.9+4733	107.732300	47.553001	S4 0707+47	BL Lac	LSP	1.292	none	···
J0712.7+5033	108.187599	50.550598	GB6 J0712+5033	BL Lac	LSP	0.502	opt	···
J0713.0+5738	108.259804	57.634499	GB6 J0713+5738	BCU	ISP	···	gam	···
J0713.8+1935	108.464699	19.587900	MG2 J071354+1934	FSRQ	LSP	0.540	none	···
J0718.0+4536	109.515900	45.616299	S4 0714+45	FSRQ	LSP	0.940	none	···
J0719.3+3307	109.839996	33.123199	B2 0716+33	FSRQ	LSP	0.779	both	4.92 (14.91)
J0720.0-3507	110.004402	−35.122601	AT20G J071959-350448	BCU	LSP	···	none	···
J0721.3+0405	110.347504	4.091400	PMN J0721+0406	FSRQ	LSP	0.665	none	···
J0721.9+7120	110.488197	71.340500	S5 0716+71	BL Lac	ISP	0.127	both	−5.89 (33.53)
J0725.2+1425	111.323997	14.421200	4C +14.23	FSRQ	LSP	1.038	none	···
J0726.4-4727	111.613098	−47.458900	PMN J0726-4728	FSRQ	LSP	1.686	none	···
J0729.1+5703	112.285698	57.055801	TXS 0724+571	FSRQ	LSP	0.426	none	···
J0730.3-1141	112.577599	−11.688800	PKS 0727-11	FSRQ	LSP	1.589	none	···
J0730.5-0535	112.635399	−5.584200	TXS 0728-054	BL Lac	ISP	···	none	···
J0733.5-5445	113.385201	−54.759300	SUMSS J073334-544544	BCU	LSP	···	none	···
J0733.6+3649	113.419601	36.822498	GB6 J0733+3650	BCU	LSP	···	none	···
J0733.8+0455	113.472198	4.928200	GB6 J0733+0456	FSRQ	LSP	3.010	none	···
J0734.0+5021	113.524498	50.357201	TXS 0730+504	FSRQ	LSP	0.720	none	···
J0734.4-7711	113.611801	−77.185204	PKS 0736-770	BCU	LSP	···	none	···
J0738.1+1742	114.538696	17.706600	PKS 0735+17	BL Lac	LSP	0.424	both	−0.20 (44.72)
J0739.2+0137	114.820000	1.621600	PKS 0736+01	FSRQ	LSP	0.189	both	11.20 (12.89)

Table A1 – *continued*

4FGL Name	RA deg	Dec deg	Association	Class	SED class	redshift	Flares	Lags days
J0742.6+5443	115.671501	54.727001	GB6 J0742+5444	FSRQ	LSP	0.720	opt	···
J0742.9-5242	115.739998	−52.703300	PMN J0742-5241	BCU	LSP	···	none	···
J0743.0-5622	115.769798	−56.376801	PMN J0743-5619	FSRQ	LSP	2.319	none	···
J0743.6-3805	115.906197	−38.093700	PMN J0743-3804	BCU	LSP	···	opt	···
J0746.4+2546	116.602097	25.767799	B2 0743+25	FSRQ	LSP	2.987	opt	···
J0746.5+2730	116.627602	27.515301	OI 272	FSRQ	LSP	1.690	none	···
J0746.6-4754	116.669403	−47.915501	PMN J0746-4755	BL Lac	HSP	···	none	···
J0747.3-3310	116.832802	−33.177799	PKS 0745-330	BL Lac	LSP	···	none	···
J0748.0-1638	117.005898	−16.643700	TXS 0745-165	BCU	LSP	···	none	···
J0748.3+4928	117.082397	49.474800	NVSS J074837+493040	BL Lac	···	···	none	···
J0748.6+2400	117.163803	24.016600	OI 275	FSRQ	LSP	0.410	both	999.90 (999.90)
J0749.3+4453	117.348198	44.891800	SDSS J074916.88+445232.1	BCU	LSP	0.559	none	···
J0750.8+1229	117.700996	12.494000	OI 280	FSRQ	···	0.889	both	999.90 (999.90)
J0751.0+7908	117.767799	79.139397	JVAS J0750+7909	BCU	LSP	···	none	···
J0752.2+3313	117.982597	33.236099	OI 380	FSRQ	···	1.936	both	−1.13 (7.26)
J0753.9+0923	118.490700	9.390400	TXS 0751+095	BCU	LSP	···	opt	···
J0754.4-1148	118.610497	−11.805200	TXS 0752-116	BL Lac	LSP	···	none	···
J0754.7+4823	118.692902	48.393200	GB1 0751+485	BL Lac	LSP	0.377	opt	···
J0757.1+0956	119.285599	9.949100	PKS 0754+100	BL Lac	LSP	0.266	opt	···
J0800.4-2257	120.111298	−22.957199	PMN J0800-2302	BCU	LSP	···	none	···
J0800.9+4401	120.245697	44.018101	B3 0757+441	BL Lac	LSP	1.072	none	···
J0801.1+6444	120.293297	64.743797	RX J0801.0+6444	BL Lac	···	0.200	none	···
J0803.2-0337	120.824699	−3.618900	TXS 0800-034	FSRQ	HSP	0.365	none	···
J0803.5+2046	120.888298	20.767799	GB6 B0800+2046	BCU	LSP	···	none	···
J0804.0-3629	121.007599	−36.485401	NVSS J080405-362919	BL Lac	···	···	none	···
J0804.5+0414	121.132797	4.239300	TXS 0802+043	BCU	···	···	none	···
J0805.1+7744	121.289101	77.744102	WN B0759.6+7754	BCU	LSP	···	none	···
J0805.2-0110	121.300400	−1.181000	PKS B0802-010	FSRQ	LSP	1.388	none	···
J0805.4+6147	121.355698	61.793701	TXS 0800+618	FSRQ	LSP	3.033	none	···
J0805.4+7534	121.361603	75.576599	RX J0805.4+7534	BL Lac	HSP	0.121	none	···
J0806.5+4503	121.628403	45.060501	B3 0803+452	FSRQ	LSP	2.102	none	···
J0807.1-0541	121.779800	−5.684200	PKS 0804-05	BL Lac	ISP	···	none	···
J0807.7-1206	121.933701	−12.104300	CRATES J080736.06-120745.9	BCU	LSP	···	none	···
J0808.2-0751	122.065002	−7.855600	PKS 0805-07	FSRQ	LSP	1.837	both	1.36 (9.41)
J0809.3+4053	122.330002	40.895401	S4 0805+41	FSRQ	LSP	1.418	none	···
J0809.8+5218	122.461700	52.314301	1ES 0806+524	BL Lac	HSP	0.138	opt	···
J0811.4+0146	122.861000	1.775600	OJ 014	BL Lac	LSP	1.148	none	···
J0814.2-1013	123.550903	−10.217200	NVSS J081411-101208	BL Lac	ISP	···	none	···
J0814.6+6430	123.665398	64.504997	GB6 J0814+6431	BL Lac	LSP	0.239	opt	···
J0816.3+5739	124.099701	57.661598	SBS 0812+578	BL Lac	ISP	0.054	none	···
J0816.4-1311	124.112297	−13.197300	PMN J0816-1311	BL Lac	HSP	0.046	none	···
J0816.7-2420	124.191597	−24.342699	PMN J0816-2421	BCU	LSP	···	none	···
J0817.8-0934	124.473396	−9.577700	TXS 0815-094	BL Lac	LSP	···	none	···
J0818.2+4222	124.557198	42.381901	S4 0814+42	BL Lac	LSP	0.530	none	···
J0821.1+1007	125.299301	10.128700	SDSS J082054.81+100609.4	BCU	LSP	0.956	none	···
J0824.4+2440	126.108101	24.670900	B2 0821+24	FSRQ	LSP	1.242	none	···
J0824.7+5552	126.197701	55.881599	OJ 535	FSRQ	LSP	1.417	none	···
J0824.9+3915	126.236099	39.257401	4C +39.23	FSRQ	LSP	1.216	none	···
J0825.9-2230	126.499100	−22.505501	PKS 0823-223	BL Lac	LSP	0.910	both	13.27 (35.45)
J0830.8+2410	127.701500	24.172701	S3 0827+24	FSRQ	LSP	0.939	both	14.94 (44.52)
J0831.8+0429	127.973198	4.494100	PKS 0829+046	BL Lac	LSP	0.174	both	1.36 (21.72)
J0833.9+4223	128.475906	42.398899	OJ 451	FSRQ	LSP	0.249	none	···
J0836.2+2141	129.051102	21.697100	MG2 J083615+2138	BCU	···	···	none	···
J0836.5-2026	129.130905	−20.447399	PKS 0834-20	FSRQ	LSP	2.752	none	···
J0839.8+0105	129.963303	1.087700	PKS 0837+012	FSRQ	LSP	1.123	both	1.17 (19.43)
J0841.3-3554	130.340607	−35.904099	NVSS J084121-355506	BL Lac	HSP	···	none	···
J0842.3-6053	130.597900	−60.891899	PMN J0842-6053	BCU	···	···	gam	···
J0843.0-0853	130.773895	−8.887800	PMN J0843-0848	BCU	···	···	none	···
J0844.2+5312	131.050903	53.214100	NVSS J084411+531250	BL Lac	LSP	0.435	none	···
J0849.4-2911	132.351105	−29.186300	NVSS J084922-291149	BCU	ISP	···	none	···
J0849.8-3541	132.451599	−35.687698	PMN J0849-3541	BCU	LSP	···	both	999.90 (999.90)
J0850.0+4855	132.508301	48.921700	GB6 J0850+4855	BL Lac	LSP	···	both	999.90 (999.90)

Table A1 – *continued*

4FGL Name	RA deg	Dec deg	Association	Class	SED class	redshift	Flares	Lags days
J0850.1-1212	132.541199	−12.212100	PMN J0850-1213	FSRQ	LSP	0.566	none	···
J0851.5+5528	132.880493	55.479401	GB6 J0851+5528	BL Lac	LSP	···	opt	···
J0852.5-5755	133.141800	−57.930401	PMN J0852-5755	BCU	LSP	···	both	999.90 (999.90)
J0854.8+2006	133.707108	20.115900	OJ 287	BL Lac	LSP	0.306	both	999.90 (999.90)
J0855.9+7144	133.975403	71.741898	GB6 J0856+7146	FSRQ	LSP	0.542	none	···
J0856.6-1105	134.169601	−11.099300	PMN J0856-1105	BL Lac	LSP	···	none	···
J0857.9-1949	134.491104	−19.817499	PKS 0855-19	FSRQ	LSP	0.659	none	···
J0900.6-7408	135.172104	−74.143997	AT20G J085959-741401	BCU	LSP	···	none	···
J0900.7-1243	135.175095	−12.720100	TXS 0858-125	BCU	ISP	···	none	···
J0902.4+2051	135.617203	20.850300	NVSS J090226+205045	BL Lac	ISP	2.055	opt	···
J0904.5-3513	136.140396	−35.230801	NVSS J090442-351423	BCU	LSP	···	none	···
J0904.9-5734	136.231506	−57.583302	PKS 0903-57	BCU	LSP	0.695	both	−0.83 (21.85)
J0905.6+1358	136.401703	13.975000	MG1 J090534+1358	BL Lac	HSP	···	opt	···
J0906.3-0905	136.582703	−9.092500	PMN J0906-0905	BL Lac	···	···	none	···
J0909.1+0121	137.296707	1.355700	PKS 0906+01	FSRQ	LSP	1.024	none	···
J0909.7-0230	137.446396	−2.514300	PKS 0907-023	FSRQ	LSP	0.957	gam	···
J0910.6+2247	137.674301	22.797800	TXS 0907+230	FSRQ	LSP	2.661	none	···
J0910.8+3859	137.709106	38.999901	FBQS J091052.0+390202	BL Lac	LSP	0.199	opt	···
J0912.2+4127	138.055893	41.456299	B3 0908+416B	FSRQ	LSP	2.563	gam	···
J0915.4-3027	138.875000	−30.464199	PMN J0915-3030	BCU	LSP	···	none	···
J0915.9+2933	138.986206	29.552999	Ton 0396	BL Lac	HSP	0.190	none	···
J0916.7+3856	139.189804	38.947899	4C +38.28	FSRQ	LSP	1.268	none	···
J0920.3-0443	140.100006	−4.731100	TXS 0917-044	BCU	LSP	···	none	···
J0920.9+4441	140.229095	44.699001	S4 0917+44	FSRQ	LSP	2.186	both	999.90 (999.90)
J0921.6+6216	140.418503	62.270802	OK 630	FSRQ	LSP	1.446	both	0.88 (3.25)
J0922.6+0434	140.666901	4.578100	GB6 J0922+0433	BCU	LSP	1.325	none	···
J0922.7-3959	140.691803	−39.986698	PKS 0920-39	FSRQ	LSP	0.595	both	1.32 (6.21)
J0923.5+3852	140.884995	38.874298	B2 0920+39	BCU	LSP	···	none	···
J0923.5+4125	140.894897	41.428299	B3 0920+416	FSRQ	LSP	1.732	none	···
J0924.0+2816	141.004898	28.275499	B2 0920+28	FSRQ	LSP	0.744	none	···
J0928.1-2035	142.047806	−20.597300	PKS 0925-203	FSRQ	LSP	0.348	gam	···
J0929.3+5014	142.326508	50.235199	GB6 J0929+5013	BL Lac	LSP	···	none	···
J0930.3+8612	142.599396	86.202103	S5 0916+864	BL Lac	LSP	···	opt	···
J0930.9-1015	142.740402	−10.256500	TXS 0928-099	BCU	LSP	···	none	···
J0931.2-8533	142.817596	−85.562599	PKS 0936-853	BCU	LSP	···	none	···
J0932.6+5306	143.158997	53.100800	S4 0929+53	FSRQ	LSP	0.597	opt	···
J0937.1+5008	144.296906	50.143700	GB6 J0937+5008	FSRQ	LSP	0.276	opt	···
J0937.9-1434	144.475098	−14.570600	NVSS J093754-143350	BL Lac	ISP	0.287	opt	···
J0939.3-1732	144.835999	−17.541800	TXS 0936-173	BCU	LSP	···	none	···
J0940.0-2828	145.011597	−28.480301	TXS 0937-282	BCU	LSP	···	opt	···
J0940.7-6105	145.178802	−61.085499	MRC 0939-608	BCU	LSP	···	opt	···
J0940.9-1335	145.243805	−13.589100	TXS 0938-133	FSRQ	LSP	0.551	none	···
J0941.7+4125	145.449997	41.421600	GB6 J0941+4121	BCU	LSP	0.819	none	···
J0942.3-0800	145.585602	−8.007600	PMN J0942-0800	BL Lac	LSP	···	opt	···
J0945.2+5200	146.316193	52.005299	WISE J094452.09+520233.4	FSRQ	LSP	0.563	none	···
J0945.7+5759	146.432007	57.987099	GB6 J0945+5757	BL Lac	LSP	0.229	none	···
J0946.6+1016	146.661301	10.277000	TXS 0943+105	FSRQ	LSP	1.007	none	···
J0947.1-2541	146.781296	−25.683901	1RXS J094709.2-254056	BL Lac	···	···	none	···
J0949.0+4038	147.261795	40.636700	4C +40.24	FSRQ	LSP	1.250	none	···
J0949.2+1749	147.315506	17.830000	TXS 0946+181	FSRQ	LSP	0.694	none	···
J0952.6-5048	148.156601	−50.811199	PMN J0952-5049	BCU	···	···	none	···
J0953.0-0840	148.262802	−8.669500	PMN J0953-0840	BL Lac	HSP	···	none	···
J0956.7+2516	149.176102	25.281700	OK 290	FSRQ	LSP	0.708	none	···
J0957.3-1348	149.331406	−13.814100	PMN J0957-1350	FSRQ	LSP	1.323	none	···
J0957.6+5523	149.416107	55.383801	4C +55.17	FSRQ	LSP	0.896	none	···
J0957.8+3423	149.470703	34.397499	B2 0954+34	BCU	LSP	1.810	none	···
J0958.0+4728	149.509003	47.467499	OK 492	FSRQ	LSP	1.882	gam	···
J0958.4+5042	149.605698	50.700001	7C 0955+5054	FSRQ	LSP	1.154	none	···
J0958.7+6534	149.689697	65.567802	S4 0954+65	BL Lac	LSP	0.367	both	−2.34 (16.15)
J1001.1+2911	150.293793	29.188000	GB6 J1001+2911	BL Lac	LSP	0.558	both	−13.29 (24.54)
J1006.7-2159	151.693100	−21.990999	PKS 1004-217	FSRQ	LSP	0.330	both	−22.55 (2.88)
J1007.6-3332	151.911697	−33.543201	PKS 1005-333	FSRQ	LSP	1.837	none	···

Table A1 – *continued*

4FGL Name	RA deg	Dec deg	Association	Class	SED class	redshift	Flares	Lags days
J1008.0+0620	152.013596	6.347500	MG1 J100800+0621	BL Lac	LSP	0.650	opt	···
J1008.7-2909	152.198898	−29.155899	PMN J1008-2912	BCU	LSP	···	none	···
J1010.2-3119	152.571594	−31.320700	1RXS J101015.9-311909	BL Lac	HSP	0.143	none	···
J1010.8-0158	152.703796	−1.981700	PKS 1008-01	FSRQ	LSP	0.896	none	···
J1011.3-0427	152.825302	−4.457700	PKS B1008-041	FSRQ	LSP	1.588	none	···
J1012.7+2439	153.198898	24.663799	MG2 J101241+2439	FSRQ	LSP	1.805	gam	···
J1013.7+3444	153.448700	34.738400	OL 318	FSRQ	LSP	0.208	none	···
J1015.0+4926	153.768005	49.433601	1H 1013+498	BL Lac	HSP	0.212	both	999.90 (999.90)
J1015.6+5553	153.910507	55.889301	TXS 1012+560	FSRQ	LSP	0.677	none	···
J1016.0+0512	154.009293	5.208900	TXS 1013+054	FSRQ	LSP	1.713	opt	···
J1017.8+0715	154.472794	7.263800	GB6 J1018+0715	BCU	···	···	none	···
J1018.1+1905	154.548004	19.096300	NVSS J101808+190614	BL Lac	LSP	···	none	···
J1018.3-3124	154.591293	−31.403200	PKS 1016-311	FSRQ	LSP	0.794	both	−1.05 (2.13)
J1018.4+0528	154.617203	5.470200	TXS 1015+057	FSRQ	LSP	1.945	none	···
J1018.4+3540	154.607193	35.680199	B2 1015+35B	FSRQ	LSP	1.228	none	···
J1019.7+6321	154.926300	63.352699	GB6 J1019+6319	BL Lac	LSP	···	opt	···
J1023.1+3949	155.788498	39.822601	4C +40.25	FSRQ	LSP	1.333	both	0.25 (10.80)
J1023.8-4335	155.972504	−43.595100	RX J1023.9-4336	BL Lac	HSP	0.320	none	···
J1023.9-3236	155.996399	−32.603401	PKS 1021-323	FSRQ	LSP	1.568	none	···
J1026.9-1749	156.742401	−17.821800	1RXS J102658.5-174905	BL Lac	HSP	0.267	none	···
J1027.2+7427	156.812103	74.452400	GB6 J1027+7428	BCU	LSP	0.879	none	···
J1027.6+8251	156.922699	82.861099	2MASS J10284195+8253398	BCU	···	···	none	···
J1028.4-0234	157.121307	−2.582900	PMN J1028-0237	FSRQ	LSP	0.476	opt	···
J1031.1+7442	157.792496	74.701897	S5 1027+74	BL Lac	ISP	0.123	none	···
J1031.6+6019	157.909103	60.317799	TXS 1028+605	FSRQ	LSP	1.231	none	···
J1032.6+3737	158.173401	37.623402	B3 1029+378	BL Lac	ISP	0.528	none	···
J1033.1+4115	158.275208	41.262001	S4 1030+41	FSRQ	LSP	1.117	none	···
J1033.9+6050	158.484894	60.849300	S4 1030+61	FSRQ	LSP	1.401	both	−1.86 (20.20)
J1037.4-2933	159.356400	−29.556801	PKS 1034-293	FSRQ	LSP	0.312	both	5.18 (8.18)
J1037.7-2822	159.427399	−28.381599	PKS B1035-281	FSRQ	LSP	1.066	both	3.87 (4.97)
J1038.2-2425	159.558807	−24.423901	NVSS J103824-242355	BCU	···	···	none	···
J1038.8-5312	159.712906	−53.206902	MRC 1036-529	FSRQ	LSP	1.450	none	···
J1040.5+0617	160.149506	6.284800	GB6 J1040+0617	BL Lac	LSP	···	both	999.90 (999.90)
J1043.2+2408	160.805298	24.146000	B2 1040+24A	FSRQ	LSP	0.560	opt	···
J1045.8-2928	161.468399	−29.479500	PKS B1043-291	FSRQ	LSP	2.128	none	···
J1047.2-5517	161.800201	−55.293098	PMN J1047-5513	BCU	···	···	none	···
J1047.7+7238	161.938797	72.641998	GB6 J1047+7238	BL Lac	ISP	···	none	···
J1047.8-6216	161.960907	−62.274502	PMN J1047-6217	BCU	LSP	···	none	···
J1048.4+7143	162.106705	71.729698	S5 1044+71	FSRQ	LSP	1.150	both	−2.80 (15.42)
J1049.8+1429	162.467499	14.483500	MG1 J104945+1429	BCU	LSP	1.630	both	−8.64 (16.21)
J1050.1+0432	162.546402	4.537700	MG1 J105009+0433	FSRQ	LSP	1.217	none	···
J1054.5+2211	163.627899	22.191299	87GB 105148.6+222705	BL Lac	ISP	2.055	none	···
J1056.8+7012	164.207596	70.201897	S5 1053+70	FSRQ	LSP	2.492	both	6.83 (29.25)
J1057.2+5510	164.318298	55.180401	SDSS J105707.47+551032.2	BL Lac	HSP	2.085	none	···
J1057.3-2341	164.342300	−23.688900	PKS B1054-234	FSRQ	LSP	1.125	none	···
J1058.0+4305	164.518097	43.093800	B3 1055+433	BL Lac	LSP	···	none	···
J1058.4+0133	164.623993	1.564100	4C +01.28	BL Lac	LSP	0.890	both	−7.64 (25.17)
J1058.5+8115	164.625504	81.254700	S5 1053+81	FSRQ	LSP	0.706	opt	···
J1058.6+2817	164.650299	28.286600	GB6 J1058+2817	BL Lac	LSP	0.479	both	−1.01 (11.62)
J1058.6+5627	164.665207	56.463402	TXS 1055+567	BL Lac	ISP	0.143	opt	···
J1058.6-8003	164.660004	−80.064003	PKS 1057-79	BL Lac	LSP	0.569	none	···
J1059.2-1134	164.806305	−11.572000	PKS B1056-113	BL Lac	LSP	···	both	999.90 (999.90)
J1059.5+2057	164.878296	20.952400	MG2 J105938+2057	FSRQ	···	0.400	none	···
J1102.6+5251	165.673004	52.856899	GB6 J1102+5249	FSRQ	ISP	0.690	none	···
J1103.0+1157	165.772202	11.965400	TXS 1100+122	FSRQ	ISP	0.914	both	999.90 (999.90)
J1103.9-5357	165.975693	−53.964699	PKS 1101-536	BL Lac	LSP	···	both	999.90 (999.90)
J1104.4+0730	166.116806	7.510000	MG1 J110424+0730	BL Lac	ISP	0.630	gam	···
J1104.4+3812	166.118698	38.207001	Mkn 421	BL Lac	HSP	0.030	both	19.78 (43.58)
J1106.0+2813	166.501999	28.225401	MG2 J110606+2812	FSRQ	LSP	0.844	none	···
J1106.5-3646	166.627396	−36.772301	PMN J1106-3647	BL Lac	···	1.080	none	···
J1107.0-4449	166.774902	−44.832298	PKS 1104-445	FSRQ	LSP	1.598	none	···
J1110.5-1836	167.641098	−18.605801	CRATES J111027.78-183552.6	BL Lac	ISP	···	opt	···

Table A1 – *continued*

4FGL Name	RA deg	Dec deg	Association	Class	SED class	redshift	Flares	Lags days
J1112.5+3448	168.146896	34.802200	TXS 1109+350	FSRQ	LSP	1.949	none	···
J1113.6-1920	168.404800	−19.335899	NVSS J111348-192252	BCU	ISP	···	none	···
J1114.5-0819	168.642105	−8.322400	PKS B1112-080	FSRQ	LSP	2.078	none	···
J1117.0+2013	169.270798	20.229401	RBS 0958	BL Lac	HSP	0.139	none	···
J1118.2-4634	169.557907	−46.579498	PKS 1116-46	FSRQ	ISP	0.713	none	···
J1119.0+1235	169.765503	12.586600	OM 127	FSRQ	LSP	2.126	none	···
J1121.4-0553	170.364105	−5.899700	PKS 1118-05	FSRQ	LSP	1.297	opt	···
J1123.4-2529	170.868301	−25.488001	NVSS J112325-252858	FSRQ	···	0.148	none	···
J1124.9+4934	171.242798	49.567402	GB6 J1124+4933	BL Lac	HSP	···	none	···
J1125.5-3557	171.392899	−35.958099	PMN J1125-3556	BL Lac	ISP	0.284	opt	···
J1125.9+2005	171.491196	20.091200	4C +20.25	FSRQ	LSP	0.133	opt	···
J1127.0-1857	171.763397	−18.964001	PKS 1124-186	FSRQ	LSP	1.048	opt	···
J1127.4+5648	171.864807	56.803200	S4 1124+57	FSRQ	LSP	2.890	none	···
J1127.8+3618	171.963898	36.313999	MG2 J112758+3620	FSRQ	LSP	0.884	none	···
J1128.0+5924	172.003403	59.401501	TXS 1125+596	FSRQ	LSP	1.795	none	···
J1129.1+3703	172.295898	37.064400	CRATES J112916+370317	BL Lac	LSP	0.445	none	···
J1129.2-0529	172.311493	−5.487400	NVSS J112914-052856	BCU	···	···	none	···
J1129.5+3034	172.380402	30.578899	87GB 112657.9+305242	BCU	ISP	0.435	none	···
J1131.0+3815	172.754501	38.256500	B2 1128+38	FSRQ	LSP	1.733	both	11.26 (5.71)
J1132.7+0034	173.196106	0.573700	PKS B1130+008	BL Lac	ISP	1.223	none	···
J1135.1+3014	173.788406	30.234400	CRATES J113514+301001	BL Lac	LSP	···	none	···
J1136.2+3407	174.074997	34.129002	MG2 J113627+3408	FSRQ	LSP	1.337	none	···
J1136.4+6736	174.117905	67.612701	RX J1136.5+6737	BL Lac	HSP	0.136	none	···
J1136.4+7009	174.121902	70.153702	Mkn 180	BL Lac	HSP	0.045	opt	···
J1139.0+4033	174.763702	40.561699	CRATES J113903+403303	BCU	LSP	2.360	none	···
J1143.1+6122	175.788101	61.380100	GB6 J1143+6122	BL Lac	LSP	0.475	none	···
J1145.7-6949	176.438202	−69.831398	PKS 1143-696	FSRQ	LSP	0.244	gam	···
J1146.9+3958	176.740494	39.977501	S4 1144+40	FSRQ	LSP	1.089	gam	···
J1147.0-3812	176.759995	−38.200600	PKS 1144-379	BL Lac	LSP	1.048	both	999.90 (999.90)
J1147.2-2627	176.811401	−26.464899	PMN J1147-2625	BCU	LSP	···	none	···
J1147.8-0724	176.960800	−7.414400	PKS 1145-071	FSRQ	LSP	1.342	none	···
J1148.5+2629	177.141296	26.498600	TXS 1145+268	FSRQ	LSP	0.867	none	···
J1149.5-4029	177.386505	−40.491001	PMN J1149-4029	BCU	LSP	···	opt	···
J1150.4+2418	177.602905	24.301600	OM 280	BL Lac	ISP	0.200	opt	···
J1150.6+4154	177.656296	41.909599	RBS 1040	BL Lac	HSP	0.320	none	···
J1152.3-0839	178.080795	−8.666300	PKS B1149-084	FSRQ	LSP	2.370	gam	···
J1153.0+8056	178.266403	80.935699	S5 1150+81	FSRQ	LSP	1.250	none	···
J1153.3-1104	178.342300	−11.078700	PKS B1150-108	BCU	LSP	0.269	gam	···
J1153.4+4931	178.350494	49.516899	4C +49.22	FSRQ	LSP	0.334	none	···
J1154.0+4037	178.514496	40.632000	B3 1151+408	FSRQ	LSP	0.925	none	···
J1154.0+6018	178.518997	60.310699	RX J1154.0+6022	FSRQ	LSP	1.120	none	···
J1154.1-3243	178.542297	−32.718899	PKS 1151-324	BL Lac	LSP	···	none	···
J1156.6+0640	179.163605	6.672800	TXS 1154+069	BCU	LSP	···	none	···
J1158.5+4824	179.636505	48.416100	GB1 1155+486	FSRQ	LSP	2.028	none	···
J1159.2-2227	179.810699	−22.460501	PKS 1156-221	BCU	LSP	0.565	both	3.57 (11.94)
J1159.3-2142	179.843201	−21.703800	PMN J1159-2142	FSRQ	LSP	0.617	opt	···
J1159.5+2914	179.884003	29.244801	Ton 599	FSRQ	LSP	0.729	both	−2.52 (15.95)
J1200.2+0201	180.055099	2.017200	87GB 115739.6+021927	BCU	LSP	···	none	···
J1200.6+1229	180.173401	12.492200	GB6 J1200+1230	BL Lac	···	0.415	none	···
J1200.7+2008	180.186600	20.135401	TXS 1158+204	BCU	LSP	···	none	···
J1202.5-0528	180.629105	−5.470900	PKS 1200-051	FSRQ	LSP	0.381	none	···
J1203.1+6031	180.788101	60.518002	SBS 1200+608	BL Lac	LSP	0.065	none	···
J1204.2-0709	181.074097	−7.162700	1RXS J120417.0-070959	BL Lac	ISP	0.184	none	···
J1205.7-2635	181.432205	−26.594601	PKS 1203-26	FSRQ	LSP	0.789	none	···
J1207.7-0106	181.927597	−1.106300	AT20G J120741-010630	FSRQ	LSP	1.006	both	−4.87 (18.23)
J1208.9+5441	182.226105	54.699501	TXS 1206+549	FSRQ	LSP	1.345	none	···
J1209.4+7608	182.362503	76.137001	2MASS J12093020+7609120	BCU	ISP	···	none	···
J1209.8+1810	182.466400	18.177601	MG1 J120953+1809	FSRQ	LSP	0.845	opt	···
J1211.0-3800	182.762100	−38.015598	PMN J1211-3754	BCU	LSP	···	none	···
J1212.0-2326	183.000900	−23.449400	PMN J1212-2327	BL Lac	···	0.666	none	···
J1215.0+1656	183.774200	16.937201	TXS 1212+171	FSRQ	LSP	1.132	none	···

Table A1 – *continued*

4FGL Name	RA deg	Dec deg	Association	Class	SED class	redshift	Flares	Lags days
J1217.9+3007	184.476196	30.117701	B2 1215+30	BL Lac	HSP	0.130	both	−12.97 (15.16)
J1218.0-0028	184.513596	−0.483200	PKS 1215-002	BL Lac	LSP	0.419	none	···
J1218.5-0119	184.638794	−1.327000	PKS 1216-010	BL Lac	LSP	···	opt	···
J1220.1+3432	185.046204	34.538300	GB2 1217+348	BL Lac	LSP	···	none	···
J1220.1+7105	185.043793	71.092003	S5 1217+71	FSRQ	LSP	0.451	both	−0.33 (10.37)
J1221.3+3010	185.344894	30.167700	PG 1218+304	BL Lac	HSP	0.184	opt	···
J1221.5+2814	185.378403	28.238199	W Comae	BL Lac	ISP	0.102	none	···
J1222.5+0414	185.627106	4.238900	4C +04.42	FSRQ	LSP	0.964	gam	···
J1223.8+8039	185.970703	80.659798	S5 1221+80	BL Lac	LSP	···	none	···
J1223.9+5000	185.988007	50.008900	SBS 1221+503	FSRQ	LSP	1.064	opt	···
J1224.4+2436	186.116104	24.614201	MS 1221.8+2452	BL Lac	HSP	0.219	opt	···
J1224.7-8313	186.199005	−83.225899	PKS 1221-82	BCU	LSP	···	none	···
J1224.9+2122	186.227707	21.381399	4C +21.35	FSRQ	LSP	0.434	both	−0.33 (26.43)
J1225.0+0330	186.251907	3.509800	4C +03.23	FSRQ	LSP	0.956	none	···
J1225.5-2851	186.392197	−28.862499	AT20G J122515-284956	BCU	LSP	···	none	···
J1226.8-1329	186.718796	−13.494000	PMN J1226-1328	BL Lac	LSP	0.456	none	···
J1228.7+4858	187.179199	48.982700	TXS 1226+492	FSRQ	LSP	1.716	opt	···
J1229.0+0202	187.267502	2.045400	3C 273	FSRQ	LSP	0.158	both	999.90 (999.90)
J1229.7-5304	187.444199	−53.070400	AT20G J122939-530332	BL Lac	···	···	none	···
J1230.2+2517	187.559906	25.298300	ON 246	BL Lac	ISP	0.135	both	4.75 (38.09)
J1231.7+2847	187.934906	28.791700	B2 1229+29	BL Lac	ISP	0.236	none	···
J1233.7-0144	188.433899	−1.742800	NVSS J123341-014426	BL Lac	ISP	···	none	···
J1234.0-5735	188.519394	−57.596100	AT20G J123407-573552	BCU	ISP	···	none	···
J1238.1-4541	189.545303	−45.686100	PMN J1238-4541	BL Lac	ISP	···	none	···
J1238.3-1959	189.593597	−19.994499	PMN J1238-1959	BL Lac	LSP	···	opt	···
J1239.5+0443	189.885406	4.728400	MG1 J123931+0443	FSRQ	LSP	1.761	gam	···
J1243.9-0218	190.984497	−2.308200	PMN J1243-0218	BCU	LSP	···	none	···
J1245.1+5709	191.288300	57.158001	1RXS J124510.5+571020	BL Lac	ISP	1.545	none	···
J1246.7-2548	191.688705	−25.801800	PKS 1244-255	FSRQ	LSP	0.635	both	0.38 (29.79)
J1248.9+4840	192.244293	48.669998	87GB 124632.9+485605	BCU	LSP	1.852	none	···
J1249.3-0545	192.326401	−5.762100	GALEXASC J124919.46-054539.7	BCU	···	···	none	···
J1249.8+3707	192.459793	37.130600	2MASS J12494675+3707474	BL Lac	···	0.286	none	···
J1251.3-0201	192.835999	−2.027100	TXS 1248-017	BCU	LSP	0.335	none	···
J1253.2+5301	193.306702	53.017300	S4 1250+53	BL Lac	LSP	···	opt	···
J1253.8+6242	193.466599	62.705200	1RXS J125400.1+624303	BL Lac	LSP	0.867	none	···
J1254.2-2205	193.552094	−22.087200	NVSS J125422-220413	BCU	···	···	none	···
J1254.5+2210	193.636993	22.180799	TXS 1252+224	BL Lac	HSP	0.509	none	···
J1254.9+1138	193.733398	11.649500	ON 187	FSRQ	LSP	0.872	none	···
J1254.9-7141	193.726700	−71.693100	PKS 1251-71	BCU	···	···	none	···
J1256.1-0547	194.041504	−5.788700	3C 279	FSRQ	LSP	0.536	both	−0.89 (8.71)
J1257.2+3646	194.310303	36.770599	RX J1257.3+3647	BL Lac	ISP	0.531	none	···
J1257.8+3228	194.472794	32.472099	ON 393	FSRQ	LSP	0.806	both	−1.31 (14.33)
J1258.6-1759	194.663498	−17.995800	PKS B1256-177	FSRQ	LSP	1.956	gam	···
J1258.8-2219	194.717194	−22.325701	PKS 1256-220	FSRQ	LSP	1.303	both	1.31 (15.83)
J1259.1-2311	194.779800	−23.192499	PKS B1256-229	BL Lac	LSP	0.481	none	···
J1259.7-3223	194.944901	−32.389801	LEDA 4075145	BL Lac	LSP	0.014	gam	···
J1300.4+1416	195.119507	14.270100	OW 197	FSRQ	LSP	1.109	none	···
J1301.6+3336	195.417603	33.609699	MG2 J130126+3337	FSRQ	LSP	1.008	none	···
J1302.8+5748	195.720901	57.814602	TXS 1300+580	BL Lac	LSP	1.088	none	···
J1303.0+2434	195.757095	24.582100	MG2 J130304+2434	BL Lac	LSP	0.993	both	999.90 (999.90)
J1303.6-4622	195.923798	−46.367500	PMN J1303-4621	FSRQ	LSP	1.664	none	···
J1304.3-4353	196.088303	−43.895699	1RXS J130421.2-435308	BL Lac	HSP	···	opt	···
J1304.6-0348	196.171799	−3.813900	PKS 1302-035	FSRQ	LSP	1.250	none	···
J1307.6-4259	196.909607	−42.994999	1RXS J130737.8-425940	BL Lac	HSP	···	none	···
J1308.4-6706	197.110397	−67.108101	PKS 1304-668	BCU	LSP	···	none	···
J1308.5+3547	197.128601	35.791801	5C 12.291	FSRQ	LSP	1.055	gam	···
J1309.4+4305	197.362595	43.084999	B3 1307+433	BL Lac	ISP	0.691	opt	···
J1310.5+3221	197.632401	32.354698	OP 313	FSRQ	LSP	0.997	both	999.90 (999.90)
J1310.7-5553	197.683701	−55.886700	PMN J1310-5552	BCU	HSP	0.104	none	···
J1312.4-2156	198.110794	−21.938000	PKS 1309-216	BL Lac	HSP	1.491	opt	···
J1312.6+4828	198.169403	48.470100	GB 1310+487	BCU	LSP	0.501	none	···

Table A1 – *continued*

4FGL Name	RA deg	Dec deg	Association	Class	SED class	redshift	Flares	Lags days
J1312.8-0425	198.216995	−4.419600	PKS B1310-041	FSRQ	LSP	0.825	gam	···
J1314.7+2348	198.687897	23.812401	TXS 1312+240	BL Lac	ISP	···	opt	···
J1315.1-5333	198.797806	−53.564899	PMN J1315-5334	BL Lac	LSP	···	gam	···
J1315.9-0732	198.986603	−7.546000	NVSS J131552-073301	BL Lac	HSP	···	none	···
J1316.1-3338	199.025208	−33.636501	PKS 1313-333	FSRQ	LSP	1.210	both	−5.33 (20.12)
J1317.6+3428	199.400803	34.467602	S4 1315+34	FSRQ	LSP	1.050	none	···
J1318.2+6754	199.555801	67.915199	87GB 131701.6+681031	BCU	LSP	···	none	···
J1319.5-0045	199.877304	−0.761300	PKS B1317-005	BCU	LSP	0.891	none	···
J1319.8+7759	199.965805	77.988197	NVSS J131921+775823	BL Lac	ISP	···	none	···
J1320.7+3314	200.185394	33.237801	87GB 131814.4+332742	FSRQ	ISP	0.924	none	···
J1321.1+2216	200.295807	22.280800	TXS 1318+225	FSRQ	LSP	0.943	opt	···
J1322.0+8317	200.501495	83.284500	S5 1322+83	FSRQ	LSP	1.024	none	···
J1322.2+0842	200.550995	8.703600	NVSS J132210+084231	FSRQ	LSP	0.325	none	···
J1322.6-0936	200.663696	−9.607500	PKS B1319-093	FSRQ	LSP	1.864	gam	···
J1323.9+1405	200.976196	14.087100	RX J1323.9+1406	BL Lac	HSP	0.470	none	···
J1326.8-5256	201.720093	−52.937599	PMN J1326-5256	BL Lac	LSP	···	none	···
J1326.9+2210	201.729507	22.173201	B2 1324+22	FSRQ	LSP	1.398	none	···
J1329.0-5607	202.267197	−56.118599	PMN J1329-5608	BL Lac	LSP	···	gam	···
J1330.2+7002	202.572693	70.040604	NVSS J133025+700141	BL Lac	HSP	···	none	···
J1330.2-7003	202.561600	−70.058601	PKS 1326-697	BCU	LSP	···	none	···
J1330.7+2933	202.693497	29.553600	FIRST J133101.8+293216	BCU	LSP	···	gam	···
J1332.0-0509	203.019608	−5.161100	PKS 1329-049	FSRQ	LSP	2.150	gam	···
J1332.2+4722	203.059494	47.372799	B3 1330+476	FSRQ	LSP	0.669	none	···
J1332.6-1256	203.154297	−12.943600	PMN J1332-1256	FSRQ	LSP	1.492	gam	···
J1333.2+2725	203.322693	27.422100	MG2 J133305+2725	FSRQ	LSP	0.731	none	···
J1333.7+5056	203.439499	50.936600	CLASS J1333+5057	FSRQ	LSP	1.362	gam	···
J1337.4+5502	204.366806	55.041801	S4 1335+55	FSRQ	LSP	1.100	none	···
J1337.6-1257	204.423996	−12.951700	PKS 1335-127	FSRQ	LSP	0.539	both	8.05 (22.84)
J1337.9-1956	204.488297	−19.945000	PMN J1337-1958	BCU	LSP	···	none	···
J1338.0+6534	204.515594	65.569603	87GB 133543.8+654752	FSRQ	LSP	0.946	none	···
J1338.9+1153	204.732300	11.895600	SDSS J133859.05+115316.7	BL Lac	ISP	···	none	···
J1339.0-2400	204.756302	−24.008499	PKS 1336-237	BCU	LSP	0.657	opt	···
J1339.1-2620	204.799103	−26.335100	PKS 1336-260	FSRQ	LSP	1.510	none	···
J1339.9-0138	204.975601	−1.637800	PKS 1337-013	FSRQ	LSP	1.620	none	···
J1340.4+6926	205.109894	69.444603	TXS 1339+696	BCU	LSP	···	none	···
J1341.8-2053	205.460999	−20.890100	PKS B1339-206	FSRQ	LSP	1.582	none	···
J1344.2-1723	206.060104	−17.397800	PMN J1344-1723	FSRQ	LSP	2.490	none	···
J1345.6-3356	206.408493	−33.945301	NVSS J134543-335643	BL Lac	ISP	···	none	···
J1345.8+0706	206.464798	7.107200	TXS 1343+073	FSRQ	LSP	1.093	none	···
J1347.6-3751	206.913498	−37.863300	PMN J1347-3750	FSRQ	LSP	1.300	opt	···
J1349.5-1131	207.386902	−11.518800	PKS 1346-112	FSRQ	ISP	0.340	none	···
J1350.8+3033	207.714798	30.558800	B2 1348+30B	FSRQ	LSP	0.712	none	···
J1351.0+0029	207.757004	0.487300	PKS 1348+007	FSRQ	LSP	2.084	none	···
J1351.3+1115	207.843399	11.250200	RX J1351.3+1115	BL Lac	HSP	···	none	···
J1351.7-2912	207.942505	−29.210600	PKS 1348-289	BCU	LSP	1.034	none	···
J1352.7-2742	208.190399	−27.705200	PMN J1352-2745	BCU	LSP	···	none	···
J1353.3+1434	208.335495	14.575500	OP 186	BL Lac	LSP	0.405	none	···
J1354.8-1041	208.718002	−10.693200	PKS 1352-104	FSRQ	LSP	0.330	gam	···
J1358.1+7642	209.528305	76.706398	S5 1357+76	FSRQ	LSP	1.585	none	···
J1359.1+5544	209.784500	55.747898	87GB 135720.6+555936	FSRQ	LSP	1.014	opt	···
J1359.7+4012	209.927597	40.215302	87GB 135731.7+402612	FSRQ	LSP	0.407	none	···
J1359.8-3746	209.966797	−37.768101	PMN J1359-3746	BL Lac	ISP	0.334	none	···
J1404.8+6554	211.215805	65.904800	NVSS J140450+655428	BL Lac	LSP	0.363	none	···
J1406.1-2508	211.544495	−25.138599	NVSS J140609-250808	BL Lac	ISP	···	none	···
J1406.6-3934	211.665497	−39.572701	1RXS J140630.3-393508	BL Lac	ISP	0.370	none	···
J1407.6-4301	211.919403	−43.023399	SUMSS J140739-430231	BL Lac	LSP	···	opt	···
J1408.9-0751	212.235596	−7.857500	PKS B1406-076	FSRQ	LSP	1.493	both	22.77 (38.87)
J1410.1+0202	212.528702	2.035400	PKS 1407+022	BL Lac	LSP	···	none	···
J1411.8+5249	212.969193	52.827801	SBS 1410+530	BL Lac	HSP	0.076	none	···
J1412.9+5018	213.240906	50.300999	SDSS J141302.28+501927.4	BCU	···	1.529	none	···
J1415.5+4830	213.899200	48.514198	RX J1415.5+4830	BL Lac	LSP	0.496	none	···
J1418.4+3543	214.622894	35.719200	87GB 141615.9+355650	FSRQ	HSP	2.085	gam	···

Table A1 – *continued*

4FGL Name	RA deg	Dec deg	Association	Class	SED class	redshift	Flares	Lags days
J1418.4-0233	214.605804	−2.559400	NVSS J141826-023336	BL Lac	HSP	0.356	opt	···
J1419.4-0838	214.860001	−8.641700	NVSS J141922-083830	FSRQ	LSP	0.903	both	−2.18 (16.04)
J1419.5+3821	214.894394	38.365700	B3 1417+385	FSRQ	LSP	1.831	none	···
J1419.8+5423	214.955002	54.393700	OQ 530	BL Lac	LSP	0.153	opt	···
J1421.1-1120	215.287201	−11.339300	PMN J1420-1118	BCU	···	···	none	···
J1422.3+3223	215.637100	32.384998	OQ 334	FSRQ	LSP	0.682	both	−1.70 (14.05)
J1423.1+3738	215.792099	37.645199	NVSS J142304+373729	BL Lac	ISP	···	none	···
J1423.5-7829	215.883301	−78.498398	PKS 1418-782	FSRQ	LSP	0.788	both	−0.92 (5.47)
J1424.1-1750	216.029404	−17.844700	NVSS J142412-175010	BL Lac	HSP	0.082	none	···
J1424.2+0433	216.050797	4.562800	TXS 1421+048	BL Lac	LSP	0.665	none	···
J1424.8-6808	216.216904	−68.148903	PKS 1420-679	BCU	LSP	···	none	···
J1427.0+2348	216.755798	23.801300	PKS 1424+240	BL Lac	HSP	0.604	opt	···
J1427.6-3305	216.912994	−33.094002	PKS 1424-328	BL Lac	LSP	···	both	999.90 (999.90)
J1427.7-3215	216.946106	−32.253700	NVSS J142750-321515	BL Lac	ISP	···	none	···
J1427.9-4206	216.986603	−42.105999	PKS 1424-41	FSRQ	LSP	1.522	both	8.38 (23.28)
J1428.9+5406	217.228897	54.111401	S4 1427+543	FSRQ	LSP	3.013	none	···
J1431.1-3120	217.796204	−31.346800	PKS 1428-311	BL Lac	LSP	···	none	···
J1433.0-1801	218.253494	−18.019600	PKS 1430-178	FSRQ	LSP	2.331	none	···
J1434.7+1950	218.675003	19.847799	OQ 253	FSRQ	LSP	1.382	both	0.38 (7.69)
J1436.9+5638	219.229004	56.648998	RBS 1409	BL Lac	···	0.150	none	···
J1438.9+3710	219.740204	37.175201	B2 1436+37B	FSRQ	LSP	2.401	gam	···
J1439.7+4958	219.941101	49.977501	GB6 J1439+4958	BL Lac	LSP	···	opt	···
J1440.0-1530	220.007202	−15.515400	PKS 1437-153	BL Lac	LSP	···	opt	···
J1440.9+0609	220.242004	6.163100	PMN J1440+0610	BL Lac	ISP	0.435	none	···
J1443.9+2501	220.993301	25.029100	PKS 1441+25	FSRQ	LSP	0.939	both	−27.27 (28.54)
J1443.9-3908	220.990799	−39.148102	PKS 1440-389	BL Lac	HSP	0.065	both	999.90 (999.90)
J1445.9-1626	221.497803	−16.449800	PKS B1443-162	BL Lac	LSP	···	none	···
J1446.0-3039	221.522598	−30.661800	PMN J1445-3036	BCU	LSP	···	none	···
J1446.3+3111	221.590698	31.195499	MG2 J144640+3110	BCU	LSP	···	none	···
J1446.7+1719	221.688400	17.323700	S3 1444+17	FSRQ	LSP	1.024	none	···
J1448.0+3608	222.017105	36.134399	RBS 1432	BL Lac	HSP	···	opt	···
J1449.6-2137	222.421997	−21.627100	PKS B1446-214	FSRQ	LSP	0.938	none	···
J1450.4+0910	222.623505	9.181800	TXS 1448+093	FSRQ	LSP	2.611	none	···
J1451.4+6355	222.855392	63.917198	RX J1451.4+6354	BL Lac	LSP	0.650	none	···
J1453.5+3505	223.391998	35.088402	MG2 J145315+3506	FSRQ	LSP	0.721	none	···
J1454.1+1622	223.544296	16.374701	CLASS J1454+1623	FSRQ	LSP	1.276	none	···
J1454.4-3744	223.615799	−37.749901	PKS 1451-375	FSRQ	LSP	0.314	none	···
J1457.4-3539	224.365707	−35.652699	PKS 1454-354	FSRQ	LSP	1.424	both	5.82 (5.73)
J1458.6+3722	224.673294	37.372601	B3 1456+375	BL Lac	LSP	0.333	none	···
J1501.0+2238	225.256699	22.636400	MS 1458.8+2249	BL Lac	ISP	0.235	opt	···
J1503.5+4759	225.895493	47.995899	TXS 1501+481	BL Lac	LSP	0.345	none	···
J1503.6-6427	225.910004	−64.451698	AT20G J150350-642539	BCU	···	···	none	···
J1504.4+1029	226.103302	10.497800	PKS 1502+106	FSRQ	LSP	1.839	both	0.77 (21.70)
J1505.0-3433	226.258102	−34.554600	PMN J1505-3432	BL Lac	LSP	···	none	···
J1506.1+3731	226.534698	37.518299	B2 1504+37	FSRQ	LSP	0.673	gam	···
J1506.6+0813	226.674103	8.225600	PMN J1506+0814	BL Lac	ISP	0.376	none	···
J1507.2+1721	226.820694	17.351900	NVSS J150716+172103	BL Lac	ISP	0.565	none	···
J1508.4+7717	227.102005	77.292900	NVSS J150811+771819	BCU	ISP	···	none	···
J1509.8-2906	227.462601	−29.106899	AT20G J150945-290502	BCU	···	···	none	···
J1510.1+5702	227.542496	57.039799	GB 1508+5714	FSRQ	···	4.313	none	···
J1510.8+7959	227.704697	79.990997	1RXS J151026.3+795946	BCU	LSP	···	none	···
J1510.8-0542	227.706696	−5.710600	PKS 1508-05	FSRQ	LSP	1.191	none	···
J1512.2+0202	228.070206	2.040300	PKS 1509+022	FSRQ	LSP	0.220	opt	···
J1512.9-5639	228.249496	−56.655300	PMN J1512-5640	BCU	LSP	···	none	···
J1513.2-7131	228.314896	−71.520798	PMN J1512-7131	BCU	···	···	none	···
J1513.4-3231	228.369003	−32.526501	PKS 1510-324	FSRQ	LSP	1.153	none	···
J1514.7-3617	228.681198	−36.294899	PMN J1514-3617	BCU	LSP	···	none	···
J1514.8-0949	228.715698	−9.817000	PMN J1514-0948	BL Lac	LSP	···	gam	···
J1514.8-4748	228.700195	−47.814098	PMN J1514-4748	FSRQ	LSP	1.551	none	···
J1516.1+4351	229.049301	43.852699	87GB 151444.4+440102	BL Lac	ISP	···	none	···
J1516.8+3651	229.221695	36.850498	MG2 J151646+3650	BL Lac	LSP	···	none	···
J1516.9+1934	229.244202	19.580500	PKS 1514+197	BL Lac	LSP	···	none	···
J1517.7+6525	229.435593	65.424004	1H 1515+660	BL Lac	HSP	0.702	none	···

Table A1 – *continued*

4FGL Name	RA deg	Dec deg	Association	Class	SED class	redshift	Flares	Lags days
J1517.7-2422	229.425400	−24.372999	AP Librae	BL Lac	LSP	0.048	both	−5.80 (33.85)
J1518.0-2731	229.512405	−27.531300	TXS 1515-273	BL Lac	HSP	···	opt	···
J1520.5+4209	230.134705	42.160000	B3 1518+423	FSRQ	···	0.484	none	···
J1521.8+4338	230.464493	43.634399	B3 1520+437	FSRQ	LSP	2.168	none	···
J1522.1+3144	230.545395	31.739500	B2 1520+31	FSRQ	LSP	1.489	gam	···
J1522.6-2730	230.664200	−27.505899	PKS 1519-273	BL Lac	LSP	1.297	none	···
J1532.7-1319	233.197205	−13.326100	TXS 1530-131	BCU	LSP	···	gam	···
J1534.8+0131	233.724701	1.522400	PKS 1532+01	FSRQ	LSP	1.428	gam	···
J1537.7-7957	234.439499	−79.957497	PMN J1537-7958	BCU	···	···	none	···
J1539.6+2743	234.901901	27.727699	MG2 J153938+2744	FSRQ	LSP	2.196	none	···
J1544.3-0649	236.078506	−6.825500	NVSS J154419-064913	BCU	···	···	opt	···
J1546.1-1003	236.541397	−10.051000	PMN J1546-1003	BL Lac	HSP	···	none	···
J1548.3+1456	237.099899	14.946100	NVSS J154824+145702	BL Lac	ISP	0.230	gam	···
J1548.8-2250	237.201096	−22.847099	PMN J1548-2251	BL Lac	HSP	0.192	none	···
J1549.5+0236	237.385101	2.608400	PKS 1546+027	FSRQ	LSP	0.414	opt	···
J1550.7+0528	237.696503	5.472500	4C +05.64	FSRQ	LSP	1.422	both	999.90 (999.90)
J1553.5-3118	238.392303	−31.311300	1RXS J155333.4-311841	BL Lac	HSP	···	none	···
J1553.6+1257	238.401505	12.952400	PKS 1551+130	FSRQ	LSP	1.290	none	···
J1553.6-2422	238.402603	−24.368700	PKS 1550-242	FSRQ	···	0.332	gam	···
J1555.2-4149	238.824402	−41.828201	PMN J1555-4150	BCU	LSP	···	none	···
J1555.7+1111	238.931305	11.188400	PG 1553+113	BL Lac	HSP	0.360	both	26.87 (38.10)
J1559.9+2319	239.977707	23.319599	87GB 155744.0+232525	BL Lac	···	1.034	opt	···
J1603.8-4903	240.966507	−49.061699	PMN J1603-4904	BL Lac	ISP	···	none	···
J1604.5-4441	241.127701	−44.690300	PMN J1604-4441	BL Lac	LSP	···	gam	···
J1604.6+5714	241.158493	57.238098	GB6 J1604+5714	FSRQ	LSP	0.720	both	22.62 (6.93)
J1606.9+5919	241.734100	59.320099	1RXS J160709.7+592115	BL Lac	ISP	0.132	none	···
J1608.7+1029	242.176407	10.493800	4C +10.45	FSRQ	LSP	1.226	gam	···
J1610.3-3958	242.598099	−39.973701	PMN J1610-3958	FSRQ	LSP	0.518	none	···
J1610.7-6648	242.691895	−66.814697	PMN J1610-6649	BL Lac	HSP	···	none	···
J1612.4-3100	243.100098	−31.001101	NVSS J161219-305937	BL Lac	LSP	···	none	···
J1613.6+3411	243.421097	34.198200	OS 319	FSRQ	LSP	1.399	gam	···
J1617.3-5849	244.348602	−58.825699	MRC 1613-586	FSRQ	LSP	1.414	none	···
J1617.9-7718	244.480606	−77.304001	PKS 1610-77	FSRQ	LSP	1.710	both	−3.25 (4.46)
J1618.0+5139	244.515594	51.665298	TXS 1616+517	FSRQ	LSP	2.556	none	···
J1621.7-1103	245.427307	−11.059200	PMN J1621-1101	BCU	···	···	none	···
J1625.7+4134	246.447296	41.570900	4C +41.32	FSRQ	LSP	2.550	none	···
J1625.7-2527	246.445297	−25.465000	PKS 1622-253	FSRQ	LSP	0.786	none	···
J1626.0-2950	246.514999	−29.848600	PKS B1622-297	FSRQ	LSP	0.815	gam	···
J1626.6-7639	246.655304	−76.650200	PKS 1619-765	BL Lac	ISP	0.105	none	···
J1628.6+7706	247.154495	77.109901	6C B163030.4+771303	BL Lac	LSP	0.400	none	···
J1628.8-6149	247.217102	−61.831299	LQAC 247-061	FSRQ	···	2.578	none	···
J1630.7+5221	247.681503	52.354301	TXS 1629+524	BL Lac	···	1.545	none	···
J1631.2+1046	247.803604	10.775300	MG1 J163119+1051	BCU	LSP	···	none	···
J1632.2+0854	248.059692	8.904400	NVSS J163211+085608	BCU	LSP	···	none	···
J1635.2+3808	248.816803	38.140099	4C +38.41	FSRQ	LSP	1.814	both	−0.75 (17.37)
J1635.6+3628	248.922897	36.479500	MG3 J163554+3629	FSRQ	LSP	3.648	none	···
J1637.7+4717	249.434204	47.291302	4C +47.44	FSRQ	LSP	0.735	gam	···
J1637.7+7326	249.447998	73.441299	RX J1637.9+7326	BL Lac	···	···	none	···
J1638.1+5721	249.525101	57.357700	OS 562	FSRQ	LSP	0.751	none	···
J1639.2+4129	249.823807	41.496399	MG4 J163918+4127	FSRQ	LSP	0.691	none	···
J1640.4+3945	250.119003	39.762600	NRAO 512	FSRQ	LSP	1.660	none	···
J1641.9-0621	250.489197	−6.352900	TXS 1639-062	BL Lac	LSP	···	none	···
J1642.9+3948	250.734100	39.816399	3C 345	FSRQ	LSP	0.593	both	−3.72 (6.07)
J1643.5-0646	250.883408	−6.774900	NVSS J164328-064619	BL Lac	···	0.082	opt	···
J1645.6+6329	251.405106	63.495800	TXS 1645+635	FSRQ	LSP	2.379	none	···
J1647.4-6438	251.870499	−64.645401	PMN J1647-6437	BL Lac	LSP	···	none	···
J1647.5+4950	251.892303	49.833599	SBS 1646+499	BL Lac	LSP	0.049	opt	···
J1648.0+2221	252.022598	22.352301	MG2 J164800+2224	BCU	LSP	0.823	none	···
J1649.4+5235	252.363693	52.590099	87GB 164812.2+524023	BL Lac	ISP	···	opt	···
J1650.3-5045	252.589401	−50.751499	PMN J1650-5044	BL Lac	LSP	···	none	···
J1653.8+3945	253.473801	39.759499	Mkn 501	BL Lac	HSP	0.033	opt	···
J1656.0+2047	254.004593	20.784100	MG2 J165546+2043	BCU	LSP	···	none	···
J1657.0+6010	254.257507	60.167599	RGB J1656+602	FSRQ	LSP	0.623	none	···
J1657.7+4808	254.438293	48.136799	4C +48.41	FSRQ	LSP	1.669	gam	···

Table A1 – *continued*

4FGL Name	RA deg	Dec deg	Association	Class	SED class	redshift	Flares	Lags days
J1659.7-3131	254.945496	−31.520901	NVSS J165949-313047	BCU	LSP	···	none	···
J1700.0+6830	255.021500	68.504204	TXS 1700+685	FSRQ	LSP	0.301	both	2.18 (15.46)
J1701.0+6613	255.260101	66.225502	7C 1700+6616	BCU	···	···	none	···
J1703.6-6213	255.911697	−62.221500	MRC 1659-621	FSRQ	LSP	1.755	none	···
J1704.1+7647	256.036713	76.792297	NVSS J170357+764611	BCU	LSP	···	both	999.90 (999.90)
J1704.2+1234	256.059906	12.575200	NVSS J170409+123421	BL Lac	LSP	0.450	none	···
J1706.1+1000	256.539093	10.007900	NVSS J170556+100006	BCU	···	···	none	···
J1707.5+1649	256.881012	16.820601	MG1 J170732+1649	FSRQ	LSP	0.291	opt	···
J1707.9+0016	256.988586	0.273100	NVSS J170744+001750	BCU	LSP	···	none	···
J1709.7+4318	257.431610	43.310902	B3 1708+433	FSRQ	LSP	1.027	none	···
J1714.0-2029	258.522491	−20.485500	1RXS J171405.2-202747	BCU	HSP	···	none	···
J1716.1+6836	259.031494	68.606300	S4 1716+68	FSRQ	···	0.777	opt	···
J1717.5-3342	259.398499	−33.700298	TXS 1714-336	BL Lac	LSP	···	none	···
J1717.6-5154	259.402588	−51.909000	PMN J1717-5155	FSRQ	LSP	1.158	none	···
J1719.2+1745	259.806213	17.753300	PKS 1717+177	BL Lac	LSP	0.137	both	−4.45 (83.66)
J1722.6+6104	260.662415	61.073399	GB6 J1722+6105	FSRQ	LSP	2.058	none	···
J1722.7+1014	260.686005	10.234600	TXS 1720+102	FSRQ	LSP	0.732	opt	···
J1723.6-7714	260.921906	−77.237602	PKS 1716-771	BCU	LSP	···	both	999.90 (999.90)
J1724.2+4005	261.050903	40.089100	S4 1722+40	FSRQ	LSP	1.049	none	···
J1724.9+7654	261.233093	76.915199	S5 1726+76	FSRQ	LSP	0.680	none	···
J1725.0+1152	261.271301	11.874800	1H 1720+117	BL Lac	HSP	0.180	opt	···
J1725.5+5851	261.387604	58.857800	7C 1724+5854	BL Lac	ISP	0.297	opt	···
J1727.4+4530	261.852112	45.510799	S4 1726+45	FSRQ	LSP	0.717	both	−3.40 (7.67)
J1728.0+1216	262.020203	12.275600	PKS 1725+123	FSRQ	LSP	0.583	none	···
J1728.3+5013	262.077911	50.226700	I Zw 187	BL Lac	HSP	0.055	none	···
J1728.4+0427	262.122009	4.460600	PKS 1725+044	FSRQ	LSP	0.293	none	···
J1728.6-7448	262.152893	−74.803497	MRC 1722-748	BCU	···	···	none	···
J1730.6+0024	262.662811	0.409500	PKS 1728+004	FSRQ	LSP	1.335	none	···
J1733.0-1305	263.263214	−13.085800	PKS 1730-13	FSRQ	LSP	0.902	none	···
J1733.6-6054	263.424591	−60.906502	PMN J1733-6055	BCU	LSP	···	none	···
J1734.3+3858	263.598389	38.976299	B2 1732+38A	FSRQ	LSP	0.976	both	5.76 (22.04)
J1736.0+2033	264.018585	20.555901	NVSS J173605+203301	BL Lac	HSP	···	none	···
J1738.0+8717	264.500885	87.285103	6C B175708+871924	BCU	···	···	none	···
J1738.2+4000	264.559998	40.009899	NVSS J173807+400312	BCU	ISP	···	none	···
J1739.5+4955	264.885986	49.931999	S4 1738+49	FSRQ	LSP	1.545	both	999.90 (999.90)
J1740.5+5211	265.135712	52.192699	4C +51.37	FSRQ	LSP	1.381	both	999.90 (999.90)
J1740.6+5346	265.159088	53.770100	87GB 173932.3+534742	BL Lac	LSP	···	none	···
J1744.6-5713	266.155487	−57.232101	PMN J1744-5715	BL Lac	ISP	···	none	···
J1746.8-5235	266.719910	−52.586800	PMN J1747-5236	BCU	LSP	···	none	···
J1747.1-5453	266.786713	−54.894402	PMN J1747-5450	BCU	LSP	···	none	···
J1748.0+3403	267.010590	34.064098	MG2 J174803+3403	FSRQ	LSP	2.763	opt	···
J1748.6+7005	267.157990	70.096901	S4 1749+70	BL Lac	ISP	0.770	opt	···
J1749.0+4321	267.255402	43.361599	B3 1747+433	BL Lac	LSP	···	none	···
J1751.5+0938	267.877594	9.645600	OT 081	BL Lac	LSP	0.322	both	2.02 (15.08)
J1751.6+2921	267.903900	29.358200	MG2 J175143+2921	BCU	···	···	none	···
J1753.7+2847	268.433289	28.796700	B2 1751+28	FSRQ	LSP	1.118	gam	···
J1754.2+3212	268.553192	32.200699	RX J1754.1+3212	BL Lac	ISP	···	opt	···
J1754.7+3444	268.678986	34.741699	MG2 J175448+3442	BCU	···	0.016	none	···
J1759.1-4822	269.783203	−48.377701	PMN J1758-4820	BCU	···	···	none	···
J1800.6+7828	270.173004	78.467400	S5 1803+784	BL Lac	LSP	0.680	both	1.14 (11.79)
J1801.5+4404	270.377106	44.074699	S4 1800+44	FSRQ	LSP	0.663	both	−0.26 (20.25)
J1802.6-3940	270.671112	−39.668701	PMN J1802-3940	FSRQ	LSP	0.296	none	···
J1803.4-6510	270.864014	−65.173203	PKS 1758-651	FSRQ	LSP	1.199	none	···
J1806.8+6949	271.710785	69.827003	3C 371	BL Lac	LSP	0.050	opt	···
J1807.2+6429	271.808685	64.498802	7C 1807+6428	BL Lac	ISP	···	none	···
J1808.1-5013	272.032196	−50.220699	PMN J1808-5011	FSRQ	LSP	1.606	none	···
J1808.2+3500	272.065704	35.010399	MG2 J180813+3501	BL Lac	ISP	···	opt	···
J1809.7+2910	272.441498	29.170900	MG2 J180948+2910	BL Lac	···	···	none	···
J1811.0+1608	272.750000	16.147800	87GB 180835.5+160714	BL Lac	ISP	···	none	···
J1811.3+0340	272.825989	3.679400	NVSS J181118+034113	BL Lac	HSP	···	none	···
J1813.5+3144	273.387207	31.749701	B2 1811+31	BL Lac	HSP	0.117	both	−6.97 (42.66)
J1813.6+0614	273.408386	6.240800	TXS 1811+062	BL Lac	LSP	···	none	···
J1814.4+2953	273.615204	29.894300	B2 1811+29	FSRQ	···	1.351	none	···
J1816.9-4942	274.243896	−49.715801	PMN J1816-4943	FSRQ	LSP	1.700	none	···

Table A1 – *continued*

4FGL Name	RA deg	Dec deg	Association	Class	SED class	redshift	Flares	Lags days
J1818.6+0903	274.674805	9.065000	MG1 J181841+0903	FSRQ	LSP	0.354	none	···
J1823.6-3453	275.910889	−34.895199	NVSS J182338-345412	BCU	HSP	···	none	···
J1824.1+5651	276.039307	56.858501	4C +56.27	BL Lac	LSP	0.663	both	1.64 (7.99)
J1825.1-5231	276.294586	−52.528999	PKS 1821-525	BCU	LSP	···	none	···
J1829.2-5813	277.310791	−58.232300	PKS 1824-582	FSRQ	···	1.531	both	−4.67 (3.97)
J1830.0+1324	277.511993	13.413800	MG1 J183001+1323	BL Lac	ISP	···	none	···
J1830.1+0617	277.536285	6.287800	TXS 1827+062	FSRQ	LSP	0.745	none	···
J1830.2-4443	277.550415	−44.720001	PMN J1830-4441	BCU	LSP	···	none	···
J1834.7-5858	278.687408	−58.981800	PKS 1830-589	BL Lac	LSP	···	none	···
J1838.8+4802	279.714111	48.041199	GB6 J1838+4802	BL Lac	HSP	0.300	opt	···
J1839.6-7107	279.914215	−71.124298	PKS 1831-711	FSRQ	LSP	1.356	none	···
J1840.6-5545	280.174805	−55.751801	PMN J1841-5544	BCU	···	···	none	···
J1841.0+6115	280.253113	61.252201	87GB 184000.4+611120	BCU	···	···	none	···
J1841.8+3218	280.453003	32.300999	RX J1841.7+3218	BL Lac	HSP	···	none	···
J1842.4-5840	280.611206	−58.680199	1RXS J184230.6-584202	BL Lac	···	0.421	none	···
J1844.4+1547	281.117401	15.788800	NVSS J184425+154646	BL Lac	HSP	···	none	···
J1848.4+3217	282.105011	32.294998	B2 1846+32A	FSRQ	LSP	0.798	none	···
J1848.5+3243	282.145599	32.730900	B2 1846+32B	FSRQ	LSP	0.981	both	0.81 (2.88)
J1848.5+6537	282.133209	65.631302	NVSS J184822+653702	BL Lac	···	0.364	none	···
J1849.2+6705	282.319214	67.090897	S4 1849+67	FSRQ	LSP	0.657	both	−11.22 (16.73)
J1849.4+2745	282.354309	27.754200	MG2 J184929+2748	BL Lac	LSP	···	none	···
J1849.4-4313	282.362305	−43.221401	PMN J1849-4314	BL Lac	LSP	···	opt	···
J1852.4+4856	283.115997	48.935001	S4 1851+48	FSRQ	LSP	1.250	none	···
J1858.3-2511	284.575195	−25.199100	PMN J1858-2511	BCU	LSP	···	none	···
J1902.9-6748	285.743195	−67.806801	PMN J1903-6749	FSRQ	LSP	0.255	both	0.60 (31.88)
J1903.2+5540	285.807709	55.677299	TXS 1902+556	BL Lac	LSP	···	none	···
J1904.1+3627	286.034302	36.452599	MG2 J190411+3627	BL Lac	···	0.078	none	···
J1911.2-2006	287.807800	−20.113701	PKS B1908-201	FSRQ	LSP	1.119	gam	···
J1912.1-0803	288.028412	−8.058900	PMN J1912-0804	BCU	···	···	none	···
J1912.4-1222	288.118500	−12.367800	TXS 1909-124	BCU	···	···	opt	···
J1913.0-8009	288.269989	−80.157402	PKS 1903-80	FSRQ	LSP	1.756	gam	···
J1913.4-3629	288.350708	−36.488499	PMN J1913-3630	BCU	LSP	···	none	···
J1917.7-1921	289.438385	−19.362801	1H 1914-194	BL Lac	HSP	0.137	opt	···
J1918.2-4111	289.564301	−41.189301	PMN J1918-4111	BL Lac	LSP	···	none	···
J1921.8-1607	290.463287	−16.123100	PMN J1921-1607	BL Lac	ISP	···	none	···
J1922.5-7453	290.627899	−74.887604	1RXS J192244.1-74541	BCU	HSP	···	none	···
J1923.5-2104	290.876312	−21.070999	TXS 1920-211	FSRQ	LSP	0.874	none	···
J1924.8-2914	291.213593	−29.246799	PKS B1921-293	FSRQ	LSP	0.353	none	···
J1926.8+6154	291.709686	61.914600	87GB 192614.4+614823	BL Lac	HSP	···	opt	···
J1927.5+6117	291.882202	61.293999	S4 1926+61	BL Lac	LSP	···	opt	···
J1931.1+0937	292.783997	9.631400	RX J1931.1+0937	BL Lac	HSP	···	none	···
J1933.2-4539	293.314301	−45.650799	PKS 1929-457	FSRQ	LSP	0.652	none	···
J1934.3+6541	293.595215	65.688797	TXS 1933+655	FSRQ	LSP	1.687	gam	···
J1936.9-4720	294.241608	−47.340000	PMN J1936-4719	BL Lac	···	0.265	none	···
J1937.2-3958	294.309204	−39.982498	PKS 1933-400	FSRQ	LSP	0.965	none	···
J1939.5-1525	294.877197	−15.425600	PKS 1936-15	FSRQ	LSP	1.657	gam	···
J1941.3-6210	295.346802	−62.175301	PKS 1936-623	BL Lac	LSP	···	gam	···
J1942.1+4011	295.539001	40.198399	87GB 194033.4+400351	BCU	ISP	···	none	···
J1942.7+1033	295.696014	10.558400	87GB 194024.3+102612	BL Lac	HSP	···	none	···
J1944.9-2143	296.229492	−21.721600	1RXS J194455.3-214318	BL Lac	···	0.410	none	···
J1945.1-4007	296.292206	−40.120899	AT20G J194519-400557	BCU	LSP	···	none	···
J1949.5+0906	297.390198	9.105400	1RXS J194934.1+090655	BL Lac	HSP	···	none	···
J1951.8-0511	297.964996	−5.184400	PMN J1951-0509	FSRQ	LSP	1.083	opt	···
J1954.6-1122	298.669312	−11.381500	TXS 1951-115	BL Lac	LSP	0.683	opt	···
J1955.1-1604	298.777405	−16.071501	1RXS J195500.6-160328	BL Lac	HSP	···	none	···
J1955.2+1358	298.820099	13.982400	87GB 195252.4+135009	FSRQ	LSP	0.743	none	···
J1957.1-3231	299.286407	−32.524601	PKS 1953-325	FSRQ	LSP	1.242	none	···
J1958.0-3845	299.502594	−38.754700	PKS 1954-388	FSRQ	LSP	0.630	both	9.30 (16.55)
J1958.1-0711	299.533813	−7.192600	NVSS J195801-071348	BCU	···	···	none	···
J1958.3-3010	299.581207	−30.181000	1RXS J195815.6-301119	BL Lac	···	0.119	opt	···
J1959.0+3844	299.766296	38.736801	LQAC 299+038	BCU	LSP	···	none	···
J1959.1-4247	299.796295	−42.785198	PMN J1959-4246	FSRQ	LSP	2.174	none	···
J2000.0+6508	300.010986	65.147903	1ES 1959+650	BL Lac	HSP	0.047	both	999.90 (999.90)

Table A1 – *continued*

4FGL Name	RA deg	Dec deg	Association	Class	SED class	redshift	Flares	Lags days
J2000.9-1748	300.234589	−17.816401	PKS 1958-179	FSRQ	LSP	0.652	both	−2.72 (19.24)
J2001.2+4353	300.301788	43.886200	MG4 J200112+4352	BL Lac	HSP	···	none	···
J2005.1+7003	301.277588	70.062401	1RXS J200504.0+700445	BL Lac	HSP	···	none	···
J2005.5+7752	301.393005	77.882896	S5 2007+77	BL Lac	LSP	0.342	both	999.90 (999.90)
J2005.8+6424	301.463989	64.400200	87GB 200541.3+641601	FSRQ	LSP	1.574	none	···
J2005.9-2309	301.476196	−23.153099	TXS 2002-233	FSRQ	LSP	0.830	none	···
J2007.2+6607	301.814789	66.117798	TXS 2007+659	FSRQ	LSP	1.325	gam	···
J2007.3-7728	301.846588	−77.477997	PKS 2000-776	BCU	LSP	···	none	···
J2009.4-4849	302.359497	−48.824799	PKS 2005-489	BL Lac	HSP	0.071	opt	···
J2009.9+3544	302.489197	35.745998	B2 2008+35	BCU	···	···	none	···
J2010.0+7229	302.515900	72.487396	4C +72.28	BL Lac	LSP	···	none	···
J2012.0+4629	303.020386	46.487999	7C 2010+4619	BL Lac	ISP	···	both	999.90 (999.90)
J2012.2-1646	303.071899	−16.772900	PMN J2012-1646	BL Lac	LSP	···	none	···
J2015.3-1432	303.826111	−14.541700	NVSS J201525-143202	BL Lac	···	···	none	···
J2016.3-0903	304.098206	−9.062200	PMN J2016-0903	BL Lac	ISP	0.367	opt	···
J2022.3-4513	305.591095	−45.222801	PMN J2022-4513	BL Lac	ISP	···	opt	···
J2022.5+7612	305.645905	76.200699	S5 2023+760	BL Lac	LSP	0.594	opt	···
J2023.6-1139	305.903198	−11.658500	PMN J2023-1140	FSRQ	LSP	0.698	none	···
J2024.6-3252	306.158112	−32.874001	PKS 2021-330	FSRQ	LSP	1.465	none	···
J2024.8-6459	306.200989	−64.991302	PMN J2024-6458	BCU	LSP	···	none	···
J2025.2+0317	306.308502	3.289300	PKS 2022+031	FSRQ	LSP	2.210	none	···
J2025.3+3341	306.341187	33.689098	B2 2023+33	BL Lac	LSP	0.219	none	···
J2025.6-0735	306.421997	−7.594500	PKS 2023-07	FSRQ	LSP	1.388	both	4.40 (9.72)
J2029.5+4925	307.375000	49.422100	MG4 J202932+4925	BL Lac	LSP	···	none	···
J2030.2-0620	307.564087	−6.343200	TXS 2027-065	FSRQ	LSP	0.667	none	···
J2031.2-4121	307.811188	−41.357399	SUMSS J203056-411906	BCU	···	···	none	···
J2032.0+1219	308.003998	12.327900	PKS 2029+121	BL Lac	LSP	1.215	none	···
J2034.6+1154	308.650391	11.903500	TXS 2032+117	FSRQ	LSP	0.607	both	1.79 (5.76)
J2035.4+1056	308.851715	10.938000	PKS 2032+107	FSRQ	LSP	0.601	gam	···
J2036.4+6553	309.103210	65.883400	87GB 203539.4+654245	BL Lac	ISP	···	none	···
J2038.7+5117	309.693787	51.285099	3C 418	FSRQ	LSP	1.686	none	···
J2039.0-1046	309.758087	−10.773100	TXS 2036-109	BL Lac	LSP	···	none	···
J2040.5-1705	310.136414	−17.090099	TXS 2037-172	BCU	LSP	···	none	···
J2046.8-4258	311.720490	−42.969398	2MASS J20464397-4257134	BL Lac	···	···	none	···
J2049.9+1002	312.478210	10.040700	PKS 2047+098	BL Lac	LSP	···	none	···
J2050.4-2627	312.610413	−26.465900	PMN J2050-2628	FSRQ	LSP	1.633	none	···
J2052.2-5533	313.067413	−55.562401	PMN J2052-5533	BCU	···	···	gam	···
J2056.2-4714	314.071503	−47.236900	PKS 2052-47	FSRQ	LSP	1.489	both	4.67 (11.43)
J2056.5-0202	314.142212	−2.035500	PMN J2056-0205	BCU	LSP	···	none	···
J2103.8-6233	315.954712	−62.556301	PMN J2103-6232	BL Lac	ISP	···	none	···
J2104.0-3546	316.009613	−35.767799	NVSS J210353-354620	BCU	LSP	···	opt	···
J2108.2-2454	317.061493	−24.908100	AT20G J210812-245233	BCU	···	···	none	···
J2108.5+1434	317.147614	14.581200	OX 110	FSRQ	LSP	2.017	none	···
J2110.3+0808	317.575989	8.149800	PMN J2110+0810	FSRQ	LSP	1.580	none	···
J2114.8+2831	318.716492	28.522200	B2 2112+28B	FSRQ	LSP	2.345	opt	···
J2115.4+2932	318.873688	29.545601	B2 2113+29	FSRQ	LSP	1.514	both	999.90 (999.90)
J2119.6-1105	319.924103	−11.091000	PKS 2116-11	FSRQ	LSP	1.844	none	···
J2120.6-1254	320.153595	−12.909700	NVSS J212035-125443	BCU	···	0.582	none	···
J2121.0+1901	320.259796	19.032400	OX 131	FSRQ	LSP	2.180	none	···
J2123.6+0535	320.920593	5.592000	OX 036	FSRQ	LSP	1.941	none	···
J2126.3-4605	321.594788	−46.097801	PKS 2123-463	FSRQ	LSP	1.670	none	···
J2127.7+3612	321.931091	36.212502	B2 2125+35	BL Lac	HSP	···	none	···
J2130.4-4241	322.601196	−42.690399	SUMSS J213017-424319	BCU	···	···	none	···
J2131.0-2746	322.752991	−27.772699	RBS 1751	BL Lac	HSP	0.380	none	···
J2131.5-0916	322.891113	−9.268400	RBS 1752	BL Lac	HSP	0.449	none	···
J2133.9+6646	323.479309	66.777603	NVSS J213349+664706	BL Lac	HSP	···	none	···
J2134.2-0154	323.569885	−1.904200	PKS 2131-021	BL Lac	LSP	1.283	opt	···
J2134.5-2130	323.641388	−21.502899	NVSS J213430-213032	BL Lac	ISP	···	none	···
J2135.3-5006	323.836212	−50.101501	PMN J2135-5006	FSRQ	LSP	2.181	none	···
J2136.5+4259	324.141113	42.993801	TXS 2134+428	BCU	LSP	···	gam	···
J2139.4-4235	324.854614	−42.589500	MH 2136-428	BL Lac	ISP	···	both	999.90 (999.90)
J2141.7-6410	325.430511	−64.179199	PMN J2141-6411	BCU	LSP	···	gam	···
J2141.8-3727	325.462189	−37.454498	PKS 2138-377	FSRQ	LSP	0.423	none	···

Table A1 – *continued*

4FGL Name	RA deg	Dec deg	Association	Class	SED class	redshift	Flares	Lags days
J2143.1-3929	325.793091	−39.488201	PMN J2143-3929	BL Lac	HSP	0.429	none	···
J2143.5+1743	325.894196	17.730600	OX 169	FSRQ	LSP	0.211	gam	···
J2144.2+3132	326.064606	31.545700	MG3 J214415+3132	BL Lac	ISP	···	none	···
J2145.0-3356	326.253296	−33.943901	PMN J2145-3357	FSRQ	LSP	1.360	none	···
J2146.5-1344	326.644897	−13.734700	NVSS J214637-134359	BL Lac	···	0.420	none	···
J2146.8+0425	326.708008	4.426600	MG1 J214653+0427	BCU	LSP	···	none	···
J2147.1+0931	326.782898	9.518100	PKS 2144+092	FSRQ	LSP	1.113	none	···
J2147.3-7536	326.826813	−75.602402	PKS 2142-75	FSRQ	LSP	1.138	both	1.67 (2.48)
J2149.1+6104	327.289703	61.070499	4C +60.32	BCU	···	···	none	···
J2149.6+0323	327.423615	3.395900	PKS B2147+031	BL Lac	LSP	···	none	···
J2149.7+1917	327.444092	19.285900	TXS 2147+191	BCU	LSP	···	none	···
J2150.7-2810	327.698395	−28.172800	PMN J2150-2812	FSRQ	LSP	0.865	none	···
J2151.7-2749	327.925110	−27.823400	PMN J2151-2742	FSRQ	LSP	1.485	none	···
J2151.8-3027	327.965515	−30.459999	PKS 2149-306	FSRQ	LSP	2.345	none	···
J2153.8-1137	328.460907	−11.630600	PMN J2153-1136	FSRQ	LSP	1.582	none	···
J2156.3-0036	329.079712	−0.603900	PKS B2153-008	FSRQ	LSP	0.495	none	···
J2157.5+3127	329.386200	31.455200	B2 2155+31	FSRQ	LSP	1.486	none	···
J2158.1-1501	329.527496	−15.023700	PKS 2155-152	FSRQ	LSP	0.672	opt	···
J2158.8-3013	329.714111	−30.225100	PKS 2155-304	BL Lac	HSP	0.116	both	5.57 (52.07)
J2159.8-4751	329.962311	−47.851799	PMN J2200-4751	BCU	LSP	···	none	···
J2200.1+2138	330.030701	21.638201	TXS 2157+213	BL Lac	LSP	···	none	···
J2201.5-8339	330.378693	−83.663101	PKS 2155-83	FSRQ	LSP	1.865	both	−0.67 (3.08)
J2201.8+5048	330.453186	50.805302	NRAO 676	FSRQ	LSP	1.899	none	···
J2202.7+4216	330.694611	42.282101	BL Lac	BL Lac	LSP	0.069	both	−0.19 (24.32)
J2203.4+1725	330.872101	17.431801	PKS 2201+171	FSRQ	LSP	1.076	none	···
J2205.0+7432	331.271912	74.546204	S5 2205+74	BCU	LSP	···	none	···
J2206.8-0032	331.708710	−0.546100	PMN J2206-0031	BL Lac	LSP	1.053	opt	···
J2207.5-5346	331.892212	−53.771900	PKS 2204-54	FSRQ	LSP	1.215	none	···
J2207.6+0053	331.913696	0.890700	PMN J2207+0052	FSRQ	···	···	none	···
J2209.8-5028	332.473511	−50.470200	PMN J2210-5030	BCU	···	···	none	···
J2211.2-1325	332.816803	−13.418900	PKS 2208-137	FSRQ	LSP	0.392	opt	···
J2212.9-2526	333.226105	−25.433500	PKS 2210-25	FSRQ	LSP	1.833	opt	···
J2216.9+2421	334.238007	24.357500	B2 2214+24B	BL Lac	LSP	0.505	none	···
J2219.2+1806	334.812714	18.102600	MG1 J221916+1806	FSRQ	LSP	1.071	none	···
J2221.5-5225	335.390900	−52.430698	PMN J2221-5224	BL Lac	HSP	0.340	none	···
J2221.9-3504	335.497009	−35.071201	NVSS J222227-350942	FSRQ	···	0.298	none	···
J2222.8+1209	335.709808	12.156800	TXS 2220+119	BCU	LSP	···	none	···
J2225.6+2120	336.413605	21.341801	PKS 2223+21	FSRQ	LSP	1.959	none	···
J2225.7-0457	336.432098	−4.953700	3C 446	FSRQ	LSP	1.404	none	···
J2228.6-1636	337.165894	−16.607300	2MASS J22283018-1636432	BL Lac	ISP	0.525	none	···
J2229.7-0832	337.425812	−8.544700	PKS 2227-08	FSRQ	LSP	1.560	gam	···
J2230.9-7815	337.728210	−78.259399	PKS 2225-785	FSRQ	LSP	···	none	···
J2231.0-4416	337.757996	−44.279099	PKS 2227-445	FSRQ	LSP	1.326	opt	···
J2232.6+1143	338.152496	11.730600	CTA 102	FSRQ	LSP	1.037	both	−2.67 (31.53)
J2234.1-2656	338.542511	−26.937500	PMN J2234-2656	BL Lac	LSP	···	none	···
J2235.1-0623	338.799408	−6.395500	PMN J2235-0623	BCU	LSP	···	none	···
J2235.3-4836	338.840912	−48.601501	PKS 2232-488	FSRQ	LSP	0.510	none	···
J2235.8-3627	338.970795	−36.460499	NVSS J223554-362901	BL Lac	ISP	···	none	···
J2236.3+2828	339.096191	28.483200	B2 2234+28A	FSRQ	LSP	0.790	both	−0.91 (20.82)
J2236.4-2309	339.124603	−23.155199	PMN J2236-2309	BCU	LSP	···	gam	···
J2236.5-1433	339.144409	−14.555700	PKS 2233-148	BL Lac	LSP	0.325	both	11.86 (21.82)
J2237.0-3921	339.268585	−39.356998	NVSS J223708-392137	FSRQ	LSP	0.297	none	···
J2243.4-2544	340.865387	−25.736300	PKS 2240-260	BL Lac	LSP	0.774	opt	···
J2243.9+2021	340.989502	20.356501	RGB J2243+203	BL Lac	HSP	···	gam	···
J2244.2+4057	341.061401	40.959702	TXS 2241+406	FSRQ	LSP	1.171	both	−2.60 (11.93)
J2248.7-3235	342.192810	−32.592602	PKS 2245-328	FSRQ	LSP	2.268	none	···
J2248.9+2106	342.246887	21.121401	PKS 2246+208	FSRQ	LSP	1.274	both	−4.65 (5.35)
J2250.0+3825	342.514191	38.424702	B3 2247+381	BL Lac	HSP	0.119	none	···
J2250.0-1250	342.504913	−12.848500	PKS 2247-131	BCU	LSP	···	gam	···
J2250.4-4206	342.606201	−42.109501	PMN J2250-4206	BL Lac	ISP	0.119	none	···
J2250.7-2806	342.690308	−28.111401	PMN J2250-2806	BL Lac	LSP	0.525	none	···
J2251.2+5550	342.803894	55.843102	87GB 224837.7+553415	BCU	···	···	none	···
J2251.5-4928	342.878906	−49.469101	SUMSS J225128-492912	BL Lac	ISP	···	none	···

Table A1 – *continued*

4FGL Name	RA deg	Dec deg	Association	Class	SED class	redshift	Flares	Lags days
J2253.2-1232	343.308411	−12.541600	TXS 2250-127	BCU	LSP	···	opt	···
J2253.9+1609	343.496307	16.150600	3C 454.3	FSRQ	LSP	0.859	both	−1.52 (12.98)
J2254.8-2725	343.717987	−27.417101	NVSS J225453-272509	BL Lac	ISP	0.333	none	···
J2258.1-2759	344.528809	−27.984301	PKS 2255-282	FSRQ	LSP	0.926	both	6.68 (22.48)
J2258.5-8247	344.638885	−82.784401	PMN J2258-8246	BCU	ISP	···	none	···
J2259.8-1552	344.952606	−15.880900	GALEXASC J225957.26-155332.5	BCU	LSP	···	opt	···
J2300.7-2645	345.182312	−26.750200	PKS 2257-270	FSRQ	LSP	1.476	none	···
J2301.0-0158	345.262695	−1.975800	PKS B2258-022	FSRQ	LSP	0.778	both	−1.45 (27.96)
J2304.6+3704	346.172607	37.082600	1RXS J230437.1+370506	BL Lac	HSP	···	none	···
J2307.6+1451	346.922211	14.864400	MG1 J230734+1449	BL Lac	LSP	0.503	none	···
J2311.0+0205	347.766113	2.099500	NVSS J231101+020504	BL Lac	LSP	···	opt	···
J2311.0+3425	347.768188	34.422298	B2 2308+34	FSRQ	LSP	1.817	both	2.95 (13.50)
J2311.7+2604	347.930786	26.083099	MG3 J231144+2604	BCU	LSP	1.747	none	···
J2312.5+7241	348.139587	72.692299	CRATES J2312+7241	BCU	LSP	···	none	···
J2313.5+3945	348.399689	39.764400	87GB 231102.6+393314	BCU	···	···	none	···
J2315.6-5018	348.914001	−50.312698	PKS 2312-505	BL Lac	LSP	0.811	none	···
J2317.4-4533	349.356506	−45.562302	SUMSS J231731-453400	BL Lac	HSP	···	none	···
J2318.2+1915	349.556793	19.256001	TXS 2315+189	BCU	LSP	2.163	none	···
J2321.5-1619	350.385406	−16.317600	NVSS J232137-161935	BL Lac	···	0.694	none	···
J2321.7-6438	350.433197	−64.645302	PMN J2321-6438	BL Lac	ISP	···	none	···
J2321.9+3204	350.477905	32.073700	B2 2319+31	FSRQ	LSP	1.489	gam	···
J2322.6-0735	350.657593	−7.590700	PMN J2322-0736	BCU	LSP	···	none	···
J2322.8-4916	350.707703	−49.272499	SUMSS J232254-491629	BL Lac	HSP	0.380	none	···
J2323.6-0617	350.915710	−6.295300	TXS 2321-065	FSRQ	LSP	2.144	none	···
J2323.8+4210	350.974915	42.182598	1ES 2321+419	BL Lac	HSP	0.059	opt	···
J2324.7+0801	351.189606	8.028200	PMN J2324+0801	BL Lac	ISP	···	none	···
J2324.7-4041	351.181702	−40.683399	1ES 2322-409	BL Lac	HSP	0.174	opt	···
J2325.2+3957	351.315399	39.954201	B3 2322+396	BL Lac	LSP	···	none	···
J2325.4-3559	351.358612	−35.987801	CTS 0490	FSRQ	LSP	0.360	none	···
J2325.4-4800	351.350098	−48.002201	PKS 2322-482	BL Lac	ISP	0.221	opt	···
J2325.7+1821	351.436005	18.365400	MG1 J232550+1822	BCU	LSP	···	opt	···
J2326.2+0113	351.574799	1.221600	SDSS J232625.63+011208.6	BCU	LSP	0.335	opt	···
J2327.5+0939	351.895905	9.654300	PKS 2325+093	FSRQ	LSP	1.843	opt	···
J2328.3-4036	352.081696	−40.603699	PKS 2325-408	FSRQ	LSP	1.972	opt	···
J2329.3-4733	352.339386	−47.555801	PKS 2326-477	FSRQ	LSP	1.302	none	···
J2330.2+7759	352.568207	77.994698	WN B2329.2+7743	BCU	···	···	none	···
J2330.5+1102	352.628693	11.047900	4C +10.73	FSRQ	LSP	1.489	none	···
J2331.0-2147	352.763214	−21.795300	PMN J2331-2148	FSRQ	LSP	0.563	opt	···
J2334.2+0736	353.557312	7.602000	TXS 2331+073	FSRQ	LSP	0.401	none	···
J2334.8+1432	353.723297	14.534600	NVSS J233453+143214	BL Lac	LSP	0.415	none	···
J2335.4-0128	353.868805	−1.476000	PKS 2332-017	FSRQ	LSP	1.182	none	···
J2336.6-4115	354.163605	−41.257900	PKS 2333-415	FSRQ	LSP	1.406	none	···
J2338.0-0230	354.508514	−2.510600	PKS 2335-027	FSRQ	LSP	1.071	none	···
J2343.7-5624	355.934906	−56.404800	PKS 2340-567	BCU	LSP	1.240	none	···
J2345.2-1555	356.303009	−15.918200	PMN J2345-1555	FSRQ	LSP	0.621	both	2.28 (12.38)
J2347.0+5141	356.765900	51.696602	1ES 2344+514	BL Lac	HSP	0.044	none	···
J2348.0-1630	357.015991	−16.516100	PKS 2345-16	FSRQ	LSP	0.576	both	8.38 (11.04)
J2348.1-4934	357.037201	−49.570000	PKS 2346-498	BCU	LSP	···	none	···
J2349.2+4535	357.304993	45.597900	TXS 2346+453	BL Lac	···	···	none	···
J2349.4+0534	357.355804	5.579000	TXS 2346+052	FSRQ	LSP	0.419	none	···
J2350.6-3005	357.664886	−30.087000	LEDA 3231681	BL Lac	HSP	0.224	none	···
J2352.0+1750	358.013214	17.839399	CLASS J2352+1749	BL Lac	ISP	···	none	···
J2357.8-5311	359.463013	−53.191898	PKS 2355-534	FSRQ	LSP	1.006	none	···
J2358.3+3830	359.588287	38.509701	B3 2355+382	BL Lac	···	0.200	none	···
J2358.3-1021	359.582214	−10.361600	PKS 2355-106	FSRQ	LSP	1.638	opt	···
J2359.0+3922	359.754791	39.366901	B2 2356+39	FSRQ	LSP	1.198	none	···

Note. The first column gives the 4FGL name, followed by its coordinates in columns 2 and 3. In Column 4, 5, 6, we list the associated source to the γ-ray emissions, the sources class (BL Lac: BL Lac type, FSRQ: flat-spectrum radio quasars, BUC: blazar candidates of uncertain type), and the SED class (LSP: low-synchrotron peaked blazars, ISP: intermediate synchrotron peaked blazars, and HSP: high-synchrotron peaked blazars). In Column 7, the redshift is given. In Columns 8, the presence of significant flares in the optical and γ-rays light curves is display (both, opt, gam, none). Finally, in Column 9, we display the rest-frame time lag in days between optical and γ-rays flares, where a positive $\tau_{\rm lag}$ corresponds to the γ-ray emission leading to the optical emission.

Table B1. 'Orphan' flare golden sample properties.

4FGL Name	Band	Peak (MJD)	width (d)	label Fig. 7
20J0011.4+0057	gam	57564	15	A
20J0038.2−2459	opt	57930	45	a
20J0050.7−0929	opt	56477	19	b
20J0102.8+5824	opt	59124	171	c
20J0108.6+0134	gam	57581	258	B
20J0118.9−2141	opt	58349	109	d
20J0133.1−5201	gam	57764	12	C
20J0133.1−5201	gam	58077	19	C
20J0211.2+1051	opt	56882	48	e
20J0211.2+1051	opt	57050	27	e
20J0217.8+0144	opt	57758	30	f
20J0229.5−3644	gam	57212	22	D
20J0303.4−2407	opt	58701	66	g
20J0325.7+2225	gam	58460	6	E
20J0405.6−1308	gam	57574	22	F
20J0405.6−1308	gam	59571	9	F
20J0440.3−4333	gam	58365	54	G
20J0457.0−2324	opt	57037	16	h
20J0457.0−2324	opt	57252	60	h
20J0501.2−0158	gam	57258	9	H
20J0538.8−4405	opt	57744	51	i
20J0539.9−2839	gam	59208	15	I
20J0539.9−2839	gam	59319	9	I
20J0719.3+3307	opt	57324	27	j
20J0742.6+5443	opt	57106	27	k
20J0839.8+0105	opt	58448	36	l
20J0842.3−6053	gam	59600	12	J
20J0854.8+2006	opt	58947	142	m
20J0910.8+3859	opt	57090	69	n
20J0912.2+4127	gam	57318	12	K
20J0921.6+6216	gam	57752	30	L
20J0942.3−0800	opt	57722	37	o
20J1058.4+0133	gam	56700	63	M
20J1153.3−1104	gam	58467	21	N
20J1159.2−2227	gam	59332	34	O
20J1218.5−0119	opt	58872	36	p
20J1238.3−1959	opt	58545	84	q
20J1303.0+2434	opt	59366	48	r
20J1308.5+3547	gam	58970	18	P
20J1312.8−0425	gam	58658	18	Q
20J1333.7+5056	gam	59360	50	R
20J1423.5−7829	opt	59271	36	s
20J1427.6−3305	opt	58591	111	t
20J1438.9+3710	gam	57863	30	S
20J1506.1+3731	gam	57060	18	T
20J1517.7−2422	opt	58197	25	u
20J1532.7−1319	gam	56771	27	U
20J1635.2+3808	gam	56499	201	V
20J1700.0+6830	opt	56466	18	v
20J1740.5+5211	gam	59271	24	W
20J1748.6+7005	opt	56864	55	w
20J1748.6+7005	opt	59514	90	w
20J2158.8−3013	opt	57604	37	x
20J2236.5−1433	opt	58413	40	y
20J2250.0−1250	gam	57674	12	X
20J2250.0−1250	gam	58340	16	X

APPENDIX B: 'ORPHAN' FLARES

In this appendix, we list the characteristic of our 'orphan' flare golden sample.

This paper has been typeset from a TEX/LATEX file prepared by the author.